Orest V. Matveichuk, MSc

The role of flotillins and their *S*-palmitoylation in LPS-induced signaling

PhD thesis

Completed in Laboratory of Molecular Membrane Biology,
Nencki Institute of Experimental Biology
of the Polish Academy of Sciences

SUPERVISOR:

Prof. dr hab. Katarzyna Kwiatkowska

Warsaw, 2022

The research leading to these results has received funding from the European Union's Horizon 2020 research and innovation program under the Marie Sklodowska-Curie (grant No. 665735) and from the National Science Centre, Poland (grant No. 2018/29/B/NZ3/00407).

I would like to extend my deepest gratitude to Professor Katarzyna Kwiatkowska - my PhD thesis supervisor, for giving me the opportunity to perform this project, huge support, commitment as well as scientific supervision in the course of my research

I would also like to express my deepest appreciation to Aneta Hromada-Judycka, Anna Ciesielska, Gabriela Traczyk, Justyna Sobocińska, Anna Świątkowska, Kamila Prymas from the Laboratory of Molecular Membrane Biology for their knowledge, practical advice and for creating a friendly working atmosphere

I would like to extend my sincere thanks to Tomas Brdicka and all people from the Laboratory of Leukocyte Signalling, from the Institute of Molecular Genetics of the Chech Academy of Sciences for a new experience in working with mice, additional research target and a warm welcome in Prague

Table of contents

Abbreviations

17ODYA - 17- octadecynoic acid

ABE - acyl-biotin exchange

BPA - bromopalmitic acid

BSA - bovine serum albumin

CCL5/RANTES – chemokine (C-C motif) ligand 5/ regulated upon activation, normal T cell expressed and secreted

CD14 - cluster of differentiation 14

cDNA - complementary DNA

DAG – diacylglycerol

DGKε - diacylglycerol kinase-ε

DAMP - damage-associated molecular pattern

DHHC motif - Asp-His-His-Cys motif

DMEM - Dulbecco's Modified Eagle's Medium

DMSO - dimethyl sulfoxide

DRM - detergent-resistant membranes

EDTA - ethylenediaminetetraacetic acid

eIF5A2 - eukaryotic translation initiation factor 5A2

ELISA - enzyme-linked immunosorbent assay

EVs- extracellular vesicles

FBS - fetal bovine serum

GPI - glycosylphosphatidylinositol

GST - glutathione-*S*-transferase

HPRT - hypoxanthine-guanine phosphoribosyltransferase

HRP - horseradish peroxidase

HXA - hydroxylamine

IgG - immunoglobulin G

IGF-1R – insulin-like growth factor-1 receptor

IRAK - interleukin-1 receptor-associated kinase

IRF - interferon regulatory factor

Iκβ - inhibitor of NFκB

JAK1 - Janus kinase 1

LB - Luria-Bertani medium

LBP - lipopolysaccharide-binding protein

LPS - lipopolysaccharide

MD2 - myeloid differentiation protein 2

MMTS - methyl methanethiosulfonate

mRNA - messenger RNA

MEND - massive endocytosis

MyD88 - myeloid differentiation primary response 88

NFκβ - nuclear factor κβ

NLRP3 - NLR family pyrin domain-containing 3

OPAL1- outcome predictor of acute leukemia 1

PAG - phosphoprotein associated with glycosphingolipid-enriched microdomains

PAMP - pathogen-associated molecular pattern

PBS - phosphate-buffered saline

PCR - polymerase chain reaction

PEG - polyethylene glycol

$PI(4,5)P_2$ - phosphatidylinositol 4,5-bisphosphate

PMSF - phenylmethylsulfonyl fluoride

PRR - pattern recognition receptor

RT-qPCR - real-time quantitative PCR

S1P - sphingosine-1-phosphate

SDS - sodium dodecyl sulfate

SDS-PAGE - SDS polyacrylamide gel electrophoresis

siRNA - small interfering RNA

shRNA - small hairpin RNA

TBK1 - TANK-binding kinase 1

TBST - Tris-buffered saline with Tween 20

TCEP - Tris(2-carboxyethyl)phosphine

TCR - T-cell receptor

TEM -tetraspanin-enriched microdomain

TIR - Toll/interleukin-1 receptor

TIRAP - TIR domain-containing adaptor protein

TLR - Toll-like receptor

TMB - 3,3',5,5'- tetramethylbenzidine

tmTNFα - transmembrane precursor TNFα

TNFα - tumor necrosis factor α

TRAM - TRIF-related adaptor molecule

TRIF - TIR domain-containing adaptor inducing interferon-β

VSVG- vesicular stomatitis virus G protein

zDHHC - zinc finger DHHC domain-containing

Abstract

Flotillin-1 and flotillin-2 are ubiquitously expressed submembranous proteins which can associate with both the plasma membrane and endosomal compartments. Membrane-binding regions of flotillins include hydrophobic stretches and site(s) of their acylation, i.e., *N*-myristoylation and/or *S*-palmitoylation. Thanks to these structural features, flotillin-1 and -2 bind to the cytoplasmic leaflet of rafts, plasma membrane nanodomains rich in cholesterol and sphingolipids. On the other hand, flotillins undergo homo- and hetero-oligomerization and also interact directly and indirectly with numerous proteins. Therefore, flotillins can act as scaffolding proteins, facilitating the assembly of multiprotein submembrane complexes involved in various cellular processes.

The main objective of this study was to reveal the role of flotillins and their *S*-palmitoylation in TLR4 signaling triggered by bacterial lipopolysaccharide (LPS). TLR4 initiates a pro-inflammatory response aiming at the eradication of bacteria, but overreaction to LPS can lead to fatal sepsis. This fuels interest in molecular mechanisms of activation of macrophages by LPS. The rationale for undertaking the studies was: (1) results of our mass spectrometry analysis, which showed that the amount of palmitoylated flotillin-1 increased in LPS-stimulated Raw264 macrophage-like cells, suggesting its participation in LPS-triggered signaling; (2) a line of data indicating that flotillins are involved in clustering, endocytosis and cellular trafficking of raft proteins. A typical raft protein is CD14 which assists activation of TLR4 by LPS. It was therefore assumed that flotillins can affect LPS-induced signaling due to possible interplay with CD14.

To achieve the goal, lentiviral particles were used to deliver flotillin-2-specific shRNA into Raw264 cells. Several clones of cells stably depleted of flotillin-2 were obtained, which were also found to be deficient in flotillin-1. In flotillin-depleted Raw264 cells, the LPS-induced responses were diminished. The TRIF-dependent signaling pathway of TLR4 leading to activation (phosphorylation) of the IRF3 transcription factor was inhibited and the subsequent production of chemokine CCL5/RANTES was reduced. The MyD88-dependent signaling leading to IκB phosphorylation and activation of the NFκB transcription factor and production of cytokine TNFα was also reduced. However, the latter effect was most pronounced in cells stimulated with low LPS concentration. The above characteristics reflect LPS-induced responses which require the participation of CD14. Indeed, a line of data obtained in the course of this study indicates that flotillins control the cellular level of CD14 and thereby affect the LPS-induced signaling. Depletion of flotillin-1 and -2: (i) lowered CD14 mRNA level; (ii) reduced the total cellular level of CD14; (ii) decreased the amount of CD14 on the cell surface. Notably, no such changes were observed for TLR4. On the other hand, forced clustering of CD14 in the

plasma membrane (the first effect of LPS binding) induced *S*-palmitoylation of flotillin-1 and flotillin-2, indicating mutual interactions of flotillins and CD14. To detect which palmitoyl acyltransferase(s) catalyze *S*-palmitoylation of flotillins, they were co-expressed in HEK293 cells with 23 members of the zDHHC family, revealing that zDHHC5 and zDHHC8 can modify flotillins. After silencing of *Zdhhc5* or *Zdhh8* with siRNA in Raw264 cells, it was found that zDHHC5 participation is required for a response to LPS triggered in both TLR4 signaling pathways, with emphasis on the TRIF-dependent pathway, which may be linked with zDHHC5 involvement in *S*-palmitoylation of flotillins. Taken together, the data indicate that flotillins modulate the cellular level of CD14 and interact (indirectly) with CD14, thereby affecting the intensity of the LPS-induced pro-inflammatory response. Flotillins are likely to be involved in CD14 endocytosis and recycling, as well as in the transport of newly synthesized CD14 to the plasma membrane, all events may be regulated by *S*-palmitoylation of flotillins catalyzed among others by zDHHC5.

The above results were obtained, i.a., owing to the development of a modification of a technique for detecting palmitoylated protein. It involves enrichment of 17ODYA (palmitic acid analogue)-labeled proteins and their recovery from streptavidin-coupled beads. The advantage of this technique is that it allows simultaneous identification of several endogenous and overproduced palmitoylated proteins. The technique was used in a study conducted in collaboration with the Institute of Molecular Genetics ASCR in Prague and allowed the detection of *S*-palmitoylation of OPAL1, an adaptor protein of leukocytes, likely to be located in rafts.

Abstract in Polish

Flotylina-1 i flotylina-2 są powszechnie występującymi białkami podbłonowymi, które asocjują zarówno z błoną komórkową, jak i z pęcherzykami endosomalnymi. Regiony cząsteczek flotylin zaangażowane w wiązanie z błoną obejmują sekwencje hydrofobowych aminokwasów oraz miejsce (miejsca) ich acylacji, tj. *N*-mirystoilacji i/lub *S*-palmitoilacji. Dzięki tym elementom strukturalnym flotylina-1 i -2 wiążą się z listkiem cytoplazmatycznym tzw. tratw, czyli nanodomen błony komórkowej bogatych w cholesterol i sfingolipidy. Z drugiej strony, flotyliny ulegają homo- i hetero-oligomeryzacji, a także oddziałują bezpośrednio i pośrednio z licznymi białkami. W związku z tym flotyliny mogą pełnić rolę białek rusztowaniowych, ułatwiających formowanie wielobiałkowych kompleksów podbłonowych, które biorą udział w różnorodnych procesach komórkowych.

Głównym celem podjętych badań było ujawnienie roli flotylin i ich *S*-palmitoilacji w szlakach sygnałowych receptora TLR4 aktywowanego przez bakteryjny lipopolisacharyd (LPS) w makrofagach. TLR4 inicjuje kaskadę prozapalną mającą na celu eliminację bakterii, ale nadmierna reakcja organizmu na LPS może prowadzić do śmiertelnej w skutkach sepsy. To wzbudza zainteresowanie molekularnymi mechanizmami aktywacji makrofagów przez LPS. Uzasadnieniem podjęcia prezentowanych badań były: (1) wyniki naszej analizy spektrometrii mas, która wykazała, że ilość palmitoilowanej flotyliny-1 wzrasta w komórkach Raw264 linii makrofagopodobnej stymulowanych przez LPS, co sugeruje udział tego białka w indukowanych wtedy szlakach sygnałowych; (2) szereg danych wskazujących, że flotyliny biorą udział w endocytozie i transporcie komórkowym białek tratw błonowych. Typowym białkiem tratw jest CD14, które wspomaga aktywację receptora TLR4 przez LPS. Założono zatem, że flotyliny mogą wpływać na szlaki sygnałowe indukowane przez LPS ze względu na możliwe oddziaływania z białkiem CD14.

Aby zrealizować cele badawcze zastosowano cząstki lentiwirusowe i wprowadzono shRNA swoiste wobec flotiliny-2 do komórek Raw264. Uzyskano kilka klonów komórek ze stabilnie zredukowanym poziomem flotiliny-2, które okazały się również pozbawione flotyliny-1. W komórkach Raw264 zubożonych we flotyliny odpowiedź na LPS, w której pośredniczy CD14 i receptor TLR4, była znacząco osłabiona. Zależny od białka TRIF szlak sygnałowy TLR4 prowadzący do aktywacji (fosforylacji) czynnika transkrypcyjnego IRF3 był zahamowany, a następująca po nim produkcja chemokiny CCL5/RANTES była zmniejszona. Osłabieniu ulegał również szlak sygnałowy zależny od białka MyD88 prowadzący do fosforylacji IκB i aktywacji czynnika transkrypcyjnego NFκB oraz wytwarzania cytokiny TNFα. Ten ostatni efekt był jednak silniej wyrażony w komórkach stymulowanych niskim stężeniem LPS. Powyższa charakterystyka odzwierciedla odpowiedzi indukowane przez LPS, które wymagają udziału

białka CD14. Rzeczywiście, szereg danych uzyskanych w trakcie prezentowanych badań wskazuje, że flotyliny kontrolują poziom CD14 w komórkach i tym samym wpływają na szlaki sygnałowe receptora TLR4 indukowane przez LPS. Ubytek flotyliny-1 i -2: (i) obniżał poziom mRNA CD14; (ii) redukował całkowity poziom CD14 w komórkach; (ii) obniżał ilość CD14 na powierzchni komórek. Warto zauważyć, że nie zaobserwowano takich zmian w odniesieniu do receptora TLR4. Z drugiej strony, wymuszona klasteryzacja białka CD14 w płaszczyźnie błony komórkowej (pierwszy efekt wiązania LPS) indukowała *S*-palmitoilację flotyliny-1 i flotyliny-2, co wskazuje na wzajemne oddziaływania flotylin i CD14. Aby wykryć, które palmitoilotransferazy katalizują *S*-palmitoilację flotylin, białka te nadprodukowano w komórkach HEK293 wraz z 23 członkami rodziny zDHHC i ustalono, że zDHHC5 i zDHHC8 mogą modyfikować flotyliny. Po wyciszeniu *Zdhhc5* lub *Zdhhc8* w komórkach Raw264 przy użyciu siRNA stwierdzono, że oba szlakach sygnałowe receptora TLR4 aktywowanego przez LPS wymagają udziału zDHHC5, z naciskiem na szlak zależny od białka TRIF, co może być związane z udziałem zDHHC5 w *S*-palmitoilacji flotylin. Podsumowując, uzyskane dane wskazują, że flotyliny modulują komórkowy poziom CD14 i oddziałują (pośrednio) z CD14, wpływając tym samym na intensywność odpowiedzi prozapalnej indukowanej przez LPS. Flotyliny prawdopodobnie biorą udział w endocytozie i recyklingu CD14, a także w transporcie nowo zsyntetyzowanego CD14 do błony komórkowej, przy czym wszystkie te zdarzenia mogą być regulowane przez *S*-palmitoilację flotylin katalizowaną między innymi przez zDHHC5.

Powyższe wyniki uzyskano m.in. dzięki opracowaniu modyfikacji techniki wykrywania palmitoilowanych białek. Polega ona na wzbogaceniu białek znakowanych 17ODYA (analog kwasu palmitynowego) i ich odzyskaniu z kulek sprzęgniętych ze streptawidyną. Zaletą tej techniki jest to, że umożliwia jednoczesną identyfikację szeregu endogennych i nadprodukowanych palmitoilowanych białek. Technika ta została wykorzystana w badaniach przeprowadzonych we współpracy z Instytutem Genetyki Molekularnej ASCR w Pradze i umożliwiła wykrycie *S*-palmitoilacji białka adaptorowego leukocytów OPAL1, które może być zlokalizowane w tratwach błonowych.

1. Introduction

The immune system is a highly effective guardian of the human organism against myriads of infections. This resistance is based on a complex synergy between innate and adaptive components of the immune system. Adaptive immunity has developed in vertebrates and engages B and T lymphocytes, which produce antibodies directed against pathogen-derived antigens and destroy infected cells. These immune responses require specific recognition of particular antigens and are relatively slow. They also lead to the development of immunological memory due to the formation of memory B and T lymphocytes. This, in turn, facilitates a fast and effective immune response after repeated contact with a given antigen (Chaplin 2010). Innate immunity responses, characteristics of invertebrates and vertebrates, provide (along with protective barriers, such as intestinal and skin epithelia) the first line of defense against pathogens and rely on the activity of antimicrobial peptides and other toxic molecules, as well as the activity of a repertoire of pro-inflammatory mediators. In mammals, pro-inflammatory reactions are mainly induced by macrophages, dendritic cells, granulocytes, mast cells, and also some non-immune cells. Pro-inflammatory reactions are triggered by distinct proteins called pattern recognition receptors (PRRs) which detect and bind structural components of viruses, bacteria, fungi and parasites called pathogen-associated molecular patterns (PAMPs). Mammalian PRRs are divided into several classes depending on their structural characteristics and include Toll-like receptors (TLRs), C-type lectin receptors (CLRs), NOD-like receptors (NLRs), RIG-I-like receptors (RLRs), and AIM2-like receptors (ALRs) (Takeuchi and Okira, 2010; Pandey et al., 2015). This diversity of receptors gives the host an indispensable instrument to recognize a large number of pathogens and successfully defend against them.

1.1 Toll-like receptors

The best-described PRRs are those of the Toll-like family which recognize a variety of PAMPs, such as lipopolysaccharide (LPS) and other components of bacterial envelops and flagella, bacterial DNA with non-methylated CpG motifs, single and double-stranded RNA, etc. (Table 1.1). They also respond to damage-associated molecular patterns (DAMPs), like chromatin-protein complexes and other molecules released from dead cells and damaged tissues of the host (Anwar et al., 2013). However, among plenty of endogenous agonists, only a minority activates the PRRs directly, while others act indirectly, e.g., in cooperation with PAMPs. Three conditions have been proposed that should be met by DAMP directly activating TLR4 (Manček-Keber et al., 2015). The conditions can be common for other DAMP-PRR interactions:

- the agonist must activate the formation of the receptor signaling complex;

- the agonist formed synthetically or *in situ* must activate the receptor to eliminate artifacts caused by contamination of the DAMP by PAMPs;
- the agonist must create a specific molecular interaction with the receptor (which need not be similar to those of PAMP).

The identification of the *Toll* gene in Drosophila in 1985 and the discovery of the Toll participation in the immune response of this fly initiated the "age" of TLRs which have been named after the *Drosophila* protein (Anderson et. al., 1985; Lemaitre et al., 1996). The first mammalian TLR – TLR4 – was described in 1998 by Bruce Beutler's group and until today members of the TLR family have been found in living beings ranging from corals to humans (Poltorak et al., 1998). Thus, 13 genes encoding TLRs in mammals have been characterized. In humans, 10 TLRs have been identified with *TLR11-13* being pseudogenes, while in mice *Tlr10* is a pseudogene. The population of cells expressing TLRs includes the vast majority of immune cells and also endothelial, neuronal, and several other non-immune cells (Song et al., 2019; Chen et al., 2019).

TLRs are localized in the plasma membrane and endosomes and the localization determines which PAMP they recognize. The first group (TLR1, 2, 4-6 and 10) detects components of walls, membranes and flagella while the second one (TLRs 3, 7-9, 11-13) nucleic acids of microbes (Table 1.1); (Takeuchi and Akira, 2010; Pandey et al., 2015).

TLRs are transmembrane proteins with the following structure:
- the ectodomain (an extracellular or intraluminal part) which is built of leucine-rich repeats and participates in PAMP recognition;
- a single transmembrane fragment;
- the Toll/interleukin-1 receptor (TIR) domain which is necessary for induction of the downstream signaling (Gay and Gangloff, 2007; Kawai and Akira, 2010).

PAMP binding initiates homo- or heterodimerization of TLRs. This, in turn, results in the recruitment of one to four adaptor proteins, including TIR domain-containing adaptor protein (TIRAP), myeloid differentiation factor 88 (MyD88), TIR domain-containing adaptor inducing interferon-β (TRIF), and TRIF-related adaptor molecule (TRAM).

The most common is MyD88 which is used by all TLRs except TLR3 (Song et al., 2019). The fifth related adaptor protein, SARM, acts as an inhibitor of the TRIF-dependent TLR signaling in humans (Carty et al., 2006). The four adaptor proteins initiate downstream signaling leading to the ultimate activation of transcription factors, such as NFκB, IRF3 and AP1, and the production of pro-inflammatory cytokines, including TNFα, IL-6, and type I interferons, as described below in more detail for TLR4.

Table 1.1. Characteristics of mammalian TLRs

TLR	Localization	PAMPs and *DAMPs* recognized	Adaptors	Main effector cytokines	Distribution in immune cells
TLR1/ TLR2	plasma membrane	triacyl lipopeptides, *HMGB-1*	TIRAP, MyD88	IL-6, TNFα	Mo, DCs, TC, BC, NK, MΦ
TLR2/ TLR6	plasma membrane	diacyl lipopeptides, peptidoglycans, lipoteichoic acid, zymosan, *HSP*, *HMGB-1*	TIRAP, MyD88	IL-6, TNFα, IL-8, MCP-1, RANTES	Mo, DCs, MΦ, MC
TLR3	endosomes	dsRNA, *mRNA*, *HSP*, *fibrinogen*	TRIF	IFNβ	Mo, DC, TC, BC
TLR4	plasma membrane and endosomes	LPS, N^{2+}, *taxol HMGB-1, HSP, hyaluronic acid, β-amyloid*	TIRAP, MyD88, TRAM, TRIF,	TNFα, IL-6, RANTES, IFNβ, IP-10`	Mo, MΦ, DC, TC, BC
TLR5	plasma membrane	flagellin	MyD88	TNFα	Mo, MΦ, DC
TLR7	endosomes	ssRNA, *endogenous RNA*	TIRAP, MyD88	IFNα	Mo, DC, TC, BC, NK
TLR8	endosomes	ssRNA, *endogenous RNA*	MyD88	IFNα	Mo, MΦ, DC
TLR9	endosomes	unmethylated CpG DNA, *endogenous DNA*	TIRAP, MyD88	IFNα	Mo, MΦ, DC, TC, BC, NK
TLR10	plasma membrane	HIV-gp41	TIRAP, MyD88	TNFα, IL-12	Mo, DC, BC
TLR11 (murine)	endosomes	profilin from *Toxoplasmosa gondi*, flagellin	MyD88	TNFα, IL-12	MΦ, EC, DC
TLR12 (murine)	endosomes	profilin from *Toxoplasmosa gondi*	MyD88	IL12p40, INFα	DC
TLR13 (murine)	endosomes	23s rRNA (bacterial ribosomal RNA)	MyD88	IL-6, IL-12p40	MΦ, DC

Recognition of DAMPs by TLR4 is discussed in the text.
BC, B lymphocytes; DC, dendritic cells; EC, epithelial cells; ECM, extracellular matrix; HSP, heat shock protein; HMGB-1, high mobility group box-1 protein; IgG, immunoglobulin G; IL, interleukin; IFN, interferon; LPS, lipopolysaccharide; MΦ, macrophages; NK, natural killer cells; ssRNA, single-stranded RNA; TC, T lymphocytes; TNF, tumor necrosis factor.
According to Pandey et al. (2015), Song et al. (2019); Chen et al. (2019), Henrick et al. (2019).

This results in an efficient inflammatory reaction that helps combat the infection. TLR activity also modulates adaptive immune responses affecting both T and B lymphocyte-mediated responses (Fitzgerald and Kagan, 2020).

One of the most important and best-characterized receptors of the TLR family is TLR4, a receptor that enables macrophages, dendritic cells and some non-immune cells to detect the extracellular LPS, the main component of the outer membrane of Gram-negative bacteria. TLR4 is crucial for LPS-mediated pro-inflammatory responses, however, exaggerated host response to bacterial infection can cause sepsis. Prolonged low-grade inflammation leads to the development of diabetes 2 and other diseases (Takeda et al., 2003; Mitchell et al., 2007; Cani et al., 2007). Among putative DAMPs, only plant-derived taxol, Ni^{+2} and disulfide HMGB1 fulfill all the criteria mentioned above and activate TLR4 directly. Other DAMPs likely enhance the LPS-induced activation of TLR4 (Manček-Keber et al., 2015). This, however, expands a list of pathophysiological conditions involving TLR4-induced pro-inflammatory reactions and increases interest in molecular mechanisms of TLR4 activity.

1.2 Lipopolysaccharide and TLR4 activation

LPS protects Gram-negative bacteria against antibiotics, other harmful chemicals and desiccation. It consists of three parts: a hydrophobic region, called lipid A, that anchors LPS in the outer layer of the bacterial membrane, core oligosaccharide, and O-antigen (O-polysaccharide) (Rietschel et al., 1994). Lipid A consists of a phosphorylated diglucosamine backbone connected to acyl chains by ester or amide linkages. The immunostimulatory activity of LPS depends on the length, number and position of acyl chains in lipid A and also on the presence of phosphoryl groups (Steimle et al., 2016). Highly immunostimulatory LPS species, like LPS of *E. coli* (0111:B4), have lipid A that is diphosphorylated and contains 6 acyl chains with a length between 12 to 14 carbon atoms. Changes in those parameters result in a lower biological activity of LPS (Park et al., 2009; Tan et al., 2015). Lipid A is covalently linked to the LPS core region comprising 1-4 molecules of 3-deoxy-d-manno-2-octulosonic acid (KDO), hexoses and hexosamines. The core glycan residues are often modified with phosphate-containing groups. Moreover, in most Gram-negative bacteria, the core oligosaccharide is linked to O-antigen which contains several repeating units of oligosaccharides whose composition is highly variable among bacterial species. LPS molecules consisting of the three above-mentioned regions are synthesized by bacteria whose colonies have a so-called smooth phenotype earning them the name smooth LPS. LPS species produced by rough bacterial colonies are devoid of O-antigen and can be also depleted of core

oligosaccharides (Raetz and Whitfield, 2002). Smooth and rough LPS differ in their ability to trigger the TLR4-dependent signaling pathways, as described below.

The mechanism of TLR4 activation by LPS is complex since this PRR does not bind its ligand directly. In addition, LPS is released from bacteria as aggregates and can form micelles, and needs to be monomerized to activate TLR4. LPS aggregates/micelles are first recognized by lipopolysaccharide-binding protein (LBP), as shown in Fig.1.1.

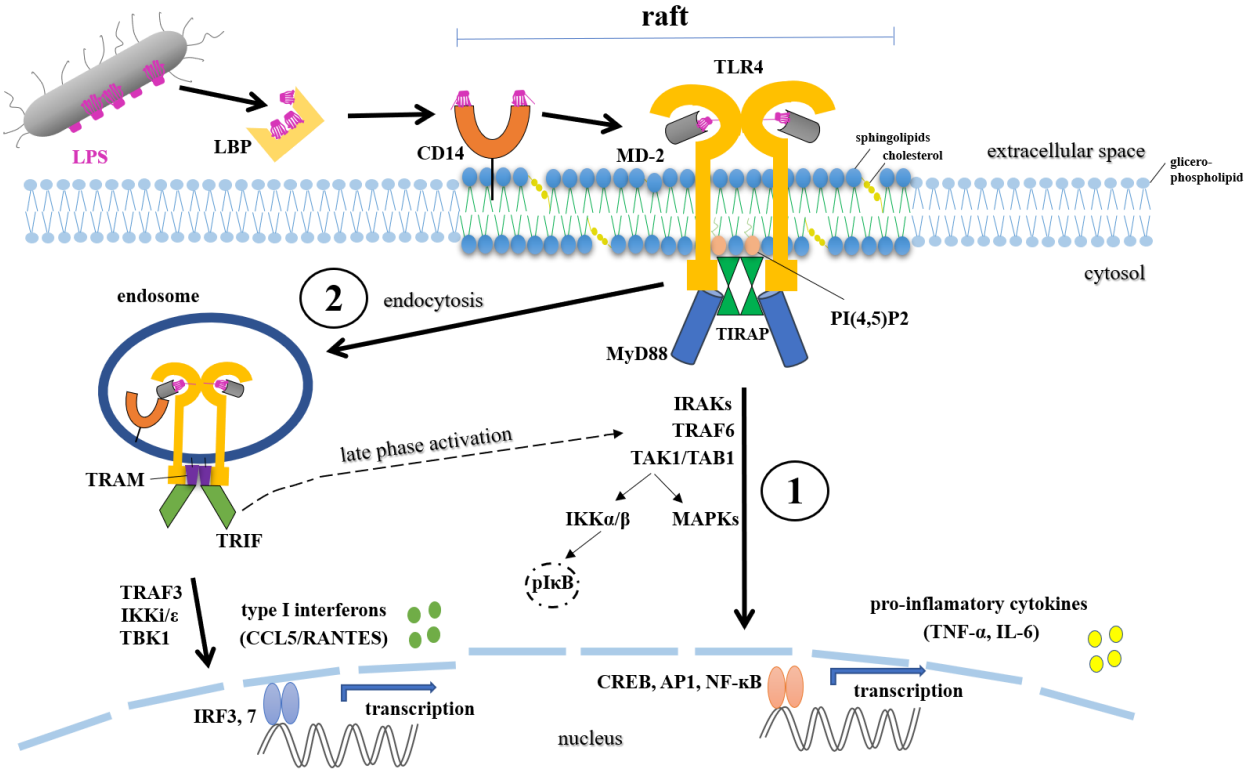

Figure 1.1 Scheme of TLR4 activation triggered by LPS. (1) MyD88-dependent signaling cascade (2) TRIF-dependent signaling cascade. See text for details.

The expression of LBP increases markedly during the acute phase of infection. LBP binds to the surface of LPS aggregates/micelles and facilitates the extraction of LPS monomers by another protein, CD14, by creating unstable triple complexes with the LPS aggregates/micelles and CD14 protein (Ryu et al., 2017). CD14 exists in two forms – a soluble protein (sCD14) found in serum and a membrane-bound glycosylphosphatidylinositol (GPI)-anchored protein (mCD14, CD14) present mainly in myeloid cells, including monocytes, macrophages and dendritic cells (Simmons et al., 1989). sCD14 is created either by cleavage of the GPI anchor of the membrane-bound CD14 or by *de novo* synthesis (Bufler et al., 1995; Ciesielska et al., 2022). While both forms of CD14 bind LPS monomers and are engaged in

TLR4 activation, only the membrane-anchored CD14 is engaged in signaling pathways of the receptor, as described below. The LPS-binding hydrophobic pocket is located at the N-terminus of CD14, while the GPI anchor is attached to its C-terminus shortly after CD14 synthesis and incorporation into the membrane of the endoplasmic reticulum (Kim et al., 2005). Upon binding of an LPS monomer, CD14 dissociates from the LPS/LBP complex and can transfer the LPS to the hydrophobic pocket of MD2 protein, which is a component of the TLR4/MD2 heterodimer. When five of the six LPS acyl chains are hidden in that pocket of MD2, the sixth one is left outside and interacts with TLR4 of another TLR4/MD2 dimer. In addition, the two phosphoryl groups of lipid A interact with the TLR4 molecule via electrostatic interactions (Park et al., 2009). By simultaneous binding to MD2 of one TLR4/MD2 complex and to the TLR4 of the adjacent TLR4/MD2 complex, LPS facilitates the formation of their "M"-shaped dimer (Park et al., 2009; Resman et al., 2009) which in turn triggers downstream signaling cascades of the receptor. This explains why LPS species which have fewer acyl chains in lipid A and/or are underphosphorylated have reduced immunostimulatory activity. They are often produced by commensal bacteria that inhabit mammalian intestines and do not trigger TLR4 activation.

Activated TLR4 launches two signaling routes (Fig. 1.1). First, the dimerized TLR4 recruits two adaptor proteins, TIRAP and MyD88 which bind to TLR4 via their TIR domains (Deguine and Barton, 2014). Additionally, TIRAP binds to phosphatidylinositol 4,5-bisphosphate ($PI(4,5)P_2$), a lipid of the inner leaflet of the plasma membrane, and this binding facilitates its interactions with TLR4 and MyD88 (Kagan and Medzhitov, 2006; Takeuchi and Akira, 2010; Patra and Choi, 2018). In turn, MyD88 recruits (via its death domain) interleukin-1 receptor-associated kinases (IRAK1, 2 and 4), leading to their autophosphorylation and activation (Lin et al., 2010). Thereby a submembranous complex called myddosome is assembled, which induces oligomerization and activation of TNF receptor-associated factor 6 (TRAF6) (Motshwene et al., 2009; Tan and Kagan, 2014). TRAF6 is an E3 ubiquitin ligase and catalyzes self-ubiquitination with ubiquitin molecules joined in a chain through Lys63 and also the formation of a free Lys63 polyubiquitin chain (Gay et al., 2014). Subsequently, TAK1-binding protein 1 (TAB1) in complex with transforming growth factor ß-associated kinase-1 (TAK1 kinase) binds to this polyubiquitin chain (Takeuchi and Okira, 2010). Activated thereby TAK1 triggers two signaling cascades. In the first path, TAK1 activates the IκB kinase complex which includes a regulatory subunit NEMO and IKKα/ß kinases, which are phosphorylated by TAK1. This leads to IKKα/ß-mediated phosphorylation and the following proteasomal degradation of IκB (inhibitor of

NF-κB) (Wang et al., 2001). Consequently, the NF-κB transcription factor (p50/p65 dimer) is released and translocates to the nucleus where induces the expression of genes encoding pro-inflammatory cytokines, such as TNFα and IL-6 (Takeuchi and Akira, 2010). TAK1 also phosphorylates and activates mitogen-activated protein kinases (MAP kinases) and thereby induces the activation of the activator protein 1 (AP-1) and cAMP-response element-binding protein (CREB) transcription factors, contributing to the expression of pro-inflammatory mediators and also some anti-inflammatory cytokines, like IL-10, which help to resolve the inflammation. Tan and Kagan reported in 2019 that in addition to the processes described above, myddosome also triggers glycolysis. Glycolysis is induced by Akt kinase, a substrate of TBK1 kinase recruited to the myddosome by TRAF6 (Tan and Kagan, 2019). The main aim of this metabolic process is to provide immune cells with energy (ATP) and metabolic intermediates required for defense responses (Ganeshan and Chawla, 2014).

After triggering the first signaling pathway, CD14/TLR4/MD2/LPS complex is internalized (Fig. 1.1). Internalization is governed by CD14, as described in more detail in the next chapter (Zanoni et al., 2011; Tan et al., 2015; Ciesielska et al., 2022). During endocytosis, TIRAP and MyD88 adaptor proteins dissociate from TLR4 and are replaced at the endosome membrane by another set of adaptor proteins, TRAM and TRIF (Kagan et al., 2008; Płóciennikowska et al., 2015a). The signaling role of TRAM resembles that of TIRAP. TRAM bind to the endosomal membrane via the N-terminal myristoyl chain and the adjacent phosphatidylinositol-binding motif, and facilitates the interaction of TLR4 with TRIF (Kagan et al., 2008; Ullah et al., 2016). The TRIF-dependent signaling begins with the binding of TRAF3, another E3 ubiquitin ligase, which initiates activation of IKKi/IKKε and TBK1 kinases (TANK-binding kinase 1) catalyzing the subsequent phosphorylation of IRF3/7 transcription factors. This is followed by dimerization of IRFs, their translocation to the nucleus, and binding to DNA target sequences which promote transcription of IFN-encoding genes and later IFN-stimulated genes. As a result, type I interferons (INFα, INFβ) and chemokines (e.g., CCL5/RANTES) are produced (Fitzgerald et al., 2003; Kawai and Akira, 2011). In addition, an interaction between TRIF and TRAF6 initiates the activation of the TAB1/TAK1 complex which leads to the production of pro-inflammatory cytokines through the late-phase activation of NF-κB and MAP kinases (Yamamoto et al., 2002; Kawai and Akira, 2006). Later, TLR4 transfers to lysosomes and is degraded (Husebye et al., 2006). Recently, a cell-specific regulatory role of integrin CD11b in the LPS-induced TLR4 endocytosis and the TRFI-dependent signaling has been indicated. The protein is required for

efficient TLR4 endocytosis in dendritic cells but inhibits TLR4-triggered signaling by promoting degradation of MyD88 and TRIF (Rosadini and Kagan, 2017).

In addition to TLR4 activation, LPS induces the production of pro-inflammatory cytokines by the NLRP3 (NLR family pyrin domain-containing 3) inflammasome. The NLRP3 inflammasome is a cytosolic protein complex composed of multiple copies of a few proteins, including NLRP3, ASC and pro-caspase-1. It is an important component of the innate immune system responsible for the processing and secretion of pro-inflammatory IL-1β and IL-18 as well as the induction of programmed cell death called pyroptosis (Patel et al., 2017). Canonical activation of the NLRP3 inflammasome requires two signals. The "priming" signal can be provided by LPS-activated TLR4 and the following activation of NFκB leading to the expression of genes encoding inflammasome proteins, such as NLRP3, and also precursors of IL-1β and IL-18. After that, a second signal is needed, which is generated by factors causing cellular stress and manifested by mitochondrial dysfunction or lysosome damage. It sets off the formation of the NLRP3 inflammasome complex and activation of caspase-1 which cleaves interleukin precursors and gasdermin D into their mature forms. Gasdermin D creates pores in the plasma membrane allowing the secretion of IL-1β and IL-18 and ultimately causes cell death by so-called pyroptosis (Guo et al., 2015). LPS can also activate the inflammasome in a non-canonical manner without TLR4 assistance. In this case, caspases 4/5 (in humans) or 11 (in mice) directly bind cytosolic LPS and induce the assembly of primed NLRP3 inflammasome, and pyroptosis (Yang et al., 2019).

1.3 The role of CD14 and rafts in LPS-induced signaling

Activation of TLR4 signaling takes place in plasma membrane nanodomains, named rafts (Wong et al., 2009; Płóciennikowska et al., 2015a). Membrane rafts are assemblies of sphingolipids, cholesterol and distinct proteins which separate laterally in the glycerophospholipid-rich milieu of the membrane. They exist in the plasma membrane, the Golgi apparatus and early/recycling endosomes. The assembly of rafts is driven by preferential interactions of saturated acyl chains of sphingolipids and cholesterol with a contribution of lipid-protein and protein-protein interactions (Lingwood and Simons, 2010; Kaiser et al., 2009; Levental et al., 2011). Owing to the distinct lipid composition, rafts are thicker and more ordered than the surrounding membrane milieu consisting mainly of unsaturated glycerophospholipids. For these reasons, raft proteins are most often modified with saturated lipids, and thereby their accommodation in rafts is energetically favorable. Thus, raft-residing proteins include GPI-linked proteins anchored in the outer leaflet of the

membrane and *S*-palmitoylated proteins which associate with the inner leaflet of the membrane. Few of the transmembrane proteins, mostly *S*-palmitoylated, also associate with rafts, including PAG and NTAL adaptor proteins involved in the immune cell signaling. It is considered that in addition to *S*-palmitoylation also the length of the transmembrane fragment and oligomerization drive the association of transmembrane proteins with rafts (Levental et al., 2010; Lorent et al., 2017).

The concept of the existence of membrane rafts was proposed by Simons and Ikonen in 1997 (Simons and Ikonen, 1997). Although initially questioned and modified, it is now widely accepted, being supported by high-resolution microscopy studies (Raghupathy et al., 2015; Stone et al., 2017). Rafts are now envisioned as highly labile nanometer-sized structures in unstimulated cells which merge upon cell simulation into more stable platforms (Podkalicka et al., 2015). These platforms can serve as sites of signal transduction owing to a concomitant local accumulation of distinct receptors and proteins involved in their signaling pathways, and also lipids involved in these pathways (Lingwood and Simons, 2010; Kusumi et al., 2012). Ample data indicate that plasma membrane rafts are sites of activation of so-called immunoreceptors such as the T-cell receptor (TCR) which cooperates with the aforementioned PAG and NTAL adaptor proteins (Horejsi and Hrdinka, 2014). Several biochemical and microscopic data also show that TLR4 associates with rafts upon LPS binding and triggers signaling with the use of raft-associated proteins and lipids such as phosphatidylinositols (Płóciennikowska et al., 2016). These data include so-called FRET and FRAP bio-imaging assays, a sensitivity of TLR4-induced signaling to the depletion or enrichment of the plasma membrane with cholesterol, and an analysis of the so-called detergent-resistant membrane (DRM) fraction which roughly reflects raft composition (Płóciennikowska et al., 2015a). The contribution of rafts to the activation of TLR4 is strengthened by the fact that CD14 is a typical raft protein.

Since CD14 is linked to the plasma membrane by the GPI-anchor and lacks a cytosolic signaling domain, it was considered that the main function of this protein is to supply LPS monomers to the TLR4/MD2 complexes (Triantafilou and Triantafilou, 2002). However, in 2005 Jiang and colleagues reported that LPS-induced activation of the TRIF-dependent signaling pathway of TLR4 in macrophages occurs only in the presence of membrane CD14 (Jiang et al., 2005). Thus, CD14-deficient macrophages stimulated with LPS displayed no IRF3 activation, no type I IFN production, and no induction of IFN-inducible genes, regardless of the smooth or rough chemotype of LPS used to simulate the cells. On the other hand, the MyD88-dependent TNFα expression could be triggered without the CD14

participation, especially by rough LPS and also by smooth LPS at concentrations ≥ 100 ng/ml (Perera et al., 1997; Jiang et al., 2005; Borzęcka et al., 2013). This can be attributed to the ability of sCD14 and albumin to deliver LPS to the TLR4/MD2 complexes in the absence of CD14 (Esparza et al., 2012) or even incorporation of LPS (especially the rough chemotype) into the plasma membrane followed by coalescence of rafts and activation of TLR4 (Płóciennikowska et al., 2015a).

Subsequent studies revealed that CD14 regulates LPS-induced endocytosis of TLR4 which is indispensable for the induction of the TRIF-dependent signaling pathways (Husebye et al., 2006, Zanoni et al., 2011). Detailed analysis showed that in unstimulated cells, CD14 undergoes slow-rate endocytosis and is degraded in lysosomes, while *de novo* synthesis of CD14 is required to replenish the cell surface pool of the protein. Recent studies revealed that a part of endocytosed CD14 can recycle back to the plasma membrane (Ciesielska et al., 2022). After binding of hexa-acylated and diphosphorylated LPS, CD14 interacts with MD2 and this interaction determines the endocytosis of CD14/TLR4/MD2/LPS complexes. Surprisingly, the signaling activity of TLR4 is dispensable for this uptake, establishing the role of TLR4 as cargo in CD14-driven endocytosis of the receptor (Zanoni et al., 2011; Tan et al., 2015). The above-described activity of CD14 and MD2 earned them the name ‘‘TAXI’’ proteins as “transporters associated with the execution of inflammation” (Tan et al., 2015). Under-acylated and under-phosphorylated forms of LPS evade the recognition by CD14 which contributes chiefly to the lack of TLR4 activation by host-adapted commensal bacteria (Tan et al., 2015).

Further studies revealed that the contribution of CD14 to TLR4 uptake is related to its influence on the $PI(4,5)P_2$ turnover. Binding of LPS to CD14 induced clustering of this protein in the plasma membrane. Clustering of CD14 is sufficient to trigger the synthesis of $PI(4,5)P_2$ via PIP5K Iα/PIP5K Iγ (Płóciennikowska et al., 2015b), with a possible engagement of Arf6 GTPase (Van Acker et al., 2014). Thus, redistribution of CD14 in the outer leaflet of rafts affects the activity of submembranous enzymes, likely due to changes in the lipid composition of rafts concomitant with the CD14 clustering. It was mentioned above that $PI(4,5)P_2$ supports the binding of the TIRAP and thereby the MyD88-dependent signaling pathway activation. On the other hand, $PI(4,5)P_2$ hydrolysis and phosphorylation are required for the subsequent endocytosis of TLR4 and the TRIF-dependent signaling and the subsequent IRF3 activation (Kagan and Medzhitov, 2006; Chiang et al., 2011; Aksoy et al., 2012). Recently, the role of the plasma membrane Ca^{+2}-permeable channel TRPM7 in the Ca^{+2} influx necessary for TLR4 endocytosis in macrophages was demonstrated and its dependence on CD14

was considered (Schappe and Desai, 2018). In summary, CD14 plays a crucial role in regulating cellular responses to LPS, not only facilitating LPS recognition by TLR4/MD2 and initiation of the MyD88-dependent pathway but also controlling TLR4/MD2/LPS endocytosis and initiation of the TRIF-dependent pathway.

An important factor affecting both TLR4 signaling pathways is the modification of proteins by lipidations, especially *S*-palmitoylation, as described below.

1.4 *S*-Palmitoylation and other protein lipidations

Protein lipidations are co- or post-translational modifications that consist in the attachment of a lipid group, including fatty acid, isoprenoid, sterol, phospholipid, or the glycosylphosphatidylinositol (GPI) anchor to a peptide chain. Lipidated proteins acquire a hydrophobic moiety that facilitates their docking in membranes. Thereby lipidations affect protein localization and functions and can also influence the tertiary structure and degradation of proteins (Werner et al, 2007; Resh 2013).

Among protein lipidations the most frequent are:

***N*-myristoylation** is mostly a co-translational attachment of the 14-carbon myristoyl chain (C14:0) to the N-terminal glycine residue (after removal of methionine) via an amide bond. This reaction is catalyzed by *N*-myristoyl transferases having two isoforms in mammals. Other fatty acids, such as palmitic acid, are also rarely used for this protein modification, justifying its broader *N*-acylation name. Eukaryotic cells do not express enzymes capable of cleaving the amide bond formed, therefore, *N*-myristoylation is irreversible. Only the IpaJ protein of *Shigella flexneri*, the bacteria causing diarrhea in humans, cleaves off the N-terminal myristoylated glycine of selected host proteins (Burnaevskiy et al., 2015). Among many *N*-myristoylated proteins is TRAM, the adaptor protein of TLR4 and also tyrosine kinases of the Src family, like Lck and Lyn pivotal in the signaling of TLR4 and TCR, and other immunoreceptors (Rowe et al., 2006; Resh 1999; Borzęcka-Solarz et al., 2017).

***S*-acylation** is a post-translational modification that involves linking a long-chain fatty acid residue derived from acyl-CoA to a cysteine residue via a thioester bond. Saturated palmitic acid (C16:0), stearic acid (C18:0) and also unsaturated palmitoleic acid (C16:1) and oleic acid (C18:1) can be used for *S*-acylation, however, most often it is a modification of proteins with the palmitic acid residue, the so-called *S*-palmitoylation. The uniqueness of *S*-palmitoylation among other lipid modifications lies in its potential reversibility (Guan and Fierke, 2011; Resh, 2016). Enzymes that catalyze *S*-palmitoylation and depalmitoylation and their selected

substrates are described in more detail below due to the importance of *S*-palmitoylation for TLR4 signaling.

***S*-prenylation** is a post-translational irreversible lipidation that consists in the attachment of a farnesyl or a geranylgeranyl moiety to a cysteine residue in the C-terminal CaaX (also CC and CXC) motif by either protein farnesyl transferase or protein geranylgeranyltransferase type I. *S*-prenylated are some monomeric GTPases, e.g., H- and N-Ras engaged in signaling cascades of various plasma membrane receptors, and Rab proteins involved in vesicular trafficking, and also important for TLR4 signaling.

***O*-acylation** is a post-transitional attachment of fatty acid residue, including palmitic acid, palmitoleic acid and octanoic acid to a serine or threonine residue via an oxyester bond (Spinelli et al., 2018). *O*-acylated are some secreted proteins (like Wnt proteins) functioning as ligands for receptors involved in embryonic development. Their lipidation is catalyzed by membrane-bound *O*-acyl transferases (MBOTs) located in the endoplasmic reticulum (Resh, 2016).

ε-*N*-acylation is a post-translational modification that involves the attachment of a fatty acid residue to the side chain of lysine via an amide linkage. The transmembrane precursor of TNFα is ε-*N*-myristoylated, in addition to its *S*-palmitoylation (Sobocińska et al., 2018a).

1.5 The role of protein *S*-palmitoylation

S-palmitoylated are both peripheral and integral membrane proteins. There are no conserved amino acid motifs containing the cysteine residue to be modified, however, some predictions are possible. Peripheral membrane proteins are often *N*-myristoylated or *S*-prenylated prior to *S*-palmitoylation. The two previous modifications, as well as polybasic motifs, provide the initial weak protein binding to a membrane which allows the subsequent *S*-palmitoylation of the protein by integral membrane palmitoyl acyltransferases. *N*-myristoylated and *S*-palmitoylated proteins are exemplified by tyrosine kinase of the Src family, including Lck and Lyn. Transmembrane proteins are often *S*-palmitoylated on a cysteine residue(s) located close to the junction of their transmembrane and cytosolic fragments. Among others, transmembrane adaptor proteins, such as PAG, SCIMP and NTAL are *S*-palmitoylated at this site and the modification is crucial for their involvement in immunoreceptor signaling (Horejsi and Hrdinka, 2014).

S-palmitoylation can target proteins to plasma membrane (micro/nano)domains. The most widespread formations of this type include membrane rafts and the tetraspanin

web (Levy et al., 2005; Charollais and Van Der Goot, 2009). Tetraspanin-enriched microdomains (TEMs) are assembled around these unique proteins which have four transmembrane helices and are *S*-palmitoylated at multiple cysteine residues (Shoham et al., 2006). *S*-palmitoylation of tetraspanins and their binding partners, such as numerous α- and β-integrin, is required for the assembly of TEMs (Yang et al, 2002; Levy and Shoham, 2005). In the case of TLR4 signaling, it was found that the level of TSPAN33 tetraspanin can regulate the degree of inflammatory gene expression in the NOTCH-depending manner (Ruiz-García et al., 2016). Another tetraspanin, CD9, plays an important role in the negative regulation of lung inflammation and the absence of this tetraspanin enhanced LPS-induced responses (Suzuki et al., 2009).

S-palmitoylation is also a major factor determining raft localization of both transmembrane and peripheral membrane proteins. This is because the saturated palmitoyl chain incorporates preferentially between ordered saturated acyl chains of lipids building the rafts. *S*-palmitoylated raft proteins include tyrosine kinases of the Src family, transmembrane hemagglutinin (HA) of influenza virus A and PAG adaptor protein (Liang et al., 2001; Veit, 2012). However, some *S*-palmitoylated proteins, like vesicular stomatitis virus G protein (VSVG) and *S*-stearoylated transferrin receptor, are excluded from rafts because the ultimate raftophilic propensity results from the combination of *S*-palmitoylation and properties of the transmembrane fragment of the protein (Senyilmaz et al., 2015; Levental et al., 2010).

The dynamic of the reversibility of *S*-palmitoylation also can define the cellular distribution of proteins and be indispensable for their functioning (Blaskovic et al., 2013). The best-known examples of this type of regulation include N- and H-Ras proteins which are excluded from the plasma membrane by depalmitoylation and transported to the Golgi apparatus where they are *S*-palmitoylated and return to the plasma membrane. The above-mentioned proteins perform different functions depending on localization and sustain growth factor-induced signaling (Rocks et al., 2005). Husseini and co-workers reported the crucial role of the PSD95 *S*-palmitoylation/depalmitoylation cycles at the postsynaptic membrane for synaptic plasticity (El-Husseini et al., 2002). Similar cycles have been recently found to control the redistribution of STAT3 from *S*-palmitoylated membrane-bound to a depalmitoylated nuclear form that was required for T helper 17 cell differentiation (Zhang et al., 2020). Studies of our group performed on Raw264 cells showed LPS-induced raft accumulation of *S*-palmitoylated Lyn kinase which resulted in inhibition of the pro-inflammatory response (Borzęcka-Solarz et al., 2017).

Recently, Ernst and co-workers reported that *S*-palmitoylation controls the anterograde transport of proteins through the Golgi complex (Ernst et al., 2018). Notably, *S*-acylation is often intertwined with other protein modifications, e.g., ubiquitination and phosphorylation and this way affects protein stability/degradation (Hach et al., 2013). For example, *S*-palmitoylation of zDHHC6 (one of the palmitoyl acyltransferases, see below) by zDHHC16 in the endoplasmic reticulum at Cys328 increases the enzymatic activity of the former but concomitantly induces its rapid degradation (Abrami et al., 2017).

1.6 Enzymes catalyzing protein *S*-palmitoylation and depalmitoylation

Palmitoyl acyltransferases were identified more than twenty years ago. Lobo et co-workers discovered that palmitoylation of Ras2 in yeast was controlled by Erf2 containing the conserved Asp-His-His-Cys (DHHC) motif located in the cysteine-rich domain (Lobo et al., 2002). At that time, independent studies of Roth and co-workers established that Akr1p, another enzyme of yeast with the DHHC motif, catalyzes *S*-palmitoylation of casein kinase Yck2 (Roth et al., 2002). Further investigations of the latter group proved the activity of 7 palmitoyl acyltransferases in yeast. They observed the elimination of protein palmitoylation in yeast strains deficient in proteins containing the DHHC motif (Roth et al., 2006).

The family of mammalian palmitoyl acyltransferases comprises 23 members (Mitchell et al., 2006). They were identified by Fukata and co-workers in 2004 by searching GenBank for mouse DHHC-coding sequences. Identified genes encoded DHHC proteins 1-23 (Fukata et al., 2004). They all have 4-6 transmembrane helices, the DHHC motif in the cysteine-rich domain and zinc finger motifs, therefore, their genes are now registered in GenBank as *Zdhhc*, and proteins are classified as palmitoyl acyltransferases of the zDHHC family (Chen et al., 2018). In this work the latter, more commonly used nomenclature is applied. When studies on palmitoyl transferases ectopically expressed in HEK293 cells are presented, both enzyme names are shown for clarity. I include Fukata's nomenclature since his laboratory kindly provided us with the collection of plasmids encoding all the mouse palmitoyl acyltransferases used in my studies. The DHHC nomenclature is in most cases the same as the zDHHC one. The exceptions include DHHC10, 11, 13, 22, 23 called zDHHC11, 23, 24, 13, 25, respectively. As shown in Fig. 1.2, the Golgi apparatus accommodates most of zDHHCs, including promiscuous zDHHC3 and zDHHC7 with a broad substrate specificity, while few palmitoyl acyltransferases, including zDHHC2, 5 and 8 are localized in the plasma membrane. zDHHC6 and 16 are localized in the endoplasmic reticulum (Jiang et al., 2018; Philippe and Jenkins, 2019). Notably, the localization of zDHHC enzymes can vary from cell to cell.

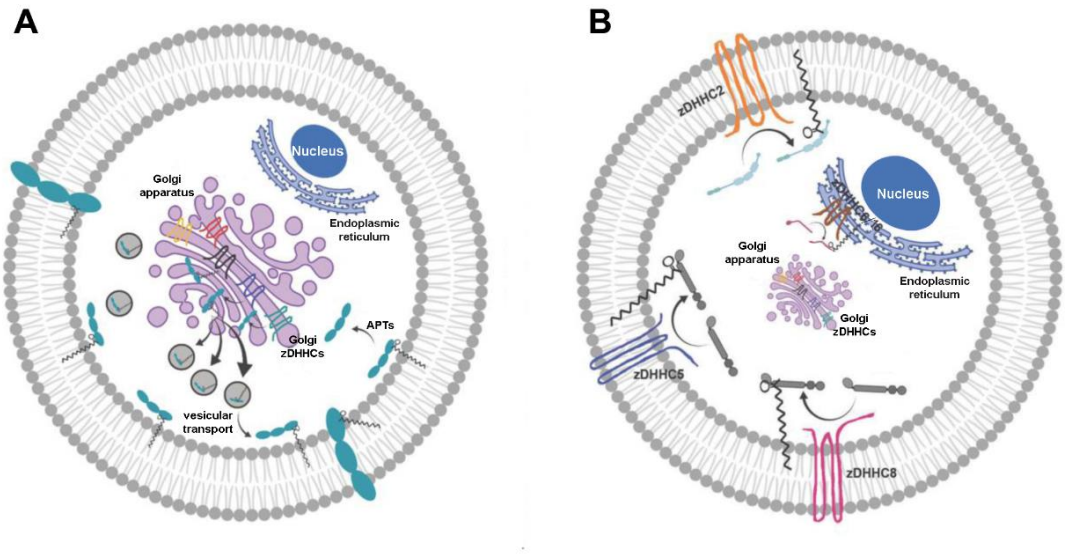

Figure 1.2 Cellular localization of mammalian zDHHCs. (**a**) Most of the enzymes of the zDHHC family are localized in the Golgi apparatus where they *S*-palmitoylate proteins which are subsequently trafficking in vesicles through the Golgi cisterns and next to the plasma membrane. (**b**) Three zDHHCs are localized in the plasma membrane, these include zDHHC2, 5 and 8, although plasma membrane localization of zDHHC7, 14, 20, 21, and 23 was also reported (Jiang et al., 2018). These enzymes are likely to catalyze *S*-palmitoylation of plasma membrane/submembranous proteins, such as flotillins. The endoplasmic reticulum harbors zDHHC6 and 16. PATs, palmitoyl acyltransferases. From Philippe and Jenkins (2019), modified.

As shown in Fig. 1.3, *S*-palmitoylation is a two-step process including the initial attachment of the palmitic acid residue (provided as palmitoyl-CoA) to the cysteine residue of the DHHC motif of the palmitoyl acyltransferase and the subsequent transfer of the fatty acyl group to the cysteine of the target protein (Jennings and Linder, 2012). The substrate selectivity of zDHHCs is regulated by few mechanisms. One is the structure of the DHHC domain (the current name of the cysteine-rich domain with the DHHC motif), e.g., zDHHC9 and 18 are specific to H-Ras and N-Ras. Another includes the presence of regulatory domains, such as the SH3 domain in zDHHC6 or PDZ-binding motifs found in the C-terminal part of zDHHC5 and zDHHC8, which contribute to the substrate recruitment (Malgapo and Linder, 2021). zDHHCs dysfunctions are a causal factor in many human diseases. The are several data pointing to the link between the zDHHC activity and cancer. For example, p53-mutant glioma development is zDHHC5-dependent (Fraser et al., 2020). *S*-palmitoylation controls also several neurological processes. Studies performed on zDHHC17 and zDHHC13 exhibited their role in Huntington's disease whereas deletion of these zDHHCs caused embryonic lethality in mice (Sanders et al., 2015; Skotte 2017).

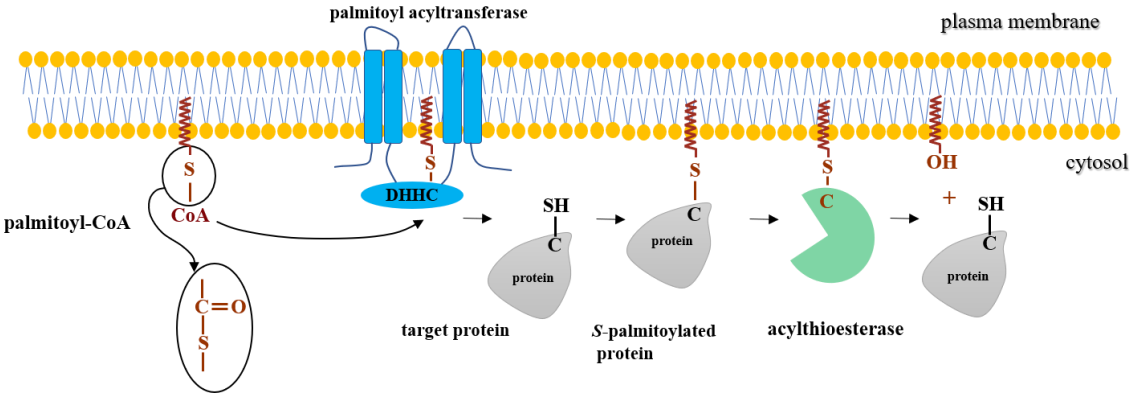

Figure 1.3 Scheme of protein *S*-palmitoylation/depalmitoylation cycle in the plasma membrane. Palmitic acid is present in an "active" form as palmitoyl-CoA thioester. In the first step of the *S*-palmitoylation reaction, palmitic acid residue binds to the cysteine residue of the DHHC motif of the palmitoyl acyltransferase and next it is transferred to a cysteine residue of a target protein. The thioester bond between the palmitic acid residue and the cysteine residue can be cleaved by acylthioesterases. The thioester bond is shown in detail in the circle on the left side of the scheme and is simplified in *S*-palmitoylated proteins.

Protein depalmitoylation is catalyzed by acyl-protein thioesterases (APTs) and palmitoyl protein thioesterases (PPTs), the latter found in lysosomes and involved in protein degradation (Verkruyse and Hofmann, 1996). On the other hand, APT1 and APT2 can participate in the depalmitoylation of *S*-acylated proteins at the cytosol/membrane interface, allowing them to be cyclically de- and repalmitoylated. Both mammalian APT1 and APT2 are *S*-palmitoylated which enhances their reactivity toward membrane-bound substrates (Vartak et al., 2014). For example, *S*-palmitoylated APT1 is anchored in the plasma membrane where it can deplamitoylate H-Ras; after auto-depalmitoylation, APT1 redistributes to the Golgi apparatus where undergoes re-palmitoylation together with the H-Ras (Kong et al., 2013). The development of APT1/2 inhibitors opened a new chapter in understanding the roles of these APTs. However, inhibition or knockdown of APT1/2 did not impair palmitate turnover on PSD-95 and N-Ras proteins, unlike the α/β-hydrolase domain 17 (ABHD17) family of proteins, which were thus discovered as depalmitoylating enzymes (Lin and Conibear, 2015).

1.7 Methods of detection of protein palmitoylation

Historically, studies of protein palmitoylation were challenging due to the lack of prompt, effortless and accurate assays. The most often used approach was based on metabolic labeling of proteins with radiolabeled palmitic acid (the most common (^{3}H)-palmitic acid) with subsequent immunoprecipitation of the protein of interest, gel electrophoresis and exposure of gels to X-ray films to detect the autoradiography (Veit, 2008). Notably, this

method is not only time-consuming and potentially hazardous but also moderately sensitive. New possibilities have emerged with the development of click chemistry and acyl-biotin exchange (ABE) reactions for the detection of palmitoylated proteins. In combination with other techniques such as mass spectrometry, they have become indispensable tools for high-throughput analyses of protein palmitoylation and the identification of new palmitoylated proteins.

The first approach, click-chemistry, utilities a highly specific reaction between the azide group of a reporter tag (e.g., biotin, a fluorescent dye) with the alkyne group present at the ω carbon of a fatty acyl chain such as the commercially available palmitic acid analogue, 17-octadecynoic acid (17ODYA). Notably, in the first step of the procedure, living cells are incubated with the fatty acid analogue which is internalized, converted into palmitoyl-CoA and can be used for protein palmitoylation (Charron et al., 2009; Martin and Cravatt, 2009; Martin, 2013). After this metabolic labeling, cells are lysed and the lysates are subjected to the „click reaction" (a copper-catalyzed 1,3-dipolar cycloaddition). Labeled proteins can be identified due to the gained fluorescence or can be adsorbed on streptavidin-coated beads and analyzed by mass spectrometry. This advanced technique allowed to collect data on global profiles of protein palmitoylation in various cells, including dendritic cells and macrophage-like Raw264 cells (Chesarino et al., 2014; Sobocińska et al., 2018a). The latter analysis was performed in our laboratory and revealed the influence of LPS on the cellular palmitoylome (Sobocińska et al., 2018a). An advantage of this approach is its ability to reveal the dynamics of protein palmitoylation. Thus, pulse-chase metabolic labeling of cells in combination with the click chemistry revealed Lck palmitate turnover upon T cell activation (Zhang et al., 2010). However, the click chemistry-based approach does not identify the type of palmitoylation (*S*-, *O*- or *N*-palmitoylation). Without sophisticated modifications, it cannot be used to detect protein palmitoylation in tissues.

The second approach, ABE, is more technically demanding and detects *S*-acylation exclusively. Its main steps include cell lysis, blocking of free thiol groups in proteins by alkylation, cleavage of thioester bonds between fatty acid and cysteine residues with hydroxylamine and substitution of the fatty acid residues with a thiol-reactive biotin derivative (biotin-HPDP). Biotinylated proteins are captured on streptavidin-coated beads. Finally, the captured proteins are released from the beads and detected by immunoblotting or subjected to mass spectrometry analysis. Several modifications of this technique have been developed such as acyl-RAC. It differs by direct binding of proteins to a resin containing sulfhydryl-reactive groups (Drisdel et al., 2006; Forrester et al., 2011). Using the ABE technique Roth

and colleagues performed the first proteomics study of *S*-acylated proteins in yeast (Roth et al., 2006). The limitations of ABE result from the hydroxylamine treatment which cleaves the ester bond between the fatty acyl chain and cysteine regardless of the species of the fatty acid, therefore, ABE does not discriminate between various types of *S*-acylation. ABE will also select proteins bearing thioester linkage with compounds other than fatty acids, like ubiquitin in E2 ubiquitin ligases. Moreover, sometimes hydroxylamine treatment is insufficient to reveal the lipidation, as in the case of junction adhesion molecule C (Aramsangtienchai et al., 2016). On the other hand, since ABE does not rely on metabolic labeling of cells which can pose a stress condition, it is a really powerful technique for identifying *S*-palmitoylated proteins. In addition, taking into account the high frequency of *S*-palmitoylation compared to other *S*-acylations, most of the proteins detected with ABE bear this modification. Nowadays, ABE is widely used for proteomic profiling of *S*-acylated proteins, e.g., in Raw264 cells and immortalized B cells and also in tissues (Merrick et al., 2011; Ivaldi et al., 2012; Ziemlińska et al., 2021).

1.8 *S*-Palmitoylation of proteins involved in TLR signaling

An application of click chemistry and ABE to large-scale analysis of protein palmitoylation has shed light on *S*-palmitoylated proteins involved in innate immune responses. Among TLRs, TLR2, TLR5 and TLR10 are *S*-palmitoylated. TLR2 is *S*-palmitoylated on Cys609 localized close to the transmembrane fragment of the receptor. The modification affects cell surface localization of TLR2. Moreover, the Cys609 TLR2 mutant was not able to activate NFκB in response to microbial ligands (Chesarino et al., 2014).

Kim with colleagues has recently revealed that MyD88 is *S*-palmitoylated on two cysteine residues and the process is catalyzed by zDHHC6 and zDHHC13. *S*-palmitoylation of MyD88 on Cys113 was required for the binding of IRAK4 to MYD88 in LPS-stimulated cells. These results indicate that the MyD88-mediated signaling of TLRs can be connected with the fatty acid metabolism and suggest therapeutic targets for controlling sepsis (Kim et al., 2019).

The main pro-inflammatory cytokine – TNFα is *S*-palmitoylated and also ε-*N*-myristoylated. TNFα is synthesized as a transmembrane precursor (tmTNFα) that is *S*-palmitoylated on the juxtamembrane Cys30. This modification facilitates raft association of tmTNFα, it does not affect its proteolysis leading to the cytokine release, however, it indirectly modulates TNFα pro-inflammatory activity affecting the binding of TNFα to TNF receptor 1 (Poggi et al, 2013). On the other hand, the TNFα precursor that is ε-*N*-myristoylated on Lys19

and Lys20 accumulates in lysosomes and is degraded. Demyristoylation of tmTNFα is catalyzed by sirtuin 6 and allows its processing to mature TNFα (Jiang et al., 2013).

Our laboratory analyzed changes in protein palmitoylation induced by LPS. For this purpose Raw264 cells were metabolically labeled with 17ODYA, stimulated or not with 100 ng/ml LPS for 1 hour, lysed and 17ODYA-labeled proteins were next subjected to the click reaction with biotin-azide. After capturing on streptavidin-coated beads, proteins were identified by mass spectrometry. A comparison of proteins in unstimulated and LPS-stimulated cells revealed 154 palmitoylated proteins which were up-regulated after stimulation, 186 proteins down-regulated and 306 proteins that were not affected by the stimulation. The identified palmitoylated proteins were engaged in various cellular processes, and further detailed studies revealed 8 palmitoylated enzymes involved in the phosphatidylinositol cycle. This was in agreement with the importance of $PI(4,5)P_2$ for the TLR4 pro-inflammatory signaling, described above (Sobocińska et al., 2018b). Among up-regulated palmitoylated proteins was also flotillin-1. This attracted our attention due to the raft localization of flotillins and their involvement in signal transduction by plasma membrane receptors and also in the endocytosis of GPI-anchored proteins.

1.9 The structure and functions of flotillins

Flotillin-1 (reggie-2) and flotillin-2 (reggie-1) are widely expressed proteins of about 50 kDa encoded by two independent genes. They are found in the vast majority of living organisms, from bacteria to mammals, except for some nematodes and budding yeast (Edgar and Polak, 2001; Rivera-Milla et al., 2006). The history of flotillins began in 1997, when they were discovered by two independent groups. Lodisch's group identified these proteins in mouse lung tissue and named them "flotillins" because of the ability to "float like a ship" in the DRM fraction enriched in rafts and related caveolae (Bickel et al., 1997). The second name of flotillins - "reggies" - came from Stuermer's group which detected these proteins highly expressed in regenerating axons of goldfish retinal ganglion cells (Schulte et al., 1997).

Flotillins are conserved proteins with the same domain structure and 50% of protein sequence identity in the case of human proteins. They contain two domains of similar size – the SPFH domain and the flotillin domain which include several protein- and lipid-binding motifs as shown in Fig. 1.4. The SPFH domain was named after proteins that share this domain, including stomatin, prohibitin, flotillin and HflC/K.

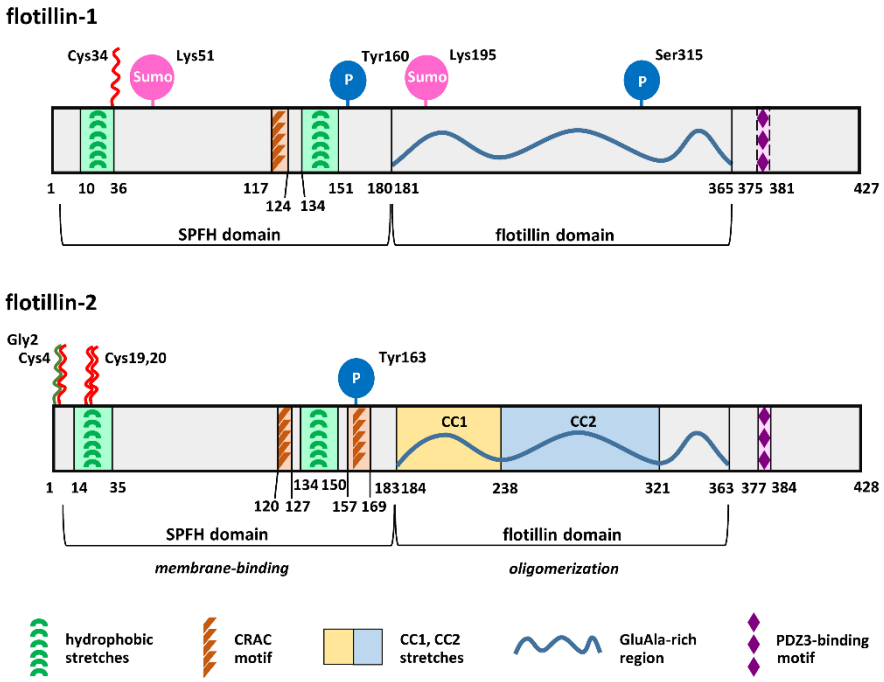

Figure 1.4 Schematical structure of human flotillin-1 and flotillin-2. *N*-myristoylation and *S*-palmitoylation are marked by green and red zigzags, respectively. CRAC motif, cholesterol recognition/interaction amino acid consensus; CC1, CC2, coiled-coil structure 1 or 2; PDZ domain, a domain present in PSD-95, Dlg, and ZO-1/2 proteins. Flotillin-1 has a less conserved PDZ3-binding domain than flotillin-2 (Rivera-Milla et al., 2006). Flotillin-1 and -2 are phosphorylated by Fyn kinase at Tyr160 and Tyr163, respectively, flotillin-1 is also phosphorylated at Ser315 by protein kinase C (Riento et al., 2009; Thalwieser et al., 2019). Flotillin-1, if not *S*-palmitoylated, is sumoylated by the E2 ligase UBC9 (Jang et al., 2019). From Kwiatkowska, Matveichuk et al. (2020).

Owing to the presence of the SPFH domain, flotillins bind to the cytosolic leaflet of the plasma membrane and endomembranes, including endosomes. The flotillin domain mediates homo- and hetero-oligomerization of flotillins. Membrane binding of flotillins is driven by their acylation, and also the interaction of hydrophobic stretches with sphingosine and the CRAC motif with cholesterol (Fig. 1.4). The acylation pattern differs between flotillins: flotillin-1 is *S*-palmitoylated at a single Cys34 while flotillin-2 is *N*-myristoylated at Gly2 and *S*-palmitoylated at three cysteines - Cys4, Cys19, and Cys20. The hydrophobic interactions of flotillins with membrane lipids and also *S*-palmitoylation (mainly in the case of flotillin-2) determine the association of flotillins with rafts (Neumann-Giesen et al., 2004). On the other hand, the differences in acylation suggest different regulations of the membrane/raft binding of flotillins. Indeed, depalmitoylated flotillin-1 dissociates from membranes while *N*-myristoylation of flotillins allows it to bind to membranes even in the absence of *S*-palmitoylation (Neumann-Giesen et al., 2004; Jang et al., 2015). zDHHC5 was detected as the palmitoyl acyltransferase which catalyzes *S*-palmitoylation of flotillin-2 and its ability to modify flotillin-1 was also suggested (Li et al., 2012).

Importantly, flotillins interact directly or indirectly with a great number of proteins, including filamentous actin, cadherins, γ-catenin, MPP1 from the MAGUK scaffolding protein family, and proteins involved in signaling cascades, like Lyn, Fyn, Lck tyrosine kinases, Gαq, MAP kinases, and plasma membrane receptors, like EGF receptor and insulin-like growth factor-1 receptor (IGF-1R), and others (the full list of protein partners of flotillins is found in our review Kwiatkowska, Matveichuk et al., 2020). Due to these interactions on the one hand, and the membrane binding on the other, homo- and hetero-oligomers of flotillins play the role of scaffolds enabling the assembly of multiprotein complexes involved in the functioning of plasma membrane receptors, the plasma membrane dynamics, and vesicular transport:

a) Signaling (EGF receptor clustering, phosphorylation and downstream signaling, sorting and lysosomal degradation; internalization of TLR3 ligand; TCR raft association and recycling; IGF-1R anterograde transport and signaling). (Amaddii et al., 2012; Fork et al., 2014; Jang et al., 2015; Redpath et al., 2019).
b) Endocytosis (GPI-proteins, amyloid precursor protein; proteoglycans e.g. syndecan-1, leucine-rich amelogenin peptide, fluid-phase uptake). (Stuermer et al., 2001; Glebov et al., 2006; Riento et al., 2009; Fekri et al., 2019).
c) Protein trafficking (recycling of AMPA receptor, MT1-MMP metalloproteinase, TCR, dopamine transporter, E-cadherin) (Cremona et al., 2011; Bodrikov et al., 2017; Planchon et al., 2018).
d) Cytoskeleton remodeling (axon regeneration, filopodia formation, cell spreading) (Neumann-Giesen et al., 2004, 2007; Munderloh et al., 2009).

Flotillins are also enriched in extracellular vesicles (EVs) involved in intercellular communication. Due to the presence of the CRAC motifs, flotillins contribute to the recruitment of cholesterol to multivesicular bodies and the subsequent secretion of this lipid in EVs. Also, flotillin-1 and flotillin-2 could modulate the content of caveolin-1 and annexin-2 in EVs (Strauss et al., 2010; Phuyal et al., 2014).

Recent studies show that *S*-palmitoylation of flotillin-1 at the single Cys34 allows the protein to perform some functions independently of flotillin-2. These activities include regulation of the transport of IGF-1R from the endoplasmic reticulum to the plasma membrane (Jang et. al., 2015) and the translocation of non-palmitoylated flotillin-1 to the nucleus for upregulation of the Snail transcription factor (Jang et al., 2019).

An increased level of flotillins was found in many types of cancers (tumors), including prostate and breast cancers. A recent meta-analysis revealed that elevated flotillin-1 and/or -

2 (immunocytochemical staining of samples) are poor prognostic factors for the survival of cancer patients (Deng et al., 2018). Flotillins' contribution to the development and progression of tumors is related to their scaffolding property and, e.g., sustained Erb2-Akt and IGF-1R-Akt signaling (Pust et al., 2013; Jang et al., 2015). Also, stabilization of the Snail transcription factor by flotillin-1 is crucial for the expression of genes required for epithelial to mesenchymal transition and metastasis of prostate and breast cancers (Jang et al., 2019; Genest et al., 2022). Flotillin-mediated recycling of MT1-MMP metalloproteinase facilitates degradation of the extracellular matrix by metastatic cells (Planchon et al., 2018). On the other hand, the detection of flotillins in blood samples is of diagnostic value for Alzheimer's disease – a reduced level of flotillins in exosomes isolated from serum is a marker of the disease (Zou et al., 2018).

Surprisingly, data on the contribution of flotillins to the signaling of TLRs are scarce. Flotillins are used as markers of rafts in immunohistochemical or biochemical analyzes, and their co-localization with TLR4 indicated the association of activated TLR4 with these plasma membrane domains (Dattaroy et al., 2016). Flotillin-1 can affect the caveolin-1 level in epithelial cells and the signaling of TLR3 which depends on caveolin-mediated endocytosis of TLR3 ligand (Fork et al., 2014). Depletion of stomatin-like protein-2, a member of the SPFH family, was found crucial for raft integrity in Raw264 cells thereby affecting TLR4 activation (Chowdhury et al., 2015).

In this work, I analyzed the involvement of flotillins in TLR4 pro-inflammatory activity. It was assumed that flotillins can affect this process due to their interplay with CD14, the raft protein assisting TLR4 activation by LPS.

2. Aims of the study

Flotillin-1 and flotillin-2 are ubiquitously expressed submembranous proteins which can associate with both the plasma membrane and endosomal compartments. Membrane-binding regions of flotillins include hydrophobic stretches and site(s) of acylation. Flotillin-1 is *S*-palmitoylated at a single cysteine residue while flotillin-2 is *N*-myristoylated and *S*-palmitoylated at three cysteines. Thanks to these structural features, flotillin-1 and -2 bind to the cytoplasmic leaflet of rafts, plasma membrane nanodomains rich in cholesterol and sphingolipids. On the other hand, flotillins undergo homo- and hetero-oligomerization and also interact directly and indirectly with numerous proteins. Therefore, flotillins can act as scaffolding proteins, facilitating the assembly of multiprotein submembrane complexes involved in various cellular processes.

The main aim of this study was to reveal the role of flotillins and their *S*-palmitoylation in TLR4 signaling triggered by bacterial LPS. TLR4 initiates a pro-inflammatory response aiming at the eradication of bacteria, but overreaction to LPS can lead to fatal sepsis. This fuels interest in molecular mechanisms of activation of macrophages by LPS. The rationale for undertaking the studies was: (1) results of our mass spectrometry analysis, which showed that the amount of palmitoylated flotillin-1 increased in LPS-stimulated Raw264 macrophage-like cells, suggesting its participation in LPS-triggered signaling; (2) a line of data indicating that flotillins are involved in clustering, endocytosis, and recycling of raft proteins. A typical raft protein is CD14 which assists activation of TLR4 by LPS.

I assumed that flotillins can affect LPS-induced signaling due to possible interaction with CD14, which could be facilitated by flotillin *S*-palmitoylation.

The specific objectives of this study included:

1. Generation of Raw264 cells stably depleted of flotillins to reveal the role of flotillins in LPS-induced signaling.

2. Assessing the influence of flotillins on CD14.

3. Identification of zDHHC(s) catalyzing *S*-palmitoylation of flotillins and determination of involvement of those palmitoyl acyltransferases in LPS-induced signaling.

4. Additionally, studies conducted in collaboration with Dr. Tomas Brdicka from the Institute of Molecular Genetics ASCR in Prague aimed at revealing whether OPAL1, an adaptor protein of leukocytes, is modified by *S*-palmitoylation.

3. Materials and methods

3.1 Cell culture

Experiments were performed on three macrophage-like cell lines: Raw264.7 and J774A.1 cells and immortalized bone-marrow-derived macrophages (IBMDM) and also on HEK293 cells transfected with plasmids encoding proteins of interest.

The line of Raw264.7 macrophage-like cells was established from a tumor-induced in a male mouse by intraperitoneal injection of Abselon leukemia virus and was purchased from the American Collection of Cell Cultures (ATCC). These cells were cultured in Dulbecco's Modified Eagle's Medium (DMEM; Sigma-Aldrich) containing 10% heat-inactivated (30 min, 56°C) fetal bovine serum (FBS, Life Technologies), 4.5 g/l glucose, 4 mM L-glutamine, 50 U/ml penicillin and 50 μg/ml streptomycin (5% CO_2, 37°C). Experiments were carried out on cultures passaged every 2-3 days (when the culture reached about 80% confluency) but no more than 17-20 times. For experiments, cells were mechanically detached from the plate surface with a stream of the culture medium, pelleted by centrifugation (300×g, 3 min, RT), resuspended in a fresh medium, counted and applied at an appropriate density to plates or dishes and grown overnight.

J774A.1 macrophage-like cells were originally obtained from a tumor of a female mouse strain BALB/c. The cells were purchased from ATCC and cultured in DMEM containing 10% heat-inactivated FBS, 1 g/l glucose, 4 mM L-glutamine, 50 U/ml penicillin and 50 μg/ml streptomycin (5% CO_2, 37°C). Cells were passaged and prepared for experiments as described above.

IBMDM cells were a kind gift from Dr. Jakub Siednienko from Hirszfeld Institute of Immunology and Experimental Therapy PAS, Wroclaw. They were cultured in DMEM with 10% FBS, 4.5 g/l glucose, 100 U/ml penicillin and 100 μg/ml streptomycin.

HEK293 (immortalized human embryonic kidney cells) were originally isolated in the 1970s by Alex Van der Eb, a Dutch biologist, whose postdoc Frank Graham transformed the cell line with sheared adenovirus 5. HEK293 cells (ATCC) were cultured as Raw264.7 cells and used for overexpression of selected proteins, as described in section *3.5.2 Cell transfection*.

All cells were stored in liquid nitrogen in 40% DMEM with L-glutamine, glucose and antibiotics described above, 50% FBS, and 10% DMSO.

In the following sections of this work, the cell line names Raw264.7 and J774A.1 are used in simplified versions as Raw264 and J774, respectively.

3.2 Stimulation of cells with LPS

Raw264 cells were seeded at 1.2 $\times 10^5$/well in 48-well plates (RT-qPCR) or at 1×10^6/6-cm dishes (click-chemistry, immunoblotting) or 0.6×10^5/well in 96-well MaxiSorp™ plates (Nunc, ELISA) and cultured overnight. For stimulation, cells were overlaid with fresh DMEM/10% FBS with antibiotics described above, supplemented with 10 or 100 ng/ml smooth LPS of *Escherichia coli* O111:B4 (List Biological Laboratories) and incubated for up to 6 h (5% CO_2, 37°C). The LPS solution was prepared according to the manufacturer's recommendations. Thus, LPS was dissolved in sterile water at a concentration of 1 mg/ml (10 min shaking, 37°C) and stored at 4°C. To prepare a working solution, LPS was warmed to room temperature (RT) and vortexed for 5 min, then diluted in DMEM/10%FBS to a concentration of 10 μg/ml and added to the medium at a desired final concentration.

In a series of experiments on protein palmitoylation, cells were preincubated with 250 μM bromopalmitic acid (BPA). BPA was prepared in the form of complexes with fatty acid-free bovine serum albumin (BSA, Sigma-Aldrich) at a 4:1 molar ratio (Kwiatkowska et al., 2003), as briefly described below:

- dissolving 2.6 mg of BPA in 125 μl of chloroform and methanol at a 1:1 ratio (v:v);
- supplementing the solution with 20 mg Celite 545 (SiO_2; Sigma-Aldrich), 10-min incubation at RT with few vortexing;
- drying Celite with adsorbed BPA under a stream of nitrogen;
- suspending Celite in 1 ml of a 2 mM defatted BSA solution (132 mg BSA/ml H_2O);
- incubation with stirring (1 h, RT);
- removal of Celite by centrifugation (15,000×g, 10 min, RT);
- filtering the supernatant with BPA/BSA complexes through a 0.22 μm filter;
- dilution of prepared BPA/BSA complex (8 mM BPA with 2 mM BSA) in DMEM with 2% charcoal-stripped FBS, 2 mM L-glutamine and 30 mM Hepes, pH 7.4, to a final concentration of 250 μM BPA.

In control samples, Celite was incubated with a mixture of BPA-free chloroform and methanol and processed as above. Cells were incubated with BPA for 1 h and next metabolically labeled with 17ODYA and stimulated with LPS (see section *3.6.1 Click chemistry with biotin-azide*). BPA was present at a concentration of 250 μM during cell labeling and stimulation.

3.3 Cross-linking of CD14 on the cell surface

CD14 was cross-linked on the surface of J774 cells (Fig. 3.1) essentially as described in (Płóciennikowska et al., 2015b). For this purpose, cells were seeded at 1×10^6/6-cm dishes, grown overnight in DMEM/10% FBS (5% CO_2, 37°C), and subjected to metabolic labeling with 17ODYA as described in section *3.6.1 Click chemistry with biotin-azide.* The next steps included:

- washing cells with ice-cold PD buffer; PD buffer was composed of 125 mM NaCl, 4 mM KCl, 10 mM $NaHCO_3$, 1 mM KH_2PO 4, 10 mM glucose, 1 mM $MgCl_2$, 1 mM $CaCl_2$, 20 mM Hepes, pH 7.4.
- incubation of cells with 1.6 µg/ml of rat IgG2a anti-CD14, clone Sa14-2 (BioLegend) or with control rat IgG2a in PD buffer (30 min, 4°C);
- washing cells with ice-cold PD buffer;
- incubation of cells with the $F(ab')_2$ fragment of donkey anti-rat IgG (Jackson ImmunoResearch) to cross-link CD14 (10 min at 37°C); to omit the cross-linking, a part of cells was incubated in PD buffer without this secondary antibody.

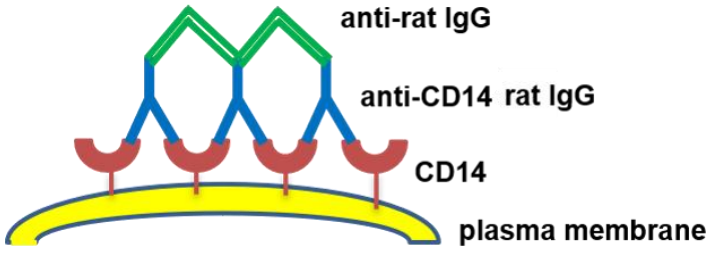

Figure 3.1 A scheme of CD14 cross-linking. CD14 was cross-linked on the cell surface of living J774 cells with a primary rat anti-CD14 IgG2a and a secondary anti-rat IgG, the $F(ab')_2$ fragment. Another set of cells was exposed to anti-CD14 only (without the secondary antibody). Controls included an application of rat IgG2a instead of rat anti-CD14 IgG2a or omitting the primary and the secondary antibodies.

Another variation of cross-linking conditions included incubation of cells with 1.6 µg/ml of rat IgG2a against CD14 for 30 min at 4°C or with PD buffer containing control rat IgG2a or in buffer without IgG (another control), followed by washing and incubation with anti-rat IgG or without IgG (control) (30 min at 4°C) and next warming of the cells for 10 min at 37°C. After cross-linking, cells were lysed, and lysates were subjected to click chemistry with biotin-azide, as described in section *3.6.1 Click chemistry with biotin-azide.*

3.4 Preparation of Raw264 cells with stably silenced *Flot2*

Raw264 cells were seeded at 1×10^4/well in 48-well plates. After 7 h, the cells were infected separately with 5 different lentiviral transduction particles (at MOI (multiplicity of

infection) = 1 or MOI=5) containing 5 different shRNA (Sigma-Aldrich) specific to mouse *Flot2* gene (NM_008028). Cells infected with non-mammalian shRNA transduction particles (Sigma-Aldrich; cat. No. SHC002V) served as a control. Cells were cultured in DMEM with 10% FBS and 4.5 g/l glucose, in the presence of 50 μg/ml streptomycin and 50 U/ml penicillin for 72 h. Then, 2 μg/ml of puromycin was added as a selection antibiotic. Every 2-3 days cells were passaged until the mortality of not infected cells reached 100% and simultaneously the survivability of cells transfected with shRNA was up to 100%. The efficiency of *Flot2* silencing was verified with RT-qPCR using primers specific to the mouse *Flot2* gene relative to *Tbp* (Table in the Section *3.6.11 RNA isolation and RT-qPCR analysis*). The reaction was carried out for the first time after 5-6 passages and was repeated 2 times in later passages. Cells selected with one type of shRNA are hereinafter referred to for simplicity as "clones", although they may have come from several different cells in which the shRNA sequence has integrated into genomic DNA at different sites. The sequences of shRNA applied to down-regulate flotillin-2 in Raw264 clones used in this study are shown in Table 3.1:

Table 3.1 shRNA sequences used for down-regulation of flotillin-2

Name of clone	Sequence 5'- 3'	cat. No.	Target sequence
1.1 or 1.5	CCGGCTCCCATGCCCTCACATTAATCTCGAGATTAAT GTGAGGGCATGGGAGTTTTTG	TRCN0000304813	3' UTR 175-194 bp
2.1 or 2.5	CCGGCTGACTGTAGAACAGATTTATCTCGAGATAAA TCTGTTCTACAGTCAGTTTTTG	TRCN0000304869	443-464 bp
3.1 or 3.5	GTACCGGACAGGGACAGCGAGAACATTTCTCGAGA AATGTTCTCGCTGTCCCTGTTTTTTTG	TRCN0000380359	3' UTR 63-83 bp
4.1 or 4.5	CCGGGCTTCACCATCAAGGATGTTTCTCGAGAAACA TCCTTGATGGTGAAGCTTTTTG	TRCN0000316514	517-539 bp
5.1 or 5.5	CCGGGCCTTCAAGTTCTACATGTATCTCGAGATACAT GTAGAACTTGAAGGCTTTTTG	TRCN0000109500	3' UTR 376-398 bp

In a series of experiments a clone of Raw264 cells depleted of diacylglycerol kinase-ε (DGKε) was used. The clone was obtained in the same way as described above by Dr. Aneta Hromada-Judycka from our laboratory.

3.5 Transfection of HEK293 and Raw264 cells

3.5.1 Expression plasmids

a) **OPAL1-Flag-Strep and OPAL1mut (**Outcome Predictor of Acute Leukemia 1)**:** The plasmid with the gene encoding mouse OPAL1 (isoform 2, NCBI reference sequence NP_666211.3) was a gift from Dr. Tomas Brdicka, Institute of Molecular Genetics AS (Chech Republic). The gene was cloned using the restriction enzymes AgeI and SalI into the pBABE

plasmid bearing ampicillin resistance gene. The protein had a 3xFLAG tag followed by a 2x Strep-tag at the C-terminus (pBABE-OPAL1). To generate the OPAL1 variant mutated at a potential *S*-palmitoylation site (pBABE-OPAL1mut), four point mutations were introduced into the OPAL1 sequence to change Cys into Ala (performed by ProteoGenixSAS, France). The following substitutions were introduced: Cys78Ala (T232G, G233C, C234T), Cys79Ala (T235G, G236C, C237T), Cys80Ala (T238G, G239C) and Cys82Ala (T244G, G245C, C246T).

OPAL1-Myc: The gene encoding OPAL1 was subcloned from the pBABE vector into the pcDNA3.1/Myc-His A vector (Invitrogen) using HindIII/XbaI restriction enzymes and the following primers bearing respective restriction sites: forward (5'-AACAAGCTTACCATGG AGAGGAGAAGGCTC-3'), reverse (5'-GAATCTAGAGCTCGGGGAGCCAC-3'). Next, the STOP codon was introduced after the Myc tag using site-directed mutagenesis and primers: forward 5'-CTCATCTCAGAAGAGGATCTGTAAATGCATACCGGTCATCATCAC-3", reverse 5'-GTGATGATGACCGGTATGCATTTACAGATCCTCTTCTGAGATGAG-3' (pcDNA-OPAL-Myc).

b) **Flotillin-1 and flotillin-2**: pCMV6-Entry-Myc-DDK plasmids encoding the mouse *Flot1* gene NM_008027 (cat. No. MR206823) and *Flot2* gene NM_001040403 (cat. No. MR222238) were ordered from OriGene (United States). Both proteins have a Myc tag followed by a FLAG tag at the C-terminus (pCMV6-Flot1 and pCMV6-Flot2).

c) **zDHHCs**: pEF-BOS plasmids encoding 23 mouse zDHHCs (alternatively called DHHCs, as described in Introduction, section *1.6 Enzymes catalyzing protein S-palmitoylation and depalmitoylation*) tagged with HA at the C-terminus were obtained from Prof. Masaki Fukata (National Institutes of Natural Science, Okazaki, Japan). In control samples, an empty plasmid pcDNA3.1/Hygro(+) (Invitrogen) was used instead of plasmids encoding zDHHCs (Fukata et al., 2006). The comparison of the DHHC and the zDHHC nomenclature together with GenBank accession numbers of all the enzymes are presented in the work of Ohno and co-workers (2012).

d) **wild-type CD14, CD14-VSVG, CD14-VSVGmut:** The pUNO-mCD14 plasmid encoding mouse CD14 was from InvivoGen. To generate CD14-VSVG fusion protein, the sequence encoding the GPI-anchor signal of CD14 (C-terminal 21 amino acids) was removed and the remaining part of the protein was fused at the C-terminus with the transmembrane and cytoplasmic fragments (49 C-terminal amino acids) of viral protein VSVG (G protein of vesicular stomatitis virus). For this, CD14 cDNA (devoid of the signal sequence) and VSVG cDNA were amplified by PCR using the pUNO-mCD14 and pCMV-VSVG (Addgene) as

respective templates. The two PCR products were ligated with pcDNA3.1/Hygro(+)-3xHA (Invitrogen) to add the HA tag at the C-terminus of the protein. Next, the obtained CD14-VSVG-3xHA fusion cDNA was amplified, purified and ligated with the pUNO1 vector yielding pUNO-CD14-VSVG used in experiments. CD14-VSVGmut was prepared by substituting Cys489 of the VSVG (*S*-palmitoylation site) with alanine by site-directed mutagenesis. The two plasmids were prepared by MSc Gabriela Traczyk from our lab, and details of the procedure, including primers used, are described in (Sobocińska et al., 2018b).

E. coli DH5α or TOP10 were transformed with plasmids described above, seeded in culture flasks in 50 ml of LB medium (10% peptone, 10%, NaCl, 5% yeast extract, pH 7.4) which contained a selective antibiotic (50 μg/ml kanamycin, 100 μg/ml ampicillin or 100 μg/ml blasticidin). The cultivation was carried out overnight with shaking at 37°C. Plasmids were purified using GenElute Endotoxin-free Plasmid HP Midiprep (Sigma-Aldrich) according to the manufacturer's instruction. The purity of obtained DNA was analyzed in Denovix (DS-11 series spectrophotometer) at λ= 230, 260 and 280 nm. The A260/A280 and A260/A230 ratios were in the range of 1.75-1.95. All plasmids were examined by sequencing (Genomed) and used for HEK293cell transfection.

3.5.2 Overexpression of proteins

Plasmids from a, d: HEK293 cells were seeded at 1×10^6/10-cm culture dish and grown overnight in DMEM/10% FBS (37°C, 5% CO2). DNA/FuGene HD (Promega) complexes were prepared in 500 μl of Opti-MEM (Life Technologies) at a ratio of 1 μg DNA: 3 μl FuGene HD (Promega) reagent. Cells were transfected with 1 μg of pBABE-OPAL1 or pcDNA-OPAL-Myc or pUNO-mCD14 or 6 μg of pBABE-OPAL1mut or pUNO-CD14-VSVG or pUNO-CD14-VSVGmut. Optionally, the amount of DNA was supplemented with an empty pcDNA plasmid to obtain 6 μg of DNA per sample, then 18 μl of FuGene HD was added to the mixture. After 15 min incubation at RT, the solution was added dropwise to the cell culture. After 24/48 h of transfection, the DNA was removed and cells were used for further experiences. The effectiveness of transfection was assessed by the immunoblotting technique.

Plasmids from b, c: HEK293 cells were seeded at 6×10^5/6-cm culture plates and grown overnight in DMEM/10% FBS (37°C, 5% CO2). pCMV6-Flot1 or pCMV6-Flot2 was mixed with pEF-BOS carrying a selected gene of zDHHC (23 genes tested). The two plasmids were used at a 1:1 ratio (200 ng of Flot1- or Flot2-plasmid and 200 ng of zDHHC-plasmid) or at a 1:3 ratio (200 ng of Flot1- or Flot2-plasmid and 200 ng of each of the three individual

zDHHC-plasmids. DNA/FuGene HD complexed were prepared in 250 µl of Opti-MEM (Life Technologies) at a ratio of 1 µg DNA: 3 µl FuGene HD reagent. After 24 hours of transfection, the DNA was removed and cells were used for further experiments. The effectiveness of transfection was assessed by the immunoblotting technique.

3.5.3 siRNA cell transfection

Raw264 cells were harvested by centrifugation (400×g, 10 min, RT), suspended at 1.2×10^5 in 300 µl of DMEM/10%FBS and transferred to 48-well plates. Then siRNA/Lipofectamine RNAiMAX (Invitrogen) complexes were prepared in 100 µl of Opti-MEM (Life Technologies) at a ratio of 40 pmol siRNA to 2 µl Lipofectamine RNAiMAX reagent. siRNA used are listed in Table 3.2 below. Cells were grown for another 18 h and used for further experiments. The effectiveness of gene silencing was assessed using qPCR.

Table 3.2 List of used siRNA

siRNA	Company	Catalog No.
zDHHC8	Qiagen	S101476
zDHHC5	Qiagen	S101476118
AllStars negative control	Qiagen	1027280

3.6 Analysis of protein palmitoylation with click chemistry

3.6.1 Click chemistry with biotin-azide

HEK293 cells were seeded at 6×10^5/6-cm culture plates, Raw264 and J774 cells at 1×10^6/6-cm culture plates and grown overnight in DMEM/10% FBS (37°C, 5% CO_2). To prepare 100 mM 17ODYA for cell labeling, 0.28 mg 17ODYA was dissolved in 10 µl DMSO and the solution was mixed with 2% charcoal-stripped FBS (Yount et al., 2011) at a 1:40 ratio (v:v) to allow forming complexes between 17ODYA and BSA. The mixture was sonicated in a water bath for 4 min (37°C), vortexed for 2 min, heated for 2 min at 37°C and all the steps were repeated 2 times. Then, the solution was diluted 50 times in DMEM containing 30 mM Hepes, pH 7.4, to a final concentration of 50 µM 17ODYA, 0.05% DMSO and 2% FBS. In the same way, a control solution containing 0.05% DMSO and 2% FBS was prepared. Cells were incubated with 50 µM 17ODYA or 0.05% DMSO for 1.5 or 4 h (37°C, 5% CO_2), subsequently were either left unstimulated or were stimulated with 100 ng/ml LPS which was added to the culture plates for 1h (37°C, 5% CO_2), as described in section *3.6.2. Stimulation*

of cells with LPS. 17ODYA-labeled J774 cells were subjected to cross-linking of CD14, as described in section *3.6.3. Cross-linking of CD14 on the cell surface*. After 17ODYA-labeling and stimulation/cross-linking, cells were washed two times with ice-cold phosphate-buffered saline (PBS), transferred to Eppendorf tubes and centrifuged (400×g, 5 min, 4°C). Pelleted cells were lysed in 640 µl of SDS buffer (4% SDS, 150 mM NaCl, 50 mM triethanolamine, pH 7.4, with 250 U/ml Benzonase (Sigma-Aldrich), EDTA-free protease inhibitor mixture (Roche), and phosphatase inhibitors (10 mM p-nitrophenyl phosphate, 1 mM Na_3VO_4, 50 mM phenylarsine phosphate)) and vortexed (15 min, RT). Then, the lysates were subjected to Cu(I)-catalyzed click reaction with biotin-azide. For this purpose, cell lysates were supplemented with 500 µM biotin-azide (Azide-PEG3-biotin conjugate, Sigma-Aldrich) in 1 mM Tris (2-carboxyethyl) phosphine hydrochloride (TCEP, Sigma-Aldrich), 100 µM Tris[(1-benzyl-1H-1,2,3-triazole-4-yl)methyl]amine (TBTA, Sigma-Aldrich) and 1 mM $CuSO_4$ (final concentrations), vortexed, and incubated for 1.5 h at RT in the darkness. To remove unreacted biotin, proteins were precipitated by adding four volumes of methanol, one volume of chloroform, and three volumes of H_2O with subsequent vortexing (Wessel and Flugge, 1984). Precipitated proteins were pelleted by centrifugation (10,000xg, 25 min, RT), washed once with methanol and air-dried for 5–10 min.

In a series of experiments on the incorporation of 17ODYA into CD14, proteins were precipitated with eight volumes of methanol (-20°C, 18 h), pelleted by centrifugation (9,000xg, 30 min, 4°C), washed twice with methanol (-20°C) and air-dried as above. Samples were also subjected to delipidation according to (Folch et al., 1957). For this, proteins precipitated with methanol were resuspended in 200 µl of 0.73% NaCl, sonicated, supplemented with 0.8 ml of chloroform:methanol (2:1, v:v), vortexed and supplemented with 9 ml of cold methanol. After 1 h (-20°C) precipitated proteins were collected by centrifugation (4,000xg, 50 min, 4°C) and air-dried as above.

Pelleted proteins were dissolved in 140 µl of the SDS buffer containing 10 mM EDTA and protein concentration was measured using Denovix (DS-11 series spectrophotometer). Equal amounts of total protein (most often 2 mg) were taken from each sample for further analysis. Protein solutions were diluted to 0.5% SDS with 1.2 ml of Brij buffer (1% Brij 97 (Sigma-Aldrich), 150 mM NaCl, 50 mM triethanolamine, pH 7.4, protease inhibitors (aprotinin, leupeptin, and pepstatin, 10 µg/ml each, and 1 mM PMSF) and phosphatase inhibitors, as above), supplemented with 0.2 ng/ml of in-house prepared biotinylated glutathione S-transferase (GST) - see the section *3.6.2 Purification and biotinylation of PFO-GST and GST*. A quantity of 20 µl was withdrawn from these solutions as input samples.

Biotin-tagged proteins were enriched on streptavidin-coupled agarose beads (25 µl per sample, ThermoFisher Scientific) during 1.5-h incubation (at RT with end-over-end rotation). The beads were washed extensively with 1 ml of 4 M urea in 10 mM Hepes, pH 7.4, (once for 1 min), 1 ml of 1% SDS in PBS (two times for 1 min) and 1 ml of PBS (two times for 1 min) and pelleted by centrifugation (400×g, 3 min). The procedure of washing the beads was selected in preliminary experiments described in Fig. 3.2.

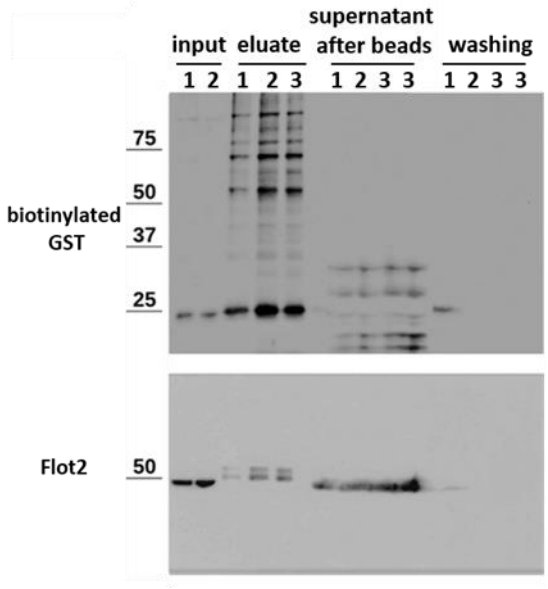

Figure 3.2 Variants washing the streptavidin beads. Various methods of washing streptavidin beads before the elution step were examined. For this, lysates of 17ODYA-labeled Raw264 cells (2 mg/ml protein concentration) supplemented with 0.2 ng/ml GST-biotin (input) were incubated with streptavidin beads, as described in the text, washed in 3 different solutions and subjected to protein elution. About 2 % of input cell lysate was loaded on the gel. The harshest washing of the beads (lanes 1) with 8 M urea, 10% acetonitrile, PBS+1%SDS, PBS, and H_20 (one washing with each solution) could lead to desorption of some proteins. Milder washing (lanes 2) included one wash with 4 M urea, two with PBS+1%SDS, and two with PBS and gave better results with no protein desorption. Similar results were obtained for the mildest type of washing (lanes 3), which included two washes with PBS+1%SDS and once with PBS, however, it could potentially leave some proteins bound unspecifically to streptavidin beads. Therefore, washing 2 was selected for further analyses.

After washing, biotinylated proteins were eluted from streptavidin beads according to the following procedure:

- adding 150 µl H2O and heating from 37°C to 70°C (~1 °C per 10 s), followed by shaking for 5 min at 70°C; centrifugation to collect supernatant;
- adding 150 µl H2O and heating from 50°C to 70°C (~1 °C per 10 s), followed by shaking for 5 min at 70°C (Holmberg et al., 2005); centrifugation to collect supernatant;
- adding 100 µl 2x SDS-sample buffer, followed by shaking for 5 min at 95°C; centrifugation to collect supernatant;
- adding 100 µl 2x SDS-sample buffer with 14% β-mercaptoethanol (Jenne and Famulok, 1999) and 5 mM EDTA, followed by shaking for 5 min at 95°C; centrifugation to collect supernatant;
- adding 100 µl H_2O, followed by shaking for 5 min at 95°C, centrifugation to collect supernatant.

All eluted fractions were combined and proteins were precipitated with 3.2 ml of 100% acetone (Sigma-Aldrich) at -80°C (30 min), air-dried and dissolved in 40 µl of 2x SDS-sample

buffer (5 min, 95°C). From 0.5% to 2% of input cell lysates were loaded on the gel along with eluted proteins. Samples were separated by SDS-PAGE, transferred to nitrocellulose (1 h, 400 mA) and proteins were detected by immunoblotting using selected antibodies as described in section 3.9. SDS-PAGE and immunoblotting.

3.6.2 Purification and biotinylation of PFO-GST and GST

The procedure of PFO-GST preparation included the following steps:

- transformation of *E. coli* BL21 with pGEX-4T-TEV-PFO plasmid carrying the gene encoding perfringolysine O with the GST tag (PFO-GST); this plasmid was obtained in our laboratory as described in Kulma et al. (2017);
- cell cultivation in 250 ml of LB medium (10% peptone, 10%, NaCl, 5% yeast extract, pH 7.4) with 100 μg/ml ampicillin (37°C, 2-3 h);
- adding IPTG when OD = 0.6, and cultivation overnight with shaking (18°C);
- collecting cells by centrifugation (5,000×g, 10 min, 4°C);
- washing cells with ice-cold PBS;
- cell lysis in 10 ml of the lysis buffer (4°C, 10 min); the lysis buffer contained 100 mM Na_2HPO4, 1 mM EGTA, 1mM EDTA, 5mM β-mercaptoethanol, 50 mM Tris, pH 8.0, 1 mM PMSF, 0.35 mg/ml lysozyme, 50 μl cocktail of protease inhibitors (Sigma-Aldrich).
- adding Triton-X-100 to the final concentration of 1%;
- sonication of lysates in an ultrasound homogenizer UP200S (15 min, 4°C, 33% amplitude, 0.3 cycle);
- centrifugation of lysates (18,000×g, 30 min, 4°C);
- purification of PFO-GST on Glutathione Sepharose 4B column (GE Healthcare) according to the manufacturer's instruction;
- elution of PFO-GST with 10 mM glutathione;
- analysis of quantity and purity of PFO-GST in column fractions with SDS-PAGE;

To obtain GST protein the following procedure was applied:

- cleavage of GST-PFO with TEV protease bound to the Glutathione Sepharose 4B column; TEV protease was expressed in *E. coli* BL21 (DE3)-RIL with plasmid pRK793 encoding TEV with His-tag (Adgene); TEV was purified by MSc Gabriela Traczyk on Ni-NTA agarose and used at 50 μg/ml;
- washing the column with buffer 1 containing 10 mM phosphorate buffer pH7.4, 150 mM NaCl, 1% Triton X-100, 5 mM DTT and buffer 2 containing 10 mM phosphorate buffer pH7.4, 150 mM NaCl, 5 mM DTT to remove PFO and TEV-protease;

- elution of GST with 10 mM glutathione;
- purification of GST in PD-10 desalting column (GE Healthcare);
- analysis of quantity and purity of GST in column fractions with SDS-PAGE.

PFO-GST and GST from the peak fractions were used for further experiments. Aliquots of both proteins were frozen in liquid nitrogen and stored at -80 °C.

The procedure of PFO-GST and GST biotinylation included the following steps:

- dilution of proteins to 2 mg/ml in 100 mM borate buffer, pH 8.8;
- incubation with sulfosuccimidylni-1-6-biotinamidohexanoate ester (Molecular Probes), which reacts with amino groups of proteins (20:1, w:w; 4 h, RT);
- separation of proteins from a free dye by gel filtration on Sephadex G-25 column (Pharmacia, Biotech);
- protein concentration measurements with the DeNovix DS-11 Series Spectrophotometer;
- protein biotinylation analysis with SDS-PAGE and immunoblotting with anti-biotin IgG-HRP (Fig. 3.3). In further experiments, biotinylated GST was used.

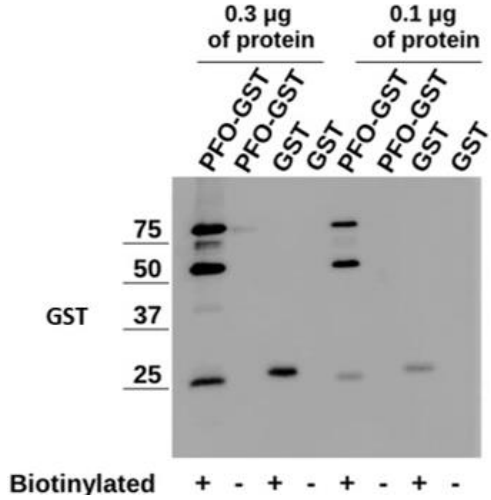

Figure 3.3 Biotinylated PFO-GST and GST. One of the critical steps in the click chemistry technique with biotin-azide is the elution of biotinylated proteins from streptavidin beads due to the strong biotin-streptavidin binding. To optimize this step, I prepared two different internal standards – biotinylated perfingolysin O-GST (PFO-GST) and biotinylated GST. Immunoblotting analysis with anti-biotin IgG-HRP showed that biotinylated PFO-GST easily degraded yielding 3 bands while biotinylated GST was stable and therefore biotinylated GST was used in further studies. It was added in equal amounts to each sample before its incubation with streptavidin beads. This allowed me to verify the accuracy of the subsequent recovery of biotinylated proteins from streptavidin beads.

3.6.3 Click chemistry on protein immunoprecipitates and in-gel fluorescence

HEK293 cells (6×10^5/6-cm cell culture plates per sample) were grown overnight in DMEM/10% FBS. Next, cells were transfected according to the procedure described in section *5.2 Cell transfection* with a plasmid encoding OPAL1-Myc. Cells were incubated for 1.5 h in 3 ml DMEM/2% charcoal-stripped FBS in the presence of 50 µM 17ODYA or 0.05% DMSO as described in section *3.6.1 Click chemistry with biotin-azide*.

To immunoprecipitated OPAL1-Myc the following procedure was applied:

- washing cells twice with PBS at 4°C;

- collecting cells in Eppendorf tubes, centrifugation (400×g, 3 min, 4°C);
- resuspending cells in 300 µl of lysis buffer (0.5% Nonidet P-40, 0.5% deoxycholate, 0.1% SDS, 100 mM NaCl, 50 mM phosphate buffer, pH 7.4, protease and phosphatase inhibitors described above, and protein thioesterase inhibitors (10 µM palmostatin, Merck, and 0.2 mM 1-hexadecanesulfonyl fluoride, Cayman Chemicals);
- incubation for 30 min at 4°C;
- centrifugation of lysates (16,000xg, 10 min, 4°C); at this stage, 20-µl aliquots were withdrawn from supernatants as input samples for SDS PAGE;
- diluting the remaining part of supernatants with two volumes of the lysis buffer without detergents;
- adding 30 µl of EZView Red agarose affinity gel bearing rabbit anti-c-Myc IgG (Sigma-Aldrich);
- incubation with end-over-end rotation (2 h at 4°C);
- washing the agarose beads (3 times) with ice-cold washing buffer (0.05% Nonidet P-40, 100 mM NaCl, 50 mM phosphate buffer, pH 7.4, protease, phosphatase, and protein thioesterase inhibitors described above);
- washing the beads with ice-cold washing buffer without detergents;
- collecting the beads by centrifugation (400×g, 5 min, 4°C);
- suspending the beads in 30 µl of ice-cold PBS containing EDTA-free protease inhibitor mixture and 1 mM PMSF.

The beads with bound proteins were subjected to the click reaction with a fluorescent tag IRDye 800CW. For this, the suspension of beads was supplemented with 1 mM TCEP, 100 µM TBTA, 1 mM CuSO4, and 10 µM IRDye 800CW-azide (LI-COR) (final concentrations). The reaction was carried out for 1 h in the darkness with gentle rotation. Then, the samples were washed as after immunoprecipitation and once in PBS, suspended in 30 µl of 1X SDS-sample buffer and heated at 95°C (5 min). Released proteins were separated by 10% SDS-PAGE, analyzed in an Odyssey CLx Imager (LI-COR), transferred onto nitrocellulose (1 h, 400 mA) and subjected to immunoblotting with mouse anti-Myc IgG.

3.7 Analysis of protein of *S*-palmitoylation with Acyl Biotin Exchange technique

HEK293 cells were seeded at 6 $\times 10^5$/6-cm culture plates and grown overnight in DMEM/10% FBS (37°C, 5% CO_2). On the next day, cells were transfected with plasmids encoding tested proteins, according to the procedure described in section *3.5.2 Cell transfection*. After 24 h, cells were washed twice with PBS (4°C), transferred to Eppendorf

tubes, centrifuged (400×g, 3 min, 4°C). Cell pellets were frozen in liquid nitrogen and stored at -80°C. For ABE, pelleted cells were lysed in 500 µl of SDS-Triton buffer (4% SDS, 1.7% Triton X-100, 150 mM NaCl, 5 mM EDTA, 50 mM Tris, pH 7.4, with 250 U/ml Benzonase and a cocktail of protease inhibitors (Roche)) and proteins were precipitated from the lysates with four volumes of methanol, one volume of chloroform, three volumes of H_2O with subsequent vortexing (Wessel and Flugge, 1984). Precipitated proteins were pelleted by centrifugation (3,000×g, 25 min, RT), washed once with methanol, air-dried for 5–10 min and dissolved in 400 µl of an SDS buffer (4% SDS, 150 mM NaCl, 5 mM EDTA, 50 mM Tris, pH 7.4) with subsequent measurement of the protein concentration with Bradford method (Bradford Ultra; Expedeon). The protein concentration was adjusted to 2 mg/ml in each sample. Next, the samples were supplemented with 5 mM TCEP to reduce protein disulfide bridges (15 min, 37°C with shaking) and with 20 mM methyl methanethiosulfonate (MMTS, Sigma-Aldrich) to block free protein thiol groups (20 min, 50°C with shaking). Proteins were precipitated three times with chloroform/methanol/water, pelleted and resuspended in 220 µl of 4% SDS buffer described above. At the next stage, samples were diluted 20 times with a buffer containing 0.2 mM biotin-HPDP (ThermoFisher), 0.2% Triton X-100 and 100 mM Hepes, pH 7.4, halved and supplemented either with hydroxylamine to a final concentration of 0.75 M (HXA+) or with a corresponding volume of 50 mM Tris, pH 7.5 (HXA-) and left for 1 h with end-over-end rotation. Then, biotinylation was stopped by three rounds of protein precipitation with methanol/chloroform/water. After the final solubilization in 170 µl in the 4% SDS buffer, protein concentration was measured using the Bradford method and small aliquots (20 µl) were withdrawn for SDS-PAGE analysis as input samples. The remaining part of each sample was transferred to a 5-ml Eppendorf tube, diluted 20 times with a buffer containing 150 mM NaCl, 0.2% SDS, 20 mM Hepes, pH 7.4, protease and phosphatase inhibitors, and supplemented with 30 µl of streptavidin-coupled agarose beads described above (end-over-end rotation, 2 h, RT). Agarose beads with bound proteins were washed four times by centrifugation (450×g, 2 min, RT) with the buffer containing 0.2% SDS described above. Finally, biotinylated proteins were eluted from beads using an agent that reduced the disulfide bond between the protein thiol group and biotin-HPDP. To do so, streptavidin-coated beads were suspended in 150 µl of buffer containing 1% β-mercaptoethanol (reducing agent), 150 mM NaCl, 0.2% SDS, 0.2% Triton X-100, 20 mM Hepes, pH 7.4, and heated with shaking for 15 min at 37°C, and after pelleting suspended in 100 µl 1X SDS-sample buffer for 5 min at 95°C. Eluates were combined and proteins were precipitated with 1 ml of cold 100% acetone (30 min, -80 °C) and pelleted by centrifugation (20,000xg, 20 min, 4 °C).

Proteins were dissolved in 2x SDS-sample buffer (5 min, 95°C with shaking), separated by SDS-PAGE, transferred to nitrocellulose (1 h, 400 mA) and analyzed by immunoblotting.

3.8 Detection and quantification of cytokines in culture supernatants

ELISA (enzyme-linked immunosorbent assay) is a plate-based assay technique that relies on the antibody-antigen interaction with subsequent colorimetric detection of this complex. Raw264 cells were seeded at 0.6×10^5/well in 96-well MaxiSorp™ plates (Nunc) in triplicate for each variant, grown overnight in DMEM/10% FBS and subsequently stimulated with 10 or 100 ng/ml LPS in 200 µl DMEM as described in section *2. Stimulation of cells with LPS*. Culture supernatants were collected after 2-6 h of cell stimulation and the levels of TNFα (Biolegend) and CCL5/RANTES (R&D Systems) were estimated by ELISA according to manufacturers' instructions. Detection was performed with a peroxidase substrate consisting of 50 µg/ml TMB/DMSO in 100 µl citrate buffer, pH 5.0, with the addition of 0.075% H_2O_2. The time of the TMB oxidation reaction varied from 5 to 20 minutes. The reaction was stopped by adding 100 µl of 2 M sulfuric acid. Measurements of the absorbance (color intensity) were performed in a Sunrise plate reader (Tecan) at $\lambda = 450$ nm and correction at $\lambda = 570$ nm. Cytokine concentrations were calculated based on a standard curve equation in Microsoft Excel. It was next normalized against protein content in cells determined by crystal violet staining (Józefowski et al., 2010). For this purpose, cells remaining on the plate after collecting the supernatant were incubated with 50 µl of 0.05% crystal violet in 20% methanol (10 min, RT). Then, the plate was washed with water, air-dried and crystal violet was extracted with 100 µl of methanol. The absorbance of samples was measured in the Sunrise plates reader at $\lambda = 595$ nm.

Alternatively, supernatants from triplicate samples for each variant were combined and examined using the mouse cytokine array panel A (R&D System). In this assay, profiles of secreted cytokines were quantified by their incubation with cytokine array membranes followed by immunoblotting performed according to the manufacturer's instructions. Immunoreactive dots were subjected to densitometric analysis in the ImageJ program and normalized against internal standards present on the membranes.

3.9 SDS-PAGE and immunoblotting

3.9.1 SDS-PAGE

Protein concentration in cell lysates was measured as described in section *3.10. Measurement of Protein concentration***.** In the case of immunoprecipitated proteins, equal volumes of samples containing proteins eluted from agarose beads with the sample buffer were applied to SDS-PAGE. Proteins were separated by 10% SDS-PAGE (at denaturing conditions of Laemmli 1970) in buffer containing 25 mM Tris, 192 mM glycine and 0.1% SDS. Protein separation was carried out in the Mighty Small II apparatus (Hoefer) at 120V. In a series of experiments with OPAL1 (in-gel fluorescence) electrophoresis was carried out at 4°C at 200 V. Prestained molecular weight standards were from BioRad.

3.9.2. Immunoblotting

The electrophoretically separated proteins were transferred from polyacrylamide gels onto nitrocellulose membrane (AppliChem) by the so-called wet transfer (Towbin et al., 1979). The transfer was performed in a buffer which consisted of 25 mM Tris, 192 mM glycine, 0.1% SDS and 20% methanol, and was carried out in a TE22 apparatus (Amersham Biosciences) for 18 h, at a constant current of 120 mA. After transfer, nitrocellulose membranes were washed once with H_2O and once with TBST buffer (150 mM NaCl, 0.05% Tween 20, 50 mM Tris, pH 7.6). Subsequently, membranes were incubated with 3% BSA/TBST for 1 h or with 5% skimmed milk/TBST for 1.5 h to block the excess protein-binding sites. To detect proteins, membranes were incubated for 1 h (RT) or overnight (4°C) with primary antibodies, and after washing (5×7 min, TBST) for 1 h with HRP-conjugated secondary antibodies. Immunoreactive bands were visualized with chemiluminescence using SuperSignal WestPico substrate (ThermoFisher Scientific) and analyzed densitometrically using the ImageJ program.

Table 3.3 List of used antibodies

Specificity of the antibody	Host	Company	Catalog No.
Primary antibody			
Flotillin-1 monoclonal IgG	Rabbit	Cell Signalling	#18634
Flotillin-2 monoclonal IgG	Rabbit	Cell Signalling	#3436
Jak1 monoclonal IgG	Rabbit	Cell Signalling	#3344
TNFα monoclonal IgG	Rabbit	Cell Signalling	#11948
HA-tag (HRP) monoclonal IgG	Mouse	Cell Signalling	#2999
DGKε polyclonal IgG	Sheep	R&D	# AF7069
zDHHC8 polyclonal IgG	Rabbit	Invitrogen	# PA5-110591
anti-eiF5A2 polyclonal IgG	Rabbit	Sigma-Aldrich	HPA029090

PAG polyclonal IgG	Rabbit	Exbio	11-409-C100
GST polyclonal IgG	Rabbit	Sigma-Aldrich	#G7781-25UL
Lyn polyclonal IgG	Rabbit	Cell Signalling	#2732
CD14 monoclonal IgG	Rat	BD Pharmingem	#553738
CD14 monoclonal IgG	Rabbit	Cell Signalling	#93882
TLR4 monoclonal IgG	Rabbit	Cell Signalling	#14358
Flag-tag monoclonal IgG	Mouse	Sigma-Aldrich	# F3165
anty-Myc monoclonal IgG	Mouse	Invitrogen	# R950-25
Actin monoclonal IgG	Mouse	BD Biosciences	# 612656
NFκB p65 XP monoclonal IgG	Rabbit	Cell Signalling	#8242
Phospho-IκBα monoclonal IgG	Rabbit	Cell Signalling	#2859
IRF3 monoclonal IgG	Rabbit	Cell Signalling	#4302
pIRF3 monoclonal IgG	Rabbit	Cell Signalling	#4947
CD14 (FITC) monoclonal IgG	Rat	eBioscience	#11-0141-82
Purified anti-mouse CD14	Rat	Biolegend	#123302
IgG2b	Rat	BD Pharmingem	# 553392
anti-biotin IgG-HRP	Goat	Sigma-Aldrich	# A4541
Secondary antibody			
anti-mouse IgG-HRP	Goat	Jackson ImmunoResearch	# 115-035-003
anti-rabbit IgG-HRP	Goat	Rockland, Calbiochem	# 611-1302
anti-rat IgG-HRP	Goat	Sigma-Aldrich	# 32160702
anti-sheep IgG-HRP	Donkey	Jackson ImmunoResearch	# 713-035-003

3.10 Determination of protein concentration

Protein concentration was measured by the DeNovix DS-11 Series Spectrophotometer which scans and measures protein absorbance at 280 nm. Alternatively, protein concentration was measured using the Bradford technique (Bradford, 1976) with Bradford Ultra dye (Expedeon). Measurements of sample absorbance were performed in a Sunrise plate reader (Tecan) at $\lambda = 595$ nm. Protein concentration was calculated based on the standard curve for BSA (5–25 μg/ml) and a standard curve equation in Microsoft Excel.

3.11 RNA isolation and RT-qPCR analysis

RNA was isolated from cells using a Universal RNA purification kit (EUR_x) and reverse-transcribed into cDNA using the High Capacity cDNA Reverse Transcription Kit (Thermo Fisher Scientific) according to the manufacturer's instructions. RT-qPCR analysis was performed in a StepOnePlus instrument using Fast SYBR Green Master Mix (Thermo Fisher Scientific). Primers (Genomed) used in experiments are shown in Table 3.4. The primers were designed by myself or by Dr. Aneta Hromada-Judycka or MSc Gabriela Traczyk from our laboratory. Prior to use, the efficiency of primers was checked by preparing a 5-point standard curve and further calculations in Microsoft Excel. All primers were constructed

according to primer design rules: lack of secondary priming sites, absence of dimerization capability, appropriate GC content, etc.

Table 3.4 List of used primers

Name of primer	Sequence 5'- 3'
Flot1_F	CCATCTCAGTCACGGGCATT
Flot1_R	GCAATCTCCGCCTCTGTCTT
Flot2_R	TGGCAAACTGGTCTCGGT
Flot2_F	TGGGCAAGAACGTACAGGAC
Tlr4_F	GCTTACACCACCTCTCAAACT
Tlt4_R	GTCTCCACAGCCACCAGATT
Cd14_F	CCAAGCACACTCGCTCAACT
Cd14_R	ATCAGTCCTCTCTCGCCCAA
Zdhhc5_F	CCGAGCCGAGGAAGATGAAG
Zdhhc5_R	CCAAGGGCAGTGATGGTCAA
Zdhhc8_F	TGGCATCCTCTTCCTCTTTGT
Zdhhc8_R	TCCTCCTTGTCCTCGTCCTC
Dgke_F	AGCCTAAACTGTGCGATTACA
Dgke_R	TTGGCGGGATGATGAGGTTTC
Ccl5_F	GCTCCAATCTTGCAGTCGTGT
Cccl5_R	CCATTTTCCCAGGACCGAGT
Tnfα_F	TGTCTCAGCCTCTTCTCATTC
Tnfα_R	TGAGGGTCTGGGCCATAGAAC
Hprt_R	GCCTCCCATCTCCTTCAT
Hprt_F	CAGTCCCAGCGTCGTGA
Tbp_R	GAGTAAGTCCTGTGCCGTAAG
Tbp_F	CAGAACAACAGCCTTCCACC

PCR conditions were the following: initial denaturation for 20 s at 95°C followed by 40 cycles comprised of denaturation for 3 s at 95°C and annealing/extension for 30 s at 60°C. Relative mRNA expression levels for investigated genes (in comparison to mRNA level for *Tbp or Hprt* gene, each variant run in triplicate) were calculated by the ΔΔCT method.

3.12 Flow cytometry

Raw264 cells were seeded at 1×10^6/well in 12-well culture plates and grown overnight in DMEM/10% FBS (37°C, 5% CO2). Cells were washed, suspended in ice-cold PBS, spun down and incubated in 2% mouse serum (Jackson ImmunoReserach) in PBS containing 0.01% NaN_3 (30 min, 4°C). The cell-surface CD14 was labeled using anti-mouse CD14 rat IgG2a conjugated with FITC (clone Sa2-8; eBioscience) for 30 min at 4°C (in the darkness). After that, cells were washed twice with cold PBS and fixed with 3% formaldehyde (15 min, RT). In control samples, the anti-CD14 IgG2a was omitted. After washing with PBS, cells were resuspended in PBS/0.01% NaN_3 and their fluorescence was determined with a Becton Dickinson FACS Calibur flow cytometer. FITC fluorescence was detected using a 530/30 nm

filter and an FL-1 detector. Cell debris was gated out by establishing a region around the population of interest on a Forward Scatter (FSC) versus Side Scatter (SSC) dot plot. Data were analyzed using BD CellQuest Pro software (BD Biosciences) and the amount of the cell surface CD14 was estimated based on the geometric mean of fluorescence intensity.

3.13 Data analysis

The significance of differences was calculated using Student's *t*-test in Microsoft Excel or, where indicated, with 2-way ANOVA and Scheffe's post hoc test. ANOVA tests were performed using the JASP software environment. Significance levels are provided in Figure legends.

4. Results

4.1 Detection of protein *S*-palmitoylation with click chemistry

Protein *S*-palmitoylation is a post-translational modification that often determines the cellular localization and functioning of proteins (Sobocińska et al., 2018a). There are two non-radioactive techniques available for its detection: one exploits so-called "click" chemistry and the second one is the ABE technique. I applied both of these techniques to follow the palmitoylation of proteins of interest. In the click-based technique, 17ODYA - palmitic acid functionalized with the alkyne group, was incorporated into living cells during 1.5 h – 4 h of incubation (Fig. 4.1). Control cells were incubated with DMSO, the 17ODYA carrier. One should bear in mind that fatty acid analogues can be used for *S*-acylation, but also for less frequent protein acylations, like *O*- and *N*-acylation (Sobocińska et al., 2018a), thus palmitoylation of a protein with 17ODYA does not reveal the nature of the chemical bond formed. In one variant of the click reaction, cells were transfected with a plasmid encoding a tagged protein (bearing, e.g., a Myc tag), then were incubated with 17ODYA and lysed in a buffer containing a non-ionic detergent, Nonidet P-40. The protein of interest was immunoprecipitated with an anti-tag antibody and subjected to the click reaction with an azide-derivative of a near-infrared dye a fluorescent dye IRDye 800CW-azide. During the click reaction, a triazole ring is formed between the dye azide group and the 17ODYA alkyne group. After separation of proteins with SDS-PAGE, the fluorescence of IRDye-azide bound to 17ODYA-alkyne, indicating a palmitoylated pool of the protein, was detected directly in a gel (Fig. 4.1, right side of the scheme).

This type of click technique is most suitable for detecting overexpressed, tagged proteins. For this reason, I developed its variation convenient for detecting endogenous proteins. In this variant of the procedure, the 17ODYA used for protein palmitoylation was detected by performing the click reaction with biotin-azide. Next, biotin-labeled proteins were enriched on streptavidin-coupled beads, according to a procedure used by us for mass spectrometry-based global profiling of palmitoylated protein in macrophage-like Raw264 cells prior to and after stimulation with LPS (Sobocińska et al., 2018b).

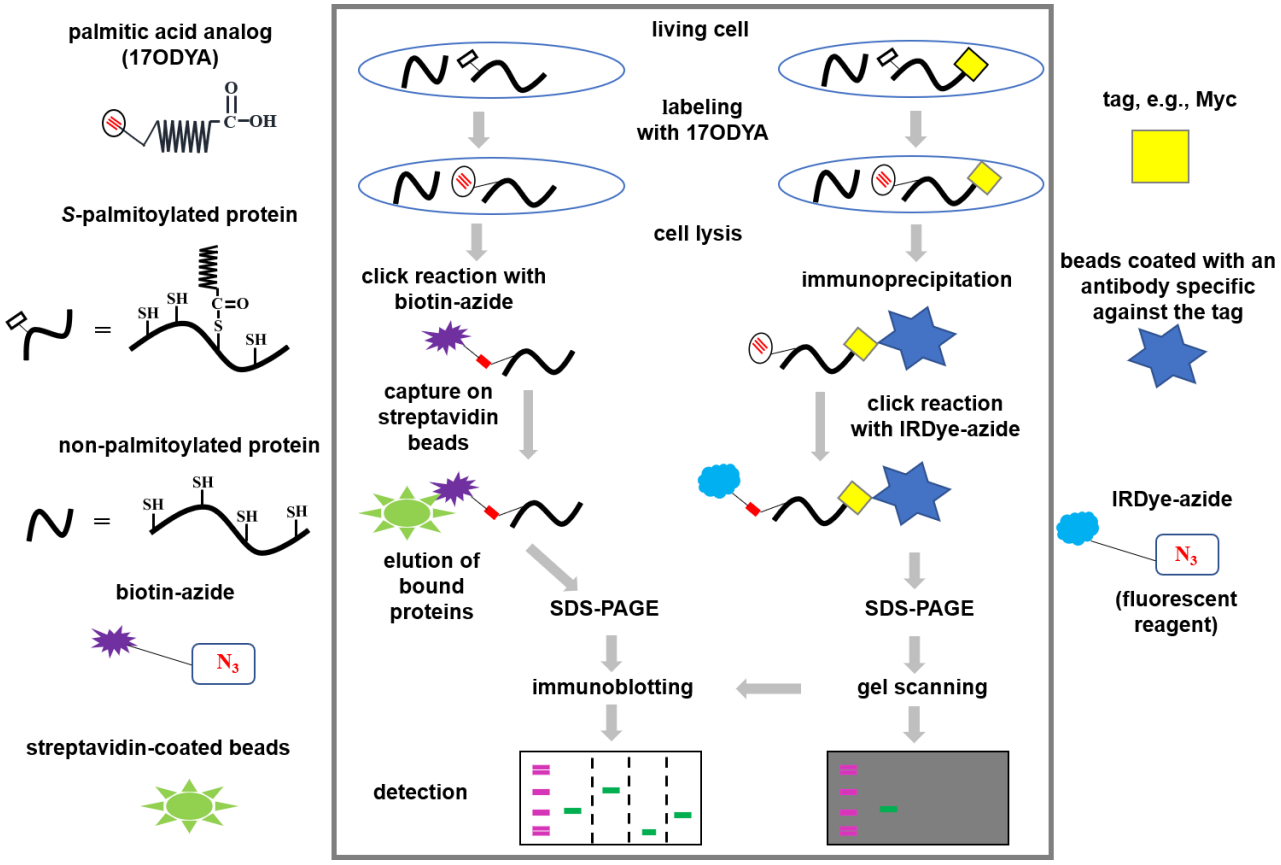

Figure 4.1. **Scheme of two procedures for detecting palmitoylated protein with the click reaction. Left side:** living cells were incubated in the presence of 17ODYA (50 μM,1.5 - 4 h, 37°C), which is an analogue of palmitic acid. Next, labeled cells were lysed and 17ODYA was detected by performing a click reaction in which the alkyne group of 17ODYA reacted with the azide group of a biotin derivative (biotin-N3). Labeled proteins were subsequently captured on streptavidin-coated beads, eluted, and analyzed by SDS-PAGE and immunoblotting. **Right side:** cells were transfected with a plasmid encoding a protein with a tag, like Myc, then labeled with 17ODYA, lysed and the overexpressed protein was immunoprecipitated with a specific antibody. Next, the click reaction was performed in which 17ODYA reacted with the azide group of a fluorescent dye (IRDye 800CW-N3). This dye generates a near-infrared fluorescent signal, therefore, the protein can be visualized in a gel. After the transfer of proteins to a nitrocellulose membrane, they can be detected by immunoblotting using an anti-tag antibody.

My goal was to elute captured proteins from streptavidin beads and identify them by immunoblotting. Since the biotin-streptavidin bond is very strong (Chivers et al., 2011), the elution of protein from beads was challenging. I found a combination of elution solutions containing H_2O and β-mercaptoethanol, as described in Materials and Methods, which allowed me to efficiently elute biotinylated proteins and analyze them using SDS-PAGE and immunoblotting with antibodies specific to proteins of interest (Fig. 1, left side of the scheme). Using this technique, it is possible to detect endogenous and also overexpressed palmitoylated proteins in cells, provided that specific antibodies for immunoblotting analysis are available. Additionally, I obtained biotinylated GST which was added to cell lysates before incubation with streptavidin beads, which served as an internal standard for protein elution efficiency. I used both click-based approaches to reveal palmitoylation of OPAL1 adaptor protein.

4.2 Detection of OPAL1 palmitoylation with click chemistry

OPAL1 is also known as WW domain-binding protein 1-like (WBP1L) and is broadly expressed in human and mouse leukocytes, including macrophages and lymphocytes. The interest in OPAL1 stems from fact that a high level of OPAL1 mRNA is a good prognostic marker in the treatment of a subset (about a quarter) of childhood acute lymphoblastic leukemia linked with the presence of ETV6-RUNX1 fusion protein (Chen et.al 2021). I took part in studies of Dr. Tomas Brdicka's group which aimed at revealing the biological functions of OPAL1 and some of its structural features that had been barely known at that time. OPAL1 is a transmembrane protein, its extracellular fragment is glycosylated while the cytoplasmic part of OPAL1, which contains several WW domain-binding motifs (L-P-X-Y or P-P-X-Y), interacts with NEDD4-family of E3 ubiquitin ligases (Fig. 4.2A). Studies of Brdicka's group indicate that OPAL1 binds and activates those enzymes which in turn catalyze ubiquitination and degradation of several proteins, including the CXCR4 receptor essential for the maintenance of hematopoiesis but is also likely to contribute to the development of leukemia. This OPAL1 activity can explain why higher *WBP1L* expression is a good prognostic in leukemia (Borna et al., 2020).

We noticed that OPAL1 contains a submembranous CCCVC motif (Fig. 4.2A) which can be a site of *S*-palmitoylation, as indicated by its similarity to *S*-palmitoylated motifs in other proteins (Sobocińska et al., 2018a). To verify this assumption, I overexpressed wild-type OPAL1 (OPAL1-Flag-Strep) in HEK293 cells and applied the click chemistry assay, described above. A brief scheme of these experiments is presented in Fig. 4.2B (panel C). After 24 h, cells were metabolically labeled with the palmitate analogue 17ODYA or exposed to DMSO, then cells were lysed, and lysates were subjected to the click reaction with biotin-azide and next supplemented with in-house prepared biotinylated GST.

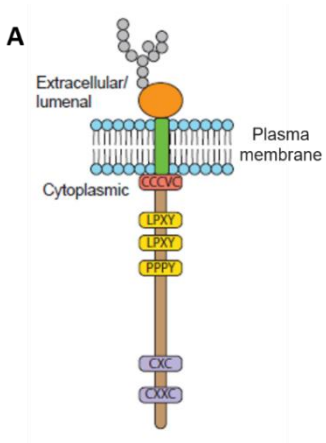

Figure 4.2 Analysis of OPAL1 palmitoylation using click chemistry. (A) Schematic representation of OPAL1 structure and its conserved sequence motifs. OPAL1 is a transmembrane adaptor protein with a very short extracellular/luminal part followed by a single transmembrane domain and a larger cytoplasmic tail. The extracellular/luminal part presumably forms a small compact domain held together by disulfide bridges formed between cysteine residues present in this part of the protein. Additionally, the extracellular part is glycosylated (grey circles). The cytoplasmic part of OPAL1 contains a submembranous CCCVC motif found here to be *S*-palmitoylated. There are also several motifs (LPXY or PPXY) potentially involved in intermolecular interactions via binding of the WW domain. The C-terminal part of OPAL1 contains CXC and CXXC domains which can potentially form intramolecular disulfide bridges. According to Borna et al. (2020).

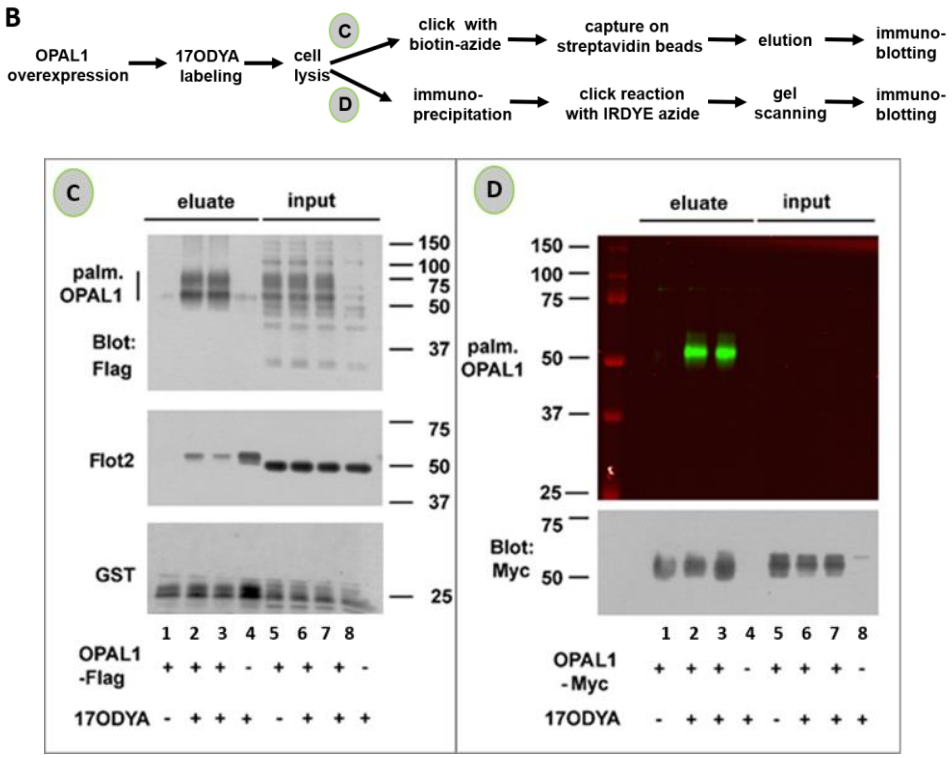

(B,C,D). Detection of palmitoylation of OPAL1. **(B)** Scheme of the procedure. HEK293 cells expressing OPAL1-Flag-Strep **(C)** or OPAL1-Myc **(D)** were labeled metabolically with 50 μM 17ODYA-or exposed to 0.05% DMSO carrier (- 17ODYA) for 1.5 h. **(C)** Lysates of cells expressing OPAL1-Flag-Strep and control cells transfected with empty vector (-OPAL1-Flag) were subjected to the click reaction with 500 μM biotin-azide. Biotin-tagged proteins were enriched on streptavidin-coupled beads, eluted, separated by SDS-PAGE and, after transfer to nitrocellulose, analyzed for the presence of overexpressed OPAL1 with mouse anti-Flag IgG (upper panel). For comparison, 2% of total cell lysate was also run as an input (lanes 5-8). Flotillin-2 was detected with rabbit IgG as a marker of endogenous palmitoylated proteins (middle panel). Visualization of GST-biotin (with rabbit anti-GST IgG) which was added to lysates(0.2 ng/ml) before incubation with streptavidin beads verified the efficiency of desorption of proteins from the beads (lower panel). Higher amounts of flotillin-2 and GST seen in the fourth lane (eluates) indicate that higher amounts of proteins were incubated with the beads in this control sample. **(D)** After lysis, OPAL1-Myc was immunoprecipitated with rabbit anti-Myc IgG and subjected to the click reaction with IRDye 800CW-azide which was visualized by in-gel fluorescence (upper panel, lanes 2-3). Cells transfected with empty vector (-OPAL1-Myc, lane 4) and cells incubated with 0.05% DMSO instead of 17ODYA (-17ODYA, lane 1) served as controls. The efficiency of immunoprecipitation of OPAL1-Myc was determined by immunoblotting with mouse anti-Myc IgG (lower panel). Results of one representative experiment of three are shown.

Biotin-tagged proteins were enriched on streptavidin-coupled beads, eluted, and analyzed by immunoblotting using anti-Flag IgG to detect OPAL1, anti-flotillin-2 IgG because flotillin-2 was used as an indicator of endogenous *S*-palmitoylated proteins, and anti-GST IgG.

It was found that OPAL1 was markedly enriched in samples derived from 17ODYA-labeled cells in comparison to control DMSO-treated ones (Fig. 4.2C, upper panel, lanes 2, 3 *vs*. lane 1) which indicated that OPAL1 was palmitoylated. A minute non-specific band was observed in cells transfected with an empty vector instead of the OPAL1-bearing one (Fig. 4.2C, upper panel, lane 4). Endogenous flotillin-2 was detected in all 17ODYA-labeled samples confirming the specific recovery of modified proteins (Fig. 4.2C, middle panel, lanes 2-4).

Immunoblotting analysis of GST verified the efficiency of desorption of biotinylated proteins from the streptavidin beads (Fig. 4.2C, lower panel).

The presence of the Strep-tag in the OPAL1-Flag-Strep protein could facilitate the binding of the protein to streptavidin beads regardless of its palmitoylation. This possibility was found unlikely owing to a negligible OPAL1 binding to the beads in samples not treated with 17ODYA, hence containing non-biotinylated OPAL1 (Fig. 4.2C, upper panel, lane 1). However, to verify OPAL1 palmitoylation, I obtained the OPAL1 construct tagged with the Myc tag instead of the Flag-Strep tag. OPAL1-Myc was overexpressed in HEK293 cells and cells were metabolically labeled with 17ODYA. After cell lysis, OPAL1-Myc was immunoprecipitated with an anti-Myc antibody and subjected to the click reaction with IRDye 800CW-azide. A scheme of this experimental approach is presented in Fig. 4.2B (panel D). Metabolic labeling of OPAL1 with 17ODYA followed by the click reaction with IRDye-azide was detected by in-gel fluorescence (Fig. 2D, upper panel, lanes 2, 3). The fluorescence was missing in control DMSO-treated samples and also in samples of control cells transfected with empty vector (Fig. 4.2D, upper panel, lanes 1 and 4, respectively). The efficiency of immunoprecipitation of OPAL1-Myc in all samples tested was confirmed by immunoblotting with an anti-Myc antibody (Fig. 4.2D, lower panel).

Taken together, obtained results show that OPAL1 is indeed labeled with 17ODYA which indicates that this protein is palmitoylated. To strengthen this conclusion, I transfected HEK293 cells with OPAL1-Flag-Strep in which all the cysteine residues in the CCCVC submembranous motif were substituted with alanine residues (Cys78Ala, Cys79Ala, Cys80Ala and Cys 82Ala). The mutated OPAL1 (OPAL1mut) was overproduced in HEK293 cells (Fig. 4.3, upper panel, lane 7), yet it was not recovered on streptavidin-coupled beads after metabolic labeling of the cells with 17ODYA and the click reaction with biotin-azide (Fig. 3, upper panel, lane 3), in contrast to wild-type OPAL1 (Fig. 4.3, upper panel, lanes 2 and 6). In control cells, transfected with empty vector or with OPAL1-Myc, no OPAL1 was detected with anti-Flag antibody, indicating the specificity of the detection of 17ODYA-labeled and biotinylated, hence palmitoylated, wild-type OPAL1-Flag-Strep (Fig. 4.3, upper panel, lanes 1 and 4). Flotillin-2 was detected in all 17ODYA-labeled samples and GST detection indicated that biotinylated proteins were recovered from streptavidin-coupled beads in comparable amounts in these samples (Fig. 4.3, middle and lower panels). In conclusion, the data indicate that OPAL1 is palmitoylated in the CCCVC motif. I verified these data using the ABE technique designed to detect *S*-palmitoylated proteins.

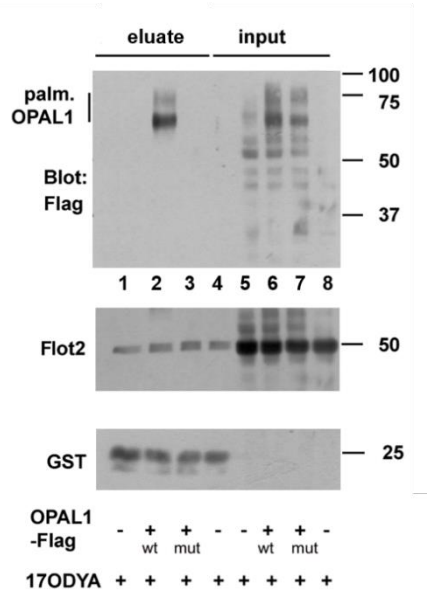

Figure 4.3. Analysis of palmitoylation of a mutated form of OPAL1 using click chemistry. HEK293 cells expressing OPAL1-Flag-Strep (lanes 2, 6), OPAL1mut (also containing the Flag-Strep tag) with the submembranous CCCVC motif substituted with AAAVA (lanes 3, 7), OPAL1-Myc (lanes 1, 5) and cells transfected with empty vector (lanes 4, 8) were metabolically labeled with palmitate analogue 17ODYA for 1.5 h. Lysates of cells were subjected to click reaction with biotin-azide. Biotinylated proteins were captured on streptavidin beads, eluted and analyzed by SDS-PAGE. The scheme of the experimental procedure is shown in Fig.1. Samples were analyzed with immunoblotting for the presence of OPAL1 with anti-Flag IgG (upper panel). For comparison, 2% of total cell lysate was also run as an input. Cells transfected with empty vector (lanes 4, 8) and cells transfected with OPAL1-Myc (lanes 1, 5) served as controls of Flag detection. Flotillin-2 was detected as a marker of endogenous palmitoylated proteins (middle panel). Visualization of GST-biotin which was added to lysates before incubation with streptavidin beads verified the efficiency of desorption of proteins from the beads (lower panel). Results of one representative experiment of two are shown.

4.3 Detection of protein *S*-palmitoylation with ABE technique

The search for non-radioactive methods of detecting *S*-palmitoylated proteins led to the development of the ABE technique, which exploits the reversible nature of this post-translational modification. Thus, the basics of the ABE technique come from the labile constitution of the thioester bond formed between the palmitic acid residue and the sulfhydryl group of the modified cysteine residue (Drisdel and Green, 2004). The thioester bond is cleaved upon hydroxylamine (HXA) treatment, thereby exposing a free sulfhydryl group at the palmitoylation site which can now react with a thiol-specific biotin derivative (biotin-HPDP).

Finally, biotinylated proteins are captured on streptavidin-coated beads and eluted with an agent cleaving the disulfide bond formed between biotin-HPDP and the modified cysteine (Drisdel and Green, 2004), and the proteins can be analyzed by SDS-PAGE and immunoblotting or processed for mass spectrometry. ABE selectivity requires thorough prior

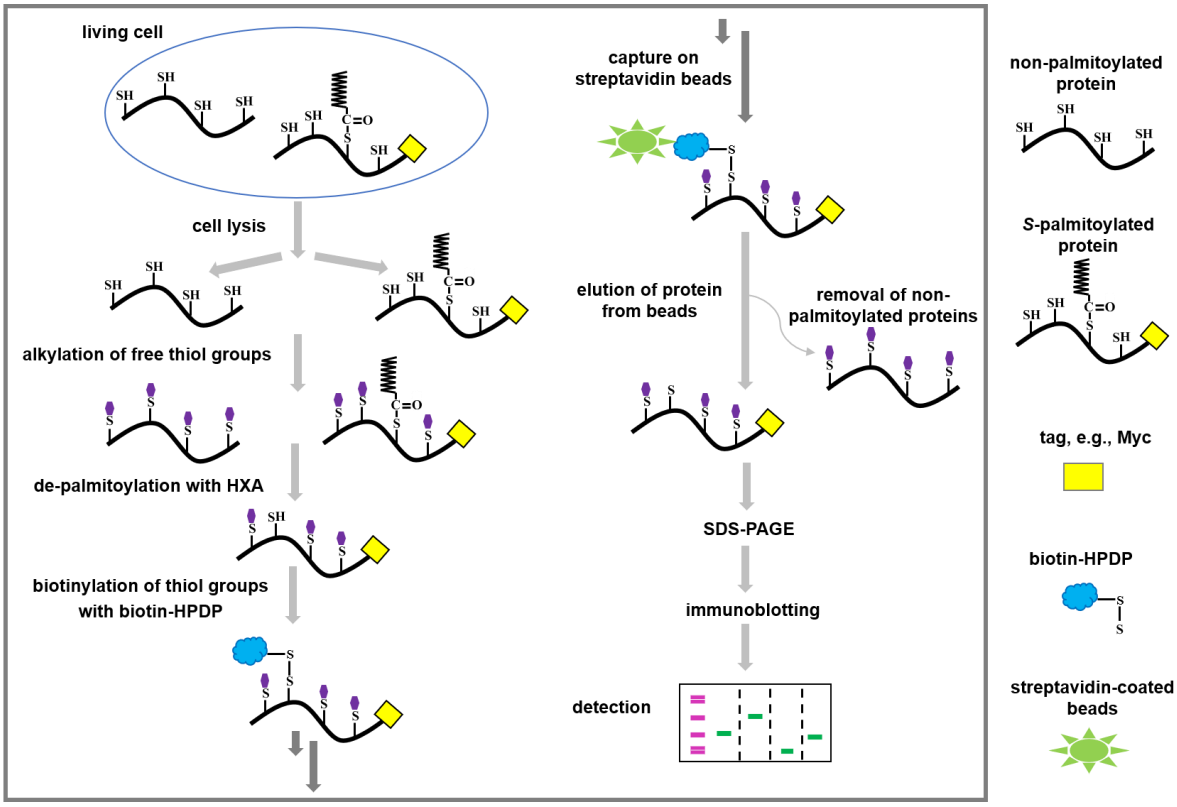

Figure 4.4. **Scheme of detection of *S*-palmitoylated proteins using acyl-biotin exchange (ABE) method.** Cells were lysed and free thiol groups of proteins were blocked by alkylation with, e.g., MMTS. Then, cleavage of thioester bonds leading to unmasking of the palmitoylated cysteine thiol groups was achieved with hydroxylamine (HXA) treatment. In the next step, the newly exposed thiol groups reacted with biotin-HPDP. Biotinylated proteins were subsequently captured on streptavidin-coated beads, eluted with an agent reducing the disulfide bond (e.g., DTT, β-mercaptoethanol), and analyzed by SDS-PAGE and immunoblotting. *S*-palmitoylation of both tagged overexpressed and endogenous proteins can be detected with this approach. An important control omitted the hydroxylamine treatment in the other half of each sample, to reveal non-specific biotinylation or streptavidin binding of proteins.

blocking of free sulfhydryl groups of proteins, which can be achieved by their alkylation, e.g., with MMTS. Tris-HCl is added to a portion of each sample instead of HXA as a control for biotinylation specificity (Fig. 4.2).

The disadvantage of the ABE technique is the detection of all *S*-acylations without distinguishing the nature of the fatty acid residue bound to a protein. The ABE procedure is also more technically demanding than the click chemistry assay (Sobocińska et al., 2018a). Nevertheless, the ABE technique is a robust instrument for detecting *S*-palmitoylated proteins which does not require metabolic labeling of cells with fatty acid analogues, therefore I used it to confirm *S*-palmitoylation of OPAL1.

4.4 Detection of OPAL1 *S*-palmitoylation with ABE technique

I performed ABE in lysates of HEK293 cells transfected with wild-type OPAL1-Flag-Strep and OPAL1mut-Flag-Strep (the latter with the mutated submembranous CCCVC motif described above). Wild-type OPAL1 was overproduced in cells (Fig. 4.5, upper panel, lanes 2, 6) and also recovered on streptavidin beads after treatment with HA but not in the control sample when the HXA treatment was omitted (Fig. 4.5, upper panel, lane 10 *vs.* 13). This control indicates that when the thioester bond between cysteine residue(s) and palmitate group was not cleaved, OPAL1 was not biotinylated and detected. In contrast, mutated OPAL1 which was overproduced in cells in comparable amounts to wild-type OPAL1 (Fig. 4.5, upper panel, lanes 3, 7) was hardly detected in the HXA-treated and -untreated samples (Fig. 4.5, upper panel, lanes 11, 14). Additionally, OPAL1 was not detected with anti-Flag antibody in control cells which were transfected with OPAL1-Myc (Fig. 4.5, upper panel, lanes 1, 5, 9) or with empty vector (Fig. 4.5, upper panel, lanes 4, 8, 12), indicating the specificity of the detection of biotinylated and *S*-palmitoylated wild-type OPAL1-Flag-Strep. Flotillin-2 used as a marker of endogenous *S*-palmitoylated proteins was found in all HXA-treated but not in HXA-untreated samples (Fig. 4.5, lower panel).

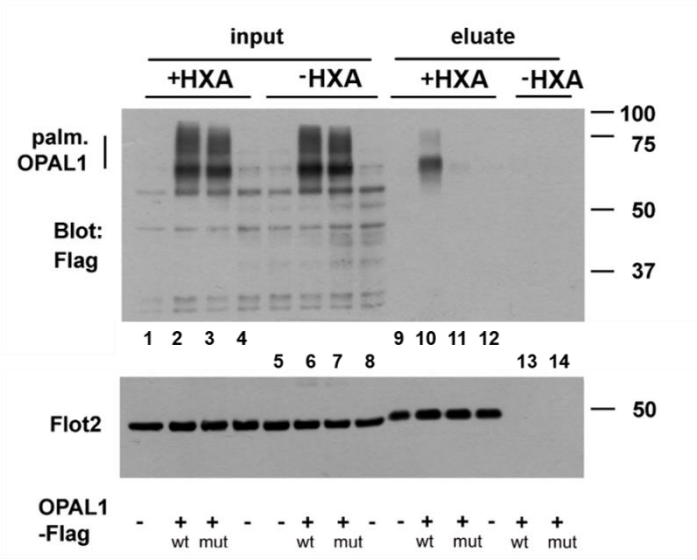

Figure 4.5. Detection of OPAL1 *S*-palmitoylation using ABE technique. HEK293 cells expressing wild-type OPAL1-Flag-Strep (lanes 2, 6, 10, 13), OPAL1mut-Flag-Strep (also containing the Flag-Strep tag) with the submembranous CCCVC motif substituted with AAAVA (lanes 3, 7, 11, 14), OPAL1-Myc (lanes 1, 5, 9) and cells transfected with empty vector (lanes 4, 8, 12) were lysed in buffer containing detergents (4% SDS, 1.7% Triton X-100) and subjected to next steps of the ABE procedure shown in Fig. 4. Acyl residues bound to proteins via thioester linkage were removed with hydroxylamine (+HXA, lanes 1-4, 9-12) yielding free cysteine residues that were previously acylated. These cysteine residues subsequently reacted with thiol-reactive biotin-HPDP, biotinylated proteins were captured on streptavidin beads and eluted (lanes 9-12). In control samples, the HA treatment was omitted (-HXA, lanes 5-8, 13-14). Samples were analyzed by SDS-PAGE and immunoblotting for the presence of OPAL1 with anti-Flag IgG (upper panel). Additionally, cells transfected with empty vector (lanes 4, 8, 12) and cells transfected with OPAL1-Myc (lanes 1, 5, 9) served as controls of Flag detection. Flotillin-2 was detected as a marker of endogenous *S*-palmitoylated proteins (lower panel). Results of one representative experiment of two are shown.

In conclusion, the results obtained with the click chemistry assay in combination with the ABE technique indicate that OPAL1 is *S*-palmitoylated in the CCCVC motif, although further studies are required to determine which cysteine(s) residue of the motif is modified. At present, the role of OPAL1 *S*-palmitoylation in its functioning in lymphocytes and macrophages also remains to be unraveled, and some propositions on this subject are considered in the Discussion.

In addition to my collaboration with Dr. Brdicka's Laboratory, I focused my studies on *S*-palmitoylation of macrophage proteins with an emphasis on proteins involved in their response to bacterial LPS, and the results of these studies are presented in the following part of this work.

4.5 Detection of palmitoylated proteins in Raw264 cells stimulated with LPS by click chemistry

LPS is a component of the outer membrane of Gram-negative bacteria. In macrophages it is recognized by the cell surface protein - CD14 - which transfers the LPS to MD2 protein associated with TLR4 triggering two pro-inflammatory signaling pathways (Poltorak et al., 1998). CD14 is anchored via its GPI moiety in the outer leaflet of the plasma membrane nanodomains rich in sphingolipids and cholesterol, named rafts (Płóciennikowska et al., 2015a). One of the mechanisms which control the association of intracellular proteins with rafts is their *S*-palmitoylation. Therefore, we reasoned that *S*-palmitoylated proteins can be crucial for the organization of signaling complexes at sites of CD14/TLR4 ligation with LPS. Indeed, our proteomic studies based on 17ODYA-labeling of Raw264 cells revealed 340 proteins whose palmitoylation was affected by the LPS stimulation, and *S*-palmitoylation of selected enzymes of the phosphatidylinositol cycle was found required for the LPS-induced signaling (Sobocińska et al., 2018b).

I performed a detailed immunoblotting analysis of palmitoylation of selected proteins from the Raw264 palmitoylome, focusing on raft proteins. A brief scheme of these experiments is presented in (Fig. 4.6A). Cells were metabolically labeled with 17ODYA or exposed to DMSO and stimulated with 100 ng/ml LPS for 1 h or left unstimulated. After lysis, the click reaction with biotin-azide was performed and next the lysates were supplemented with in-house prepared biotinylated GST. Biotin-tagged proteins were enriched on streptavidin-coupled beads, eluted according to the procedure described above, and analyzed by immunoblotting.

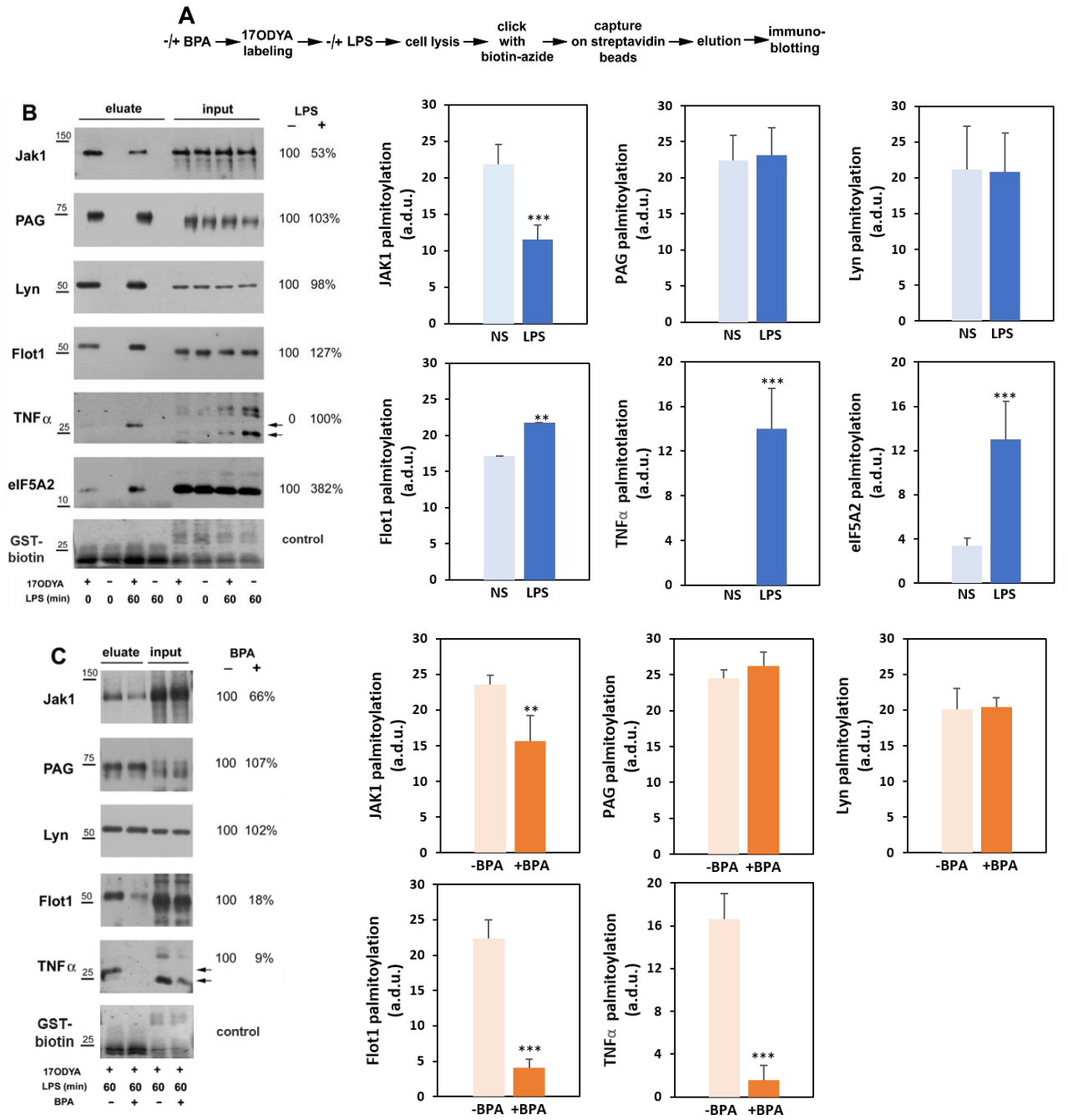

Figure 4.6. Palmitoylation of selected proteins in LPS-stimulated Raw264 cells. (*A*) Scheme of experimental procedure mirroring that shown in Fig.1 and including incubation of cells with 17ODYA (50 μM, 4h, 37°C) or 0.05% DMSO (-17ODYA), with or without LPS stimulation (100 ng/ml, 1h, 37°C in the 17ODYA presence) and finalized by elution of 17ODYA-labeled and biotin-tagged proteins from streptavidin beads and their separation by SDS-PAGE. In a series of experiments, cells were pretreated with BPA (250 μM, 1h, 37°C), labeled with 17ODYA and stimulated with LPS in the presence of the drug. **(*B, C*)** Immunoblotting analysis of palmitoylation of the indicated proteins in cells unstimulated (NS) and stimulated with LPS **(*B*)** and in cells untreated or treated with BPA and stimulated with LPS **(*C*)**. For comparison, 2% of total cell lysate (or 0.5% for eIF5A2 detection) was also run as an input. Positions of transmembrane TNFα precursor in inputs and eluates are indicated by arrows. It is seen that 17ODYA- and biotin-labeling decreased slightly migration of proteins in SDS-PAGE. The indicated set of proteins was usually detected in one nitrocellulose strip (taking advantage of their different migration in gels, or after stripping) for internal control of protein loading that was additionally verified by detection of biotinylated GST added to cell lysates prior to their incubation with streptavidin beads (the lowest panels in **B, C**). Molecular weight markers are shown on the left. Levels of palmitoylated proteins eluted from the beads were quantified by densitometry and normalized against GST-biotin; a.d.u, arbitrary density units. Data shown are mean ± s.d. from three experiments. **, ***, Significantly different at $p < 0.01$, and $p < 0.001$ from cells stimulated with LPS **(B)** or untreated with BPA **(C)**.

Thus, the amount of a protein detected in eluates reflected its palmitoylated pool prior to and after LPS stimulation, provided the elution was equally effective in all samples (as indicated by GST-biotin). As could be expected, LPS induced the production of TNFα, a major pro-inflammatory cytokine, which is synthesized as a transmembrane precursor (tmTNFα), and this protein was palmitoylated (Fig.4.6B). Indeed, the tmTNFα is *S*-palmitoylated at Cys30 located at the cytosolic boundary of its transmembrane fragment (Poggi et al., 2013). I also found that stimulation of cells with LPS markedly increased the amount of palmitoylated flotillin-1, the increase reached nearly 30% in comparison to unstimulated cells (Fig.4.6B). In contrast, in the case of two other well-known *S*-palmitoylated raft proteins, PAG adaptor protein (*S*-palmitoylated at juxtamembraneous Cys 39 and Cys42) and Lyn tyrosine kinase (*S*-palmitoylated at Cys3) no significant difference in palmitoylation was detected between unstimulated and LPS-stimulated cells (Fig.4.6B). Furthermore, the stimulation reduced by as much as 50% the amount of palmitoylated tyrosine kinase Jak1 (Fig. 4.6B). It has been found recently that Jak1 is *S*-palmitoylated at Cys541 and Cys542 (Ren et.al. 2013). The data were in full accord with our results on protein palmitoylation in Raw264 cells obtained with mass spectrometry (Sobocińska et al., 2018b). Finally, I analyzed palmitoylation of eukaryotic initiation factor 5A2 (eiF5A2) found highly upregulated in LPS-stimulated cells by the mass spectrometry analysis of Raw264 palmitoylome (Sobocińska et al., 2018b). eIF5A2 and eIF5A1 are two isoforms of an eukaryotic translation factor. These are the only known eukaryotic proteins containing an unique amino acid hypusine. My analysis confirmed that eiF5A2 was indeed palmitoylated and this eIF5A2 modification was highly upregulated in LPS-stimulated cells (Fig.4.6B). In view of a robust synthesis of proteins triggered by activated TLR4, these data suggest that palmitoylation facilitates eIF5A2 involvement in the translation of proteins engaged in immune responses of macrophages to LPS.

To study whether protein palmitoylation is essential in proinflammatory signaling pathways initiated by LPS, we used 2-bromopalmitic acid (BPA) which is considered an inhibitor of palmitoylation (Davda et al., 2013) but is also able to inhibit protein depalmitoylation (Pedro et al., 2013). To do so, Raw264 cells were treated or not with 250 μM BPA (1 h) and then stimulated with 100 ng/ml LPS (1 h) in the presence of this inhibitor. In these conditions, a considerable (exceeding 50%) reduction of LPS-induced cytokine production was observed (Sobocińska et al., 2018b). I found that BPA nonuniformly reduced palmitoylation of proteins. It did not affect palmitoylation of PAG and Lyn kinase, in contrast, it strongly reduced palmitoylation of flotillin-1, Jak1 and tmTNFα, in the latter case also affecting the total level of the protein found in input lysates (Fig.4.6C).

The above results pointed my interest toward flotillins due to their association with rafts (Kwiatkowska, Matveichuk et al., 2020) and possible interactions with CD14 (likely indirect since CD14 is anchored in the outer leaflet of rafts) that might be facilitated by flotillin-1 and flotillin-2 *S*-palmitoylation. Therefore my further studies concentrated on those proteins in LPS-stimulated cells.

4.6 Analysis of CD14 lipidation with click chemistry

Our mass spectrometry studies on LPS-induced protein palmitoylation in Raw264 cells revealed CD14 as a 17ODYA-labeled protein (Sobocińska et al., 2018b). This was surprising because CD14 has no transmembrane or intracellular fragment and is linked to the plasma membrane by the GPI anchor which precludes palmitoylation. To analyze the lipidation of CD14, I overexpressed the protein in HEK293 cells, incubated them with 17ODYA, subjected cell lysates to the click reaction with biotin-azide, and isolated biotinylated proteins as above (Fig. 4.7A). This technique is especially useful in detecting GPI-anchored proteins which are hard to be tagged at either N- or C-terminus without interfering with the proper synthesis of these proteins. This approach confirmed the incorporation of 17ODYA into CD14. However, the labeled protein constituted only a small fraction of the whole population of CD14 (Fig. 4.7B, left panel). Owing to the presence of a large hydrophobic pocket in CD14, which is located at the N-terminal part of the protein and binds LPS, we thought that 17ODYA can be trapped in the pocket. To test this assumption I added a delipidation step (Folch et. al., 1957) after the click reaction. Delipidation of samples did not eliminate the metabolic labeling of CD14 with 17ODYA, indicating that the lipid was covalently linked to the protein (Fig. 4.7B, left panel).

Then, to check whether palmitic acid can be incorporated in the GPI moiety of CD14, as described for alkaline phosphatase (Berger et al., 1998), I used a fusion construct of CD14: CD14-VSVG with removed 21 C-terminal amino acids constituting a signal sequence for attachment of the GPI moiety; this truncated CD14 was fused with the transmembrane and cytoplasmic fragment of viral protein VSVG (49 amino acids). Since this VSVG sequence has one cysteine residue, also CD14-VSVGmut was prepared, in which the cysteine was substituted with alanine. When the cysteine residue was present in the CD14-VSVG construct, high amounts of the protein were recovered from 17ODYA-labeled cells via the biotin-streptavidin binding regardless of delipidation, indicating intensive palmitoylation of the protein (Fig. 4.7B, middle panel).

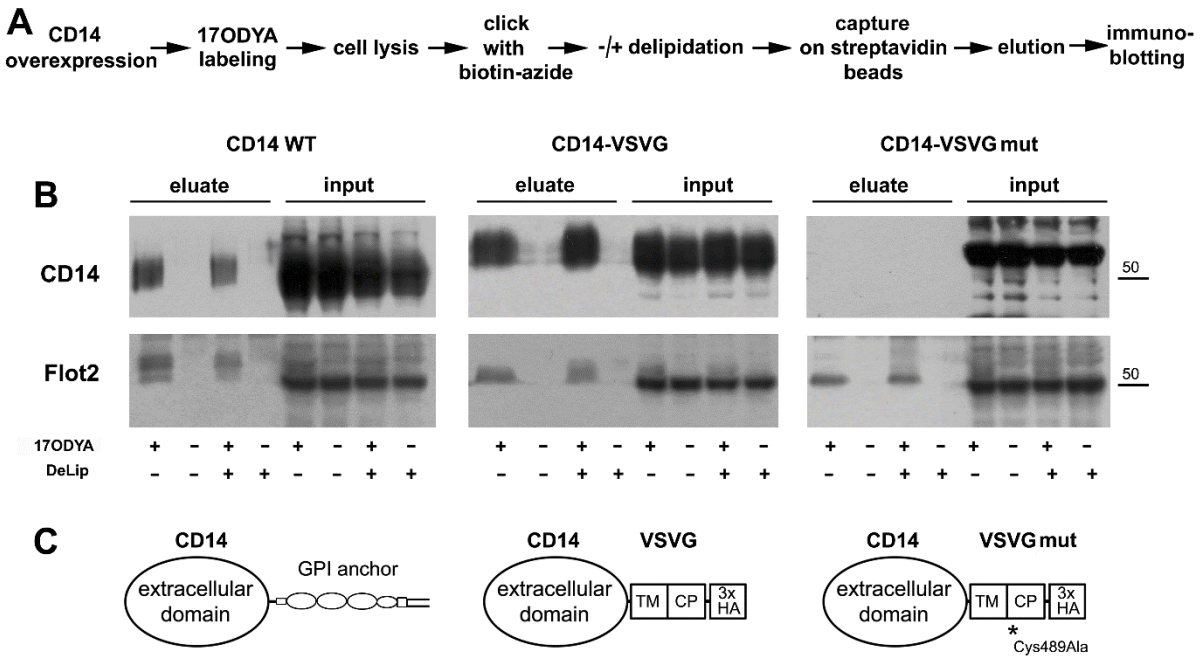

Figure 4.7 Lipidation of CD14. (**A)** Scheme of the procedure. Wild-type CD14 (WT), CD14-VSVG, or CD14-VSVGmut were expressed in HEK293 cells. Then cells were incubated in the presence of 17ODYA or exposed to DMSO carrier for 4h, lysed, and cell lysates were subjected to the click reaction with biotin-azide. Biotin-tagged proteins were enriched on streptavidin-coupled beads, eluted and separated by SDS-PAGE. A parallel set of samples was subjected to delipidation after the click chemistry reaction (DeLip). **(B)** After transfer to nitrocellulose, eluates/input lysates were analyzed for the presence of CD14 and flotillin-2. Since wild-type CD14 was not tagged, the protein was detected with an anti-CD14 antibody. **(C)** Structure of CD14 constructs. TM, CP, transmembrane and cytoplasmic fragments of VSVG, respectively. HA, HA tag. Results of one representative experiment of three are shown.

In contrast, no labeling of CD14-VSVGmut was detected (Fig. 4.7B, right panel). Flotillin-2 was used as a positive control for the recovery of palmitoylated proteins in all labeled samples.

Taken together, the data indicate, that during metabolic labeling of cells with 17ODYA, this exogenous palmitic acid analogue incorporates into the GPI anchor of CD14 which explains the proteomic data.

4.7 Expression of flotillin-2 dominates over flotillin-1 in Raw264 cells

To assess the role of flotillins in LPS-induced signaling I aimed at obtaining Raw264 cells with stably silenced expression of respective gene(s). RT-qPCR analysis indicated that the amount of flotillin-2 mRNA in Raw264 cells exceeded that of flotillin-1 about 4.7-fold. Also in J774 macrophage-like cells and in macrophages isolated from mouse peritoneum flotillin-2 mRNA prevailed over that of flotillin-1, 2.1- and 4.1-fold, respectively.

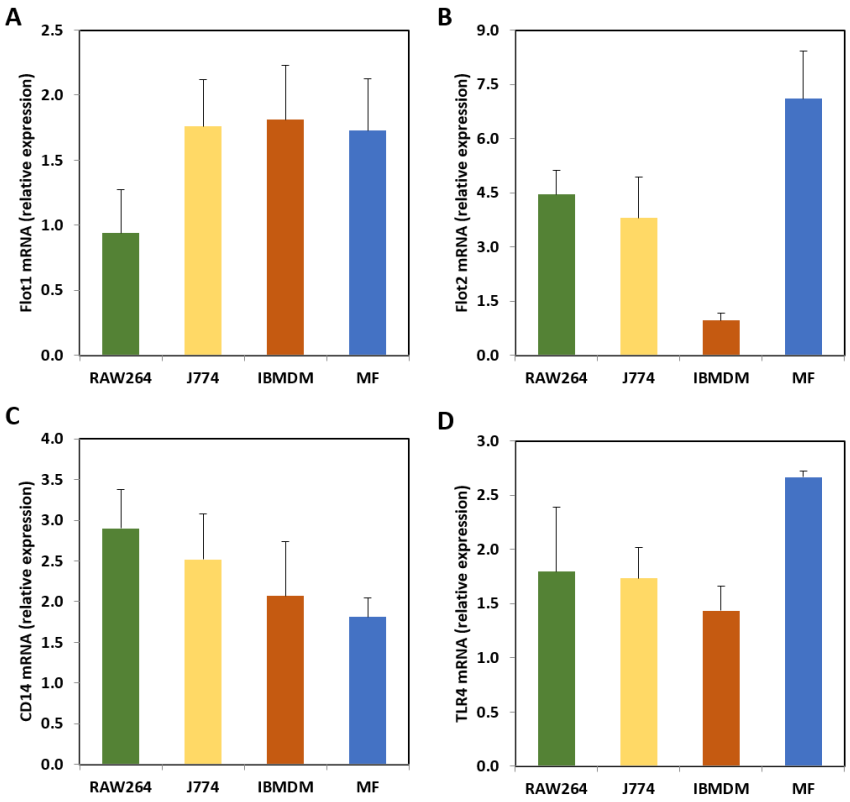

Figure 4.8 Comparative analysis of mRNA levels of flotillin-1, flotillin-2, CD14 and TLR4 in different cell lines. Analysis was performed using RT-qPCR. **(A,B,D)** *Flot1, Flot2, and Tlr4* transcripts were quantified relative to *Tbp* while **(C)** that of *Cd14* relative to *Hprt* due to comparable abundance of those transcripts. Data shown are mean ± s.d. from at least three experiments. MF – mouse peritoneal macrophages.

Only in IBMDM, a line of immortalized mouse bone marrow-derived macrophages, the expression of *Flot2* was low and flotillin-1 mRNA was 1.9-fold more abundant than flotillin-2 (Fig. 4.8A, B). Raw264 and J774 cells were relatively rich in CD14 mRNA in comparison to primary and immortalized macrophages (Fig. 4.8C). On the other hand, TLR4 mRNA level was highest in primary macrophages of all the cells tested (Fig. 4.8D). Interestingly, the relative ratio of CD14 mRNA *vs.* flotillin-2 mRNA was in a fairly narrow range of 0.25-0.66, except for IBMDM (ratio of 2.15).

Since the expression of flotillin-2 dominates over flotillin-1 in Raw264, I silenced the expression of *Flot2* in these cells and used them for studies on LPS-induced signaling.

4.8 Preparation of Raw264 clones depleted of flotillin-2 with shRNA

RNA interference has been widely used for gene silencing to study the cellular effects of the depletion of selected proteins. In my studies, I used short hairpin RNA (shRNA) enabling long-term silencing of the target gene. The delivery vehicles for shRNA to Raw264 cells were lentiviral constructs. After transfection of cells with lentiviral particles, the short

hairpin-coding sequence (after transcription to dsDNA) was integrated into the host genome, transcribed, shuttled from the nucleus to the cytoplasm and converted into RNAi degrading the target RNA, with the contribution of Dicer and the RISC complex formation.

To prepare clones of Raw264 cells depleted of flotillin-2, cells were transfected separately with 5 different lentiviral particles (bearing 5 different shRNA sequences) and one control shRNA (bearing a non-mammalian shRNA) at MOI=1 and MOI=5. The efficiency of *Flot2* silencing was verified with RT-qPCR.

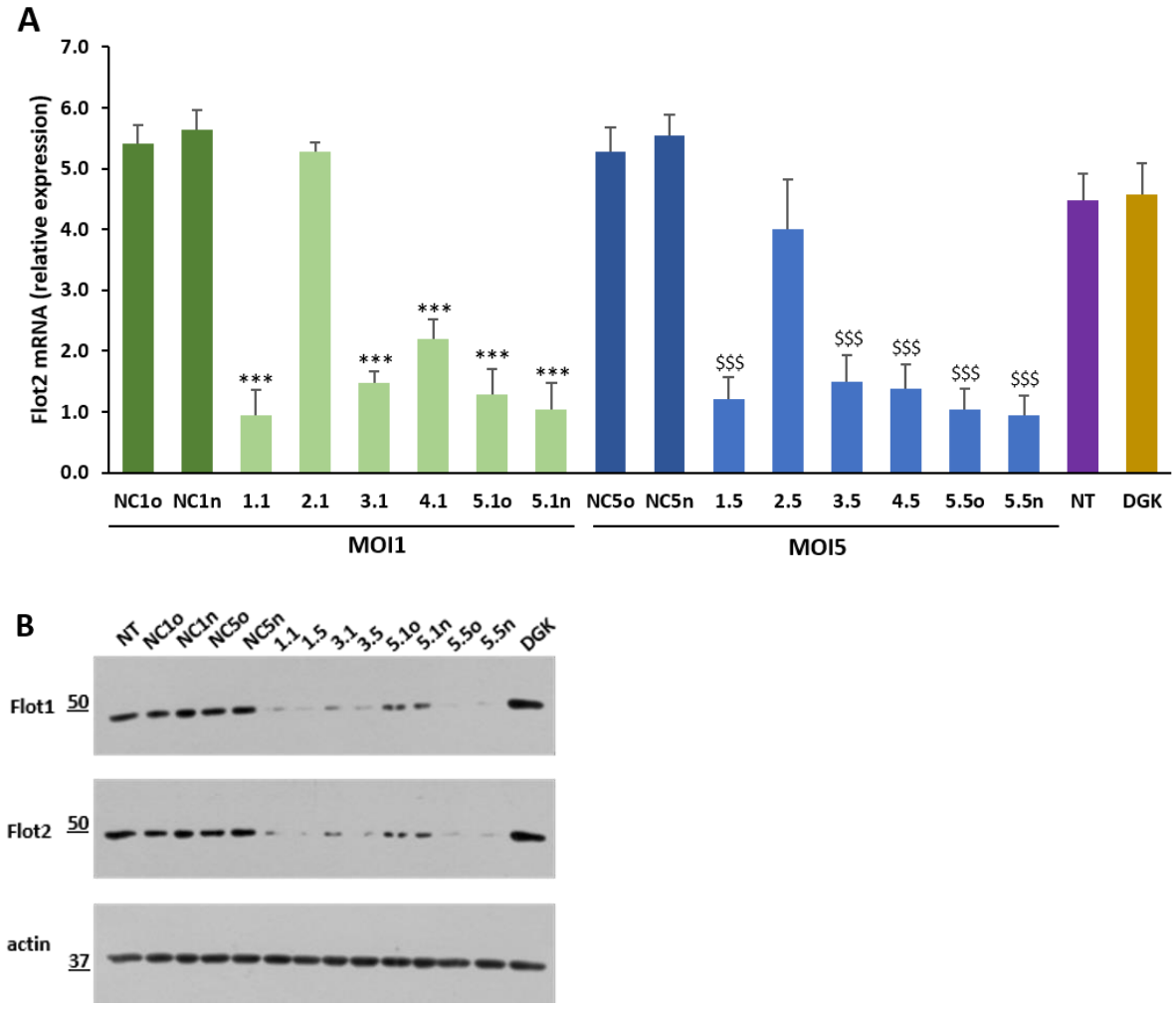

Figure 4.9. Knock-down of *Flot2* expression in Raw264 cells with the application of shRNA. (A) Five commercially available shRNA specific against *Flot2* were used to down-regulate flotillin-2. One control shRNA (NC) was applied. shRNA particles were used at MOI=1 (NC1o, NC1n, *Flot2*-silencing 1.1- 1.5) and MOI=5 (NC5o, NC5n, *Flot2*-silencing 1.5- 5.5). Some of the shRNA were applied in two independent attempts, including control shRNA (NC1o and NC1n, NC5o and NC5n) and *Flot2*-silencing shRNA 5 (5.1o and 5.1n, 5.5o and 5.5n) because the latter was most efficient in *Flot2* silencing. Analysis was performed using RT-qPCR. *Flot2* transcript was quantified relative to *Tbp* due to their comparable abundance. Data shown are mean ± s.d. from at least three experiments. *** *and* $$$, Significantly different at $p \leq .001$. (*) Show the difference of the indicated values *vs*. NC1o; ($) show the difference of the indicated values *vs.* NC5o. The same results were obtained when the mRNA levels in clones were compared to NC1n and NC5n, respectively. **(B)** Immunoblotting analysis of flotillin-1 and flotillin-2 levels in the indicated Raw264 clones. Flotillin-1 was detected after stripping of anti-flotillin-2 antibodies. Actin was visualized to verify equal loading of protein between wells. Molecular weight markers are shown on the left. Results of one representative experiment of two are shown. NT – non-transfected cells; DGK – Raw264 clone with down-regulated DGKε. The clone was obtained after transfection of cells with shRNA specific against *Dgke* (at MOI=1).

It was found that 4 applied shRNAs effectively silenced *Flot2* expression with shRNA variant 2 being the exception (Fig.4.9A). Some of the shRNAs were used in two independent attempts, including control shRNA and shRNA silencing *Flot2* number 5 (named "o" and "n"), because the latter shRNA variant was most efficient in flotillin-2 down-regulation. The average relative flotillin-2 mRNA level in obtained Raw264 clones (variants 1 and 3-5 of shRNA) reached about 1.39 at MOI=1 and 1.21 at MOI=5 in comparison to about 5.52 and 5.4 in control clones, giving reduction by about 75% and 78%, respectively (Fig.9A). The most profound reduction, reaching 80-83%, was observed in 5.5o and 5.5n clones. The level of flotillin-2 mRNA in controls increased by about 20% *vs.* non-transfected Raw264 cells and the reasons for this phenomenon remain unknown. It is of interest that the non-efficient shRNA variant 2 and also variant 4 both targeted the coding region of flotillin-2 mRNA, while all the shRNA of highest silencing potency - variants 1, 3, and 5 - targeted the 3'-untranslated region (UTR) of flotillin-2 mRNA.

Immunoblotting analysis of those clones revealed that they were virtually depleted of flotillin-2 if obtained at MOI=5 (clones 1.5, 3.5, 5.5o and 5.5n) while in those obtained at MOI=1 remnants of flotillin-2 were still detected (clones 1.1, 3.1, 5.1o and 5.1n) (Fig. 4.9B, middle panel). The analysis uncovered that the obtained cell clones also were depleted of flotillin-1. The down-regulation of flotillin-1 correlated with that of flotillin-2 at the protein level (Fig.4.9 B, upper panel), in agreement with earlier studies (Hoehne et al., 2005; Berger et al., 2013).

Most of the further experiments on the involvement of fotillins in LPS-induced signaling were performed on clones 1.5, 3.5, 5.5o and 5.5n and on the two control clones NC5o and NC5n. Clones were used for a maximum of 5 weeks (up to 10 passages) to minimize the potential recovery of *Flot2* expression.

4.9 Depletion of flotillin-2 can affect the expression of *Flot1* and *Cd14*

Further RT-qPCR analysis of Raw264 clones showed the *Flot2* silencing led to a significant reduction of flotillin-1 mRNA level, by about 29% and 21% in clones 5.5o and 5.5n, respectively, in comparison to NC5o/n control clones. A tendency for reduction was also found for CD14 mRNA in all examined clones, reaching about 33% and 43% in clones 1.5 and 5.5n, respectively. In clone 5.5o, the difference *vs.* NC5n was of borderline statistical significance (p = 0.058) (Fig.4.10). In contrast, no significant changes in TLR4 and DGKε mRNA levels were detected after *Flot2* silencing. DGKε is a lipid kinase phosphorylating diacylglycerol do phosphatic acid likely to be involved in CD14-triggered generation of

phosphatidylinositols (Sobocińska et al., 2018b), therefore cells depleted of this kinase were included in my analyses as an additional control. Notably, in a Raw264 clone selected after transfection with shRNA specific against *Dgke* (the DGK clone), DGKε mRNA was diminished by about 81% (Fig.4.10).

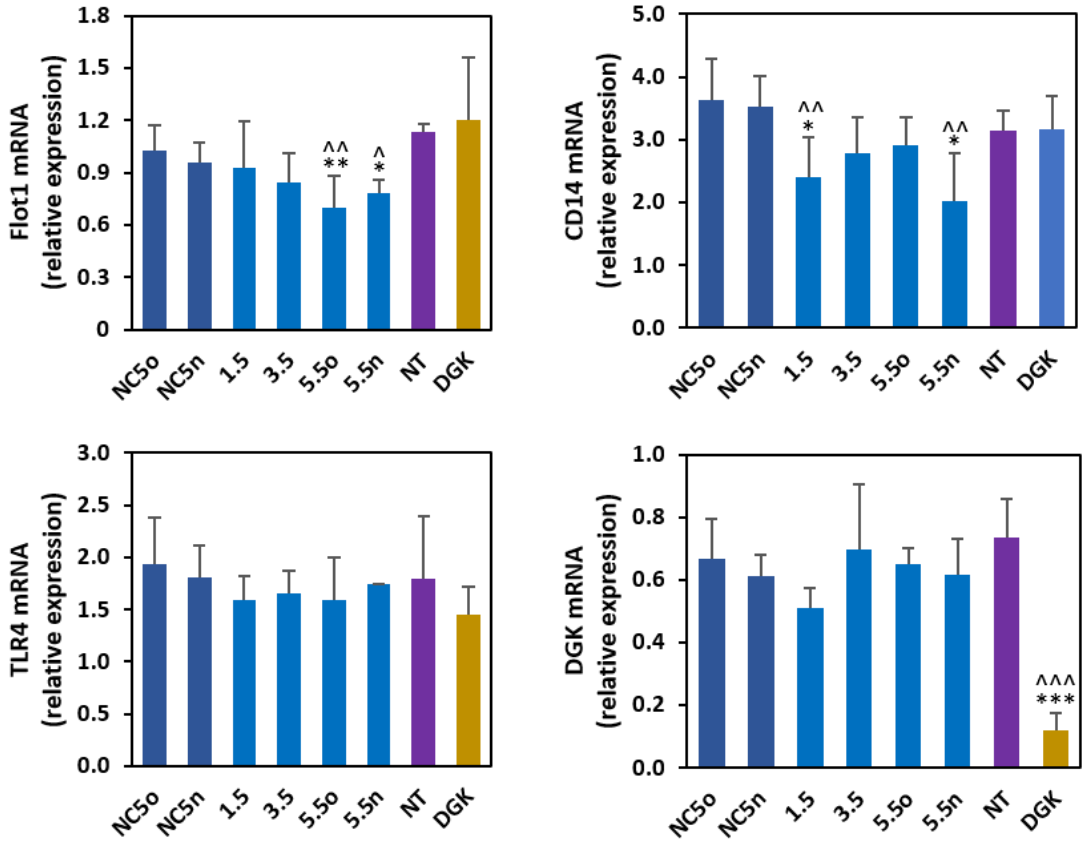

Figure 4.10 Analysis of the influence of *Flot2* knock-down on the expression of selected genes in Raw264 cells. Indicated cell clones were obtained using shRNA specific against *Flot2* (1.5, 3.5, 5.5o, 5.5n) or *Dgke* (DGK) or with control shRNA (NC5o, NC5n), as shown in Fig.9. Analysis was performed using RT-qPCR. *Flot1*, *Tlr4* and *Dgke* transcripts were quantified relative to *Tbp*, while that of *Cd14* relative to *Hprt* due to comparable abundance of those transcripts. NT – non-transfected cells. Data shown are mean ± s.d. from at least three experiments, except for *Tlr4* mRNA in 5.5n (measured once). * and ^, ** and ^^, *** and ^^^, Significantly different at $p \leq .05$, $p \leq .01$ and $p \leq .001$. (*) Show the difference of the indicated value *vs.* NC5o; (^) show the difference of the indicated value *vs.* NC5n.

4.10 Depletion of flotillin inhibits LPS-induced signaling in cells

After obtaining clones of Raw264 cells depleted in flotillin-2 and consequently in flotillin-1, I analyzed whether LPS-induced signaling was altered in these cells (clones 1.5, 5.5o compared to NC5o and NC5n controls) and in the DGK clone. For this purpose, cells were stimulated with 10 or 100 ng/ml LPS for 1 h, and the level of selected proteins known to be involved in TLR4 signaling was examined by immunoblotting and the following densitometry (Fig.4.11A, B).

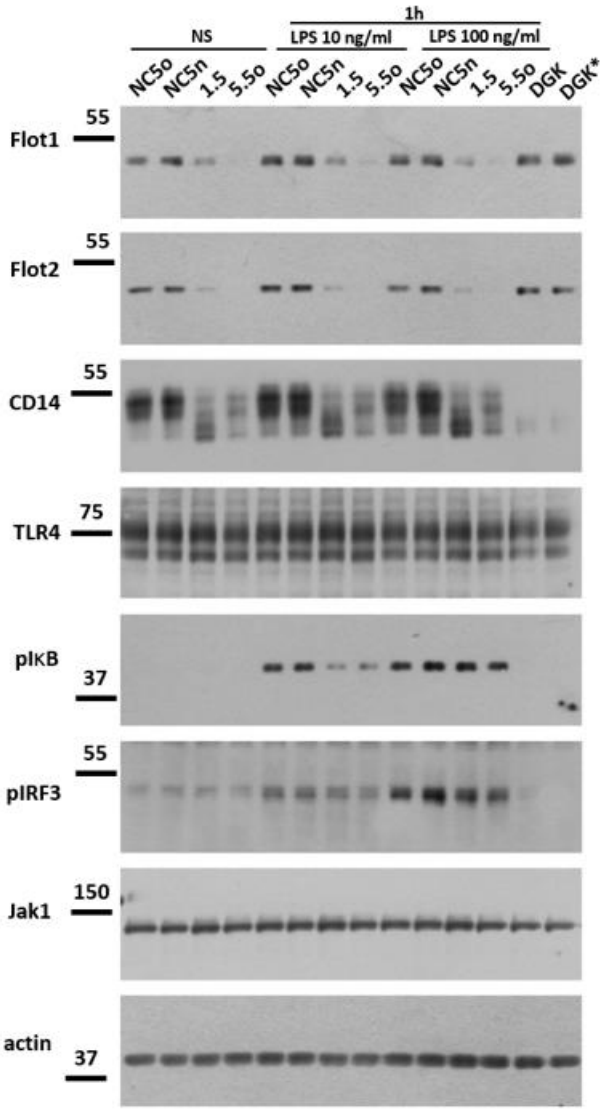

Figure 4.11a Analysis of the influence of *Flot2* knock-down on the level of flotillin-1 and -2, CD14 and TLR4, and on the phosphorylation of IκB and IRF3 in LPS-stimulated in Raw264 cells. Indicated cell clones (clones 1.5, 5.5o) were obtained using shRNA specific against *Flot2*, together with control cells (NC5o, NC5n) as shown in Fig.9. Cells were left unstimulated (NS) or were stimulated with 10 ng/ml or 100 ng/ml LPS (1h, 37°C). Proteins of cell lysates were subjected to SDS-PAGE followed by immunoblotting analysis with antibodies specific to the indicated proteins. Relative protein levels were quantified by densitometry (see Fig. 11b for results). Jak1 and actin were visualized to verify equal loading of protein between wells. Molecular weight markers are shown on the left. pIκB - phosphorylated IκB, pIRF3 - phosphorylated IRF3; . DGK – cell clone depleted of DGKε with shRNA*;* DGK* - these cells were stimulated with 10 ng/ml LPS, 1h.

Immunoblotting analysis confirmed that Raw264 cell clones 1.5 and 5.5o were strongly depleted of flotillin-2 prior to and also after stimulation with 10 or 100 ng/ml LPS. The reduction reached 68-76% on average in both clones compared to NC5o and NC5n control clones (Fig.4.11a, 4.11b-B), consistent with results shown in Fig. 9. Furthermore, it was also seen that the decrease in the level of flotillin-2 correlated with the reduction of flotillin-1 in unstimulated (by about 72%) and LPS-stimulated (by about 57-62%) cells (Fig.4.11a, 4.11b-A). This observation is additional evidence that flotillin-2 is required for the stabilization of flotillin-1, as the two proteins heterodimerize (Solis et al., 2013; Kwiatkowska, Matveichuk et al., 2020). However, I found differences in the response of both proteins to LPS stimulation. The level of flotillin-1 tended to increase in the control clones stimulated with 10 or 100 ng/ml LPS, it exceeded the resting level on average by about 31% and 39% respectively, although the differences were not statistically significant. An upward

trend in flotillin-1 level was observed even in clones 1.5 and 5.5o depleted of flotillin-2 (Fig.4.11a, 4.11b-A). In contrast to flotillin-1, the flotillin-2 level tended to decrease (non-significantly) by 5-14% in the control NC5o and NC5n clones during LPS-stimulation, and the decrease was also seen in clones 1.5 and 5.5o (Fig.4.11a, 4.11b-B). These data indicate that flotillin-1 and -2 can play different roles during the stimulation of cells with LPS.

Interestingly, the level of CD14 increased in control clones NC5o and NC5n during stimulation of cells with LPS, resembling flotillin-1. The increase in CD14 level was statistically significant, reaching on average 24% at 10 ng/ml LPS and as much as 57% at 100 ng/ml LPS compared to unstimulated controls (Fig.4.11a, 4.11b-C), in agreement with earlier reports (Prymas et al., 2020). Furthermore, the analysis uncovered that in clones 1.5 and 5.5o depleted of flotillins, the CD14 level was strongly, by about 32%, reduced in comparison to NC5o and NC5n controls and the difference remained at this level during cell stimulation with 10 and 100 ng/ml LPS (28% and 34% reduction, respectively) (Fig.4.11a, 4.11b-C). The data indicate that depletion of flotillins led to a sustained down-regulation of CD14 protein in Raw264 cells.

In striking contrast to CD14, no significant changes in the level of TLR4 were observed in 1.5 and 5.5o clones in comparison to control cells. The 1-h stimulation did not affect the TLR4 level either (Fig.4.11a, 4.11b-D). According to previously published data, the TLR4 level is markedly down-regulated after longer stimulation of cells with LPS (more than 2-h stimulation) which ends its pro-inflammatory signaling (Płóciennikowska et al., 2016).

To reveal the consequences of depletion of flotillin-1 and -2, and the following reduction of CD14 level for the LPS-induced signaling, I analyzed the activation of two transcription factors, NFκB and IRF3, which are the final targets of the two signaling cascades triggered by LPS-activated TLR4. NFκB is activated in the MyD88-dependent pathway and at a late phase of the endosomal TRIF-dependent pathway. IRF3 is activated exclusively in the TRIF-dependent manner (Björkbacka et al., 2004). Activation of NFκB is indicated by phosphorylation of its regulatory subunit IκB; in NC5o and NC5n control clones it was comparable upon stimulation with 10 and 100 ng/ml LPS (Fig.4.11a, 4.11b-E). Notably, the IκB phosphorylation was inhibited in 1.5 and 5.5o clones; the inhibition was stronger and statistically significant in cells stimulated with 10 ng/ml LPS, reaching on average 44%, in comparison to 34% reduction (non-significant) found at 100 ng/ml LPS (Fig.4.11a, 4.11b-E).

The TRIF-dependent phosphorylation of IRF3 indicating activation of this transcription factor was induced by LPS in a dose-dependent manner, and at 100 ng/ml LPS was twice that induced by 10 ng/ml LPS (Fig.4.11a, 4.11b-F). Interestingly, *Flot2* silencing

led to a comparable, significant reduction of IRF3 phosphorylation by about 29% at both LPS concentrations (Fig.4.11a, 4.11b-F).

For comparison, in the DGK clone, the CD14 level was profoundly diminished and upon stimulation with 10 ng/ml LPS both IκB and IRF3 phosphorylation were abolished (Fig.4.11a).

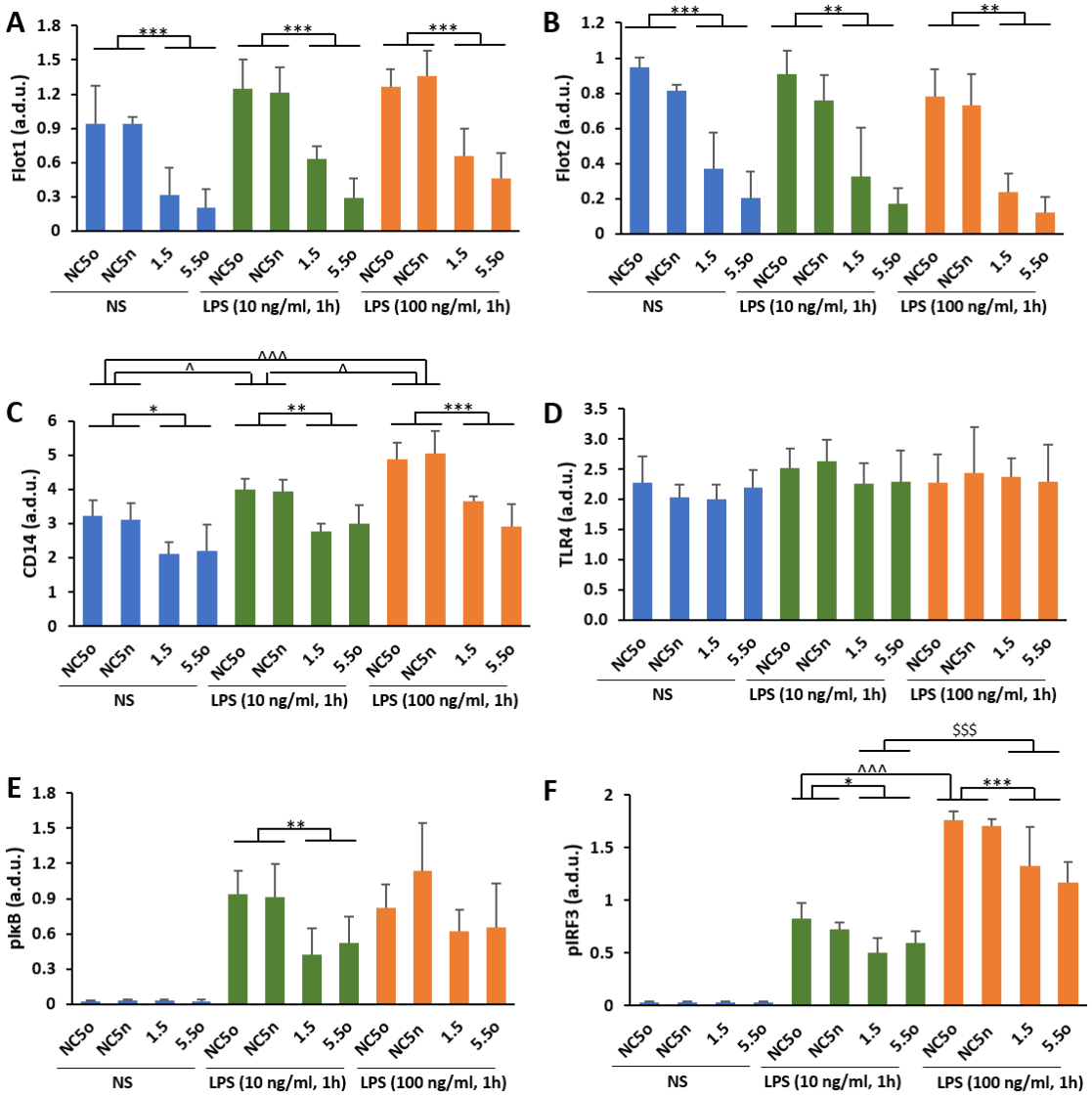

Figure 4.11b. Analysis of the influence of *Flot2* knock-down on the level of flotillin-1 and -2, CD14 and TLR4, and on the phosphorylation of IκB and IRF3 in LPS-stimulated in Raw264 cells. Relative protein levels were determined by immunoblotting followed by densitometric analysis relative to actin. Representative blots are seen in Fig.11a. a.d.u, arbitrary density units. Data shown are mean ± s.d. from at least three experiments. *, ^ and ** and ***, $$$, ^^^, Significantly different at $p \leq .05$ and $p \leq .01$ and $p \leq .001$. (*) Show the difference of the indicated group *vs.* the group of NC5o and NC5n controls; ($) show the difference between the group of flotillin-2-depleted 1.5 and 5.5o clones stimulated with 10 or 100 ng/ml LPS; (^) show the difference between the group of NC5o and NC5n controls unstimulated and stimulated with 10 or 100 ng/ml LPS. The statistical analysis was performed using 2-way ANOVA with Tukey's post hoc test.

Taken together, obtained data show a negative influence of flotillin depletion on the CD14 but not the TLR4 abundance in cells. These changes resulted in inhibition of the TRIF-dependent signaling at low (10 ng/ml) and high (100 ng/ml) LPS concentrations. In contrast, the MyD88-dependent signaling was affected more strongly at the lower LPS concentration. This profile of changes reflects the different dependence of the two TLR4 signaling pathways on the contribution of CD14 – CD14 is required for the TRIF-dependent signaling but can be dispensable for the MyD88-dependent signaling at higher LPS concentrations (Borzęcka-Solarz et al., 2017).

4.11. Assessment of CD14 surface level in flotillin-depleted cells with flow cytometry

To get further insight into the flotillin-dependent changes of the CD14 level, I applied flow cytometry to examine whether the cell surface CD14 was also affected by *Flot2* silencing in Raw264 cells. I found that in the 5.5o clone the amount of CD14 on the cell surface was lower by about 25% than in the NC5o control (Fig. 2.12A, B). The analysis also uncovered a 77% decrease in the CD14 surface level in the DGK clone (Fig. 4.12A, B), corresponding to the substantial decrease in the total CD14 amount found by immunoblotting in this clone (see Fig. 4.11b-C).

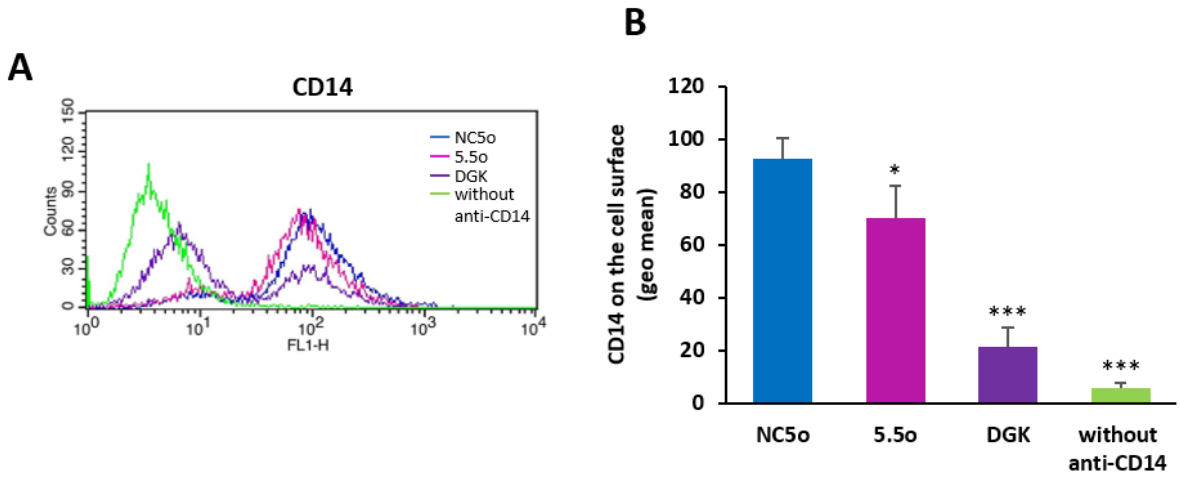

Figure 4.12 Analysis of the influence of *Flot2* knock-down on the surface level of CD14 in Raw264 cells. Unstimulated cells were detached, incubated with or without anti-CD14-FITC, fixed and analyzed with flow cytometry. **(A)** Representative plots indicating differences in CD14 cell surface level in examined cells. **(B)** The geometric mean of fluorescence intensity (geo mean) values of CD14 staining. Data shown are mean ± s.d. from four experiments. * and ***, Significantly different at $p \leq .05$ and $p \leq .001$ *vs.* NC5o. DGK – cell clone depleted of DGKε with shRNA; without anti-CD14 - Raw264 cells not-treated with anti-CD14-FITC antibody.

4.12. Depletion of flotillins reduces LPS-induced production of cytokines

To determine the ultimate impact of depletion of flotillin on pro-inflammatory responses of Raw264 cells, I used ELISA assays to analyze the amount of released TNFα and CCL5/RANTES, two cytokines produced, respectively, mainly in the MyD88-dependent and strictly in the TRIF-dependent manner (Björkbacka et al., 2004). For this purpose, cells were stimulated with 10 or 100 ng/ml LPS for 6 h.

The production of TNFα in NC5o and NC5n control clones was found to be about 2-fold higher at 10 than at 100 ng/ml LPS (Fig.4.13A). In clones 1.5, 3.5 and 5.5o depleted of flotillins, TNFα production was strongly inhibited in cells stimulated with 10 ng/ml LPS; the reduction reached 45%, 31% and 46% of control values, respectively. In contrast, the production of TNFα was not inhibited in the above-mentioned clones stimulated with 100 ng/ml LPS. Interestingly, TNFα production induced by 10 ng/ml dropped in flotillin-depleted cells to the level observed in cells stimulated with 100 ng/ml LPS (Fig.4.13A).

Analysis of CCL5/RANTES production in control clones showed that it was induced by LPS in a dose-dependent manner and was 1.5-fold higher at 100 than at 10 ng/ml LPS (Fig.4.13B). It decreased in clones 1.5, 3.5 and 5.5o by 39%, 36% and 58%, respectively, upon stimulation with 10 ng/ml LPS, resembling the effect of flotillin depletion exerted on TNFα (Fig.4.13B). However, in contrast to TNFα, the CCL5/RANTES production tended to decrease (by at least 20%) also in 1.5, 3.5 and 5.5o clones stimulated with 100/ml LPS. In the clone 5.5o, the reduction reached as much as 37% of the control value and was statistically significant (Fig.4.13B).

For comparison, the production of both cytokines was strongly inhibited, by about 79-84%, in the DGK clone regardless of the LPS concentration (Fig.4.13A, B). This corresponded to the substantial down-regulation of the total and the cell surface level of CD14 in this clone described above (see Figs 4.11b-C and 4.12).

The ELISA results for cells depleted of flotillins were consistent with the results of immunoblotting analysis of IκB and IRF3 phosphorylation in cells stimulated with 10 ng/ml LPS for 1 and 4 h (Fig.4.13C). In control cells, IκB phosphorylation was pronounced after 1 h and decreased over time of the stimulation.

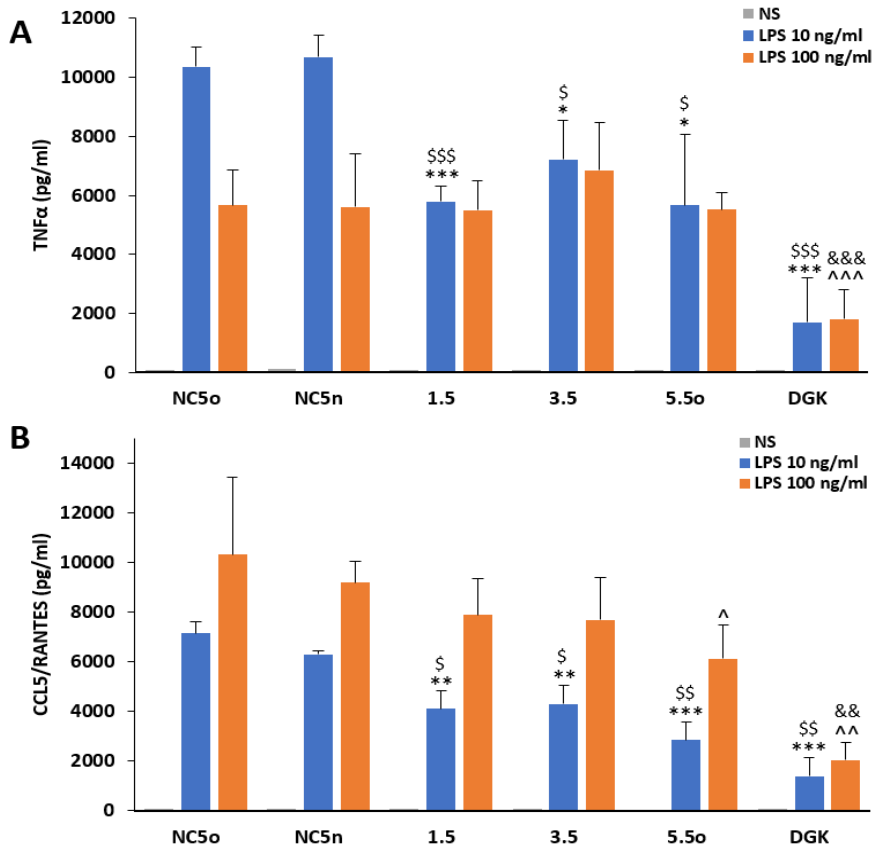

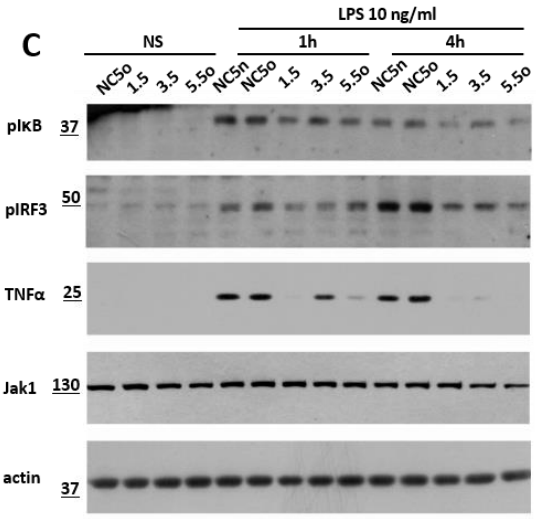

Figure 4.13 Analysis of the influence of *Flot2* knock-down on the TNFα and CCL5/RANTES production in RAW264 cells stimulated with LPS.

(A, B) Indicated Raw264 clones were unstimulated (grey) or stimulated with 10 ng/ml (blue) or 100 ng/ml (orange) LPS for 6 h. The concentration of TNFα **(A)** and CCL5/RANTES **(B)** was determined in culture supernatants with ELISA. Data shown are mean ± s.d. from three experiments. *, $ and ** and ***, $$$, &&&, ^^^, Significantly different at $p \leq .05$ and $p \leq .01$ and $p \leq .001$. (*) Show the difference of the indicated value *vs.* NC5o at 10 ng/ml LPS; ($) show the difference of the indicated value *vs.* NC5n at 10 ng/ml LPS; (^) Show the difference of the indicated value *vs.* NC5o at 100 ng/ml LPS; (&) show the difference of the indicated value *vs.* NC5n at 100 ng/ml LPS **(C)** Immunoblotting analysis of the levels of phosphorylated IκB (pIκB), phosphorylated IRF3 (pIRF3) and the transmembrane precursor of TNFα in the indicated clones of Raw264 cells. Jak1 and actin were visualized to verify equal loading of protein between samples. Molecular weight markers are shown on the left. DGK – cell clone depleted of DGKε with shRNA. Results of one representative experiment of two are shown.

It was reduced in clones 1.5, 3.5 and 5.5o at both times of stimulation. Corresponding to these data and ELISA results, the production of the transmembrane TNFα precursor was also inhibited in 1.5, 3.5 and 5.5o clones (Fig.4.13C). In contrast to IκB, IRF3 phosphorylation increased as LPS stimulation progressed. It was reduced in 1.5, 3.5 and 5.5o clones at both analyzed times of LPS stimulation (Fig.4.13C).

To sum up, obtained data indicate that the participation of flotillins is required for maximal pro-inflammatory signaling in LPS-stimulated cells. Knock-down of flotillins negatively affected TLR4 signaling and pro-inflammatory cytokine production, especially when cells were stimulated with low LPS concentration (10 ng/ml). Moreover, the TRIF-dependent signaling pathway was more affected by the lack of flotillins than the MyD88-dependent one even at the high LPS concentration (100 ng/ml). Thus, the involvement of flotillins in LPS-induced signaling is manifested in conditions that require the involvement of CD14 for TLR4 activation.

4.13 Clustering of CD14 induces palmitoylation of flotillin-1 and flotillin-2

In the next step, I undertook studies to establish the relationship between stimulation of cells with LPS and flotillin palmitoylation. Owing to the functional interplay between flotillins and proteins with the GPI anchor (Kwiatkowska, Matveichuk et al., 2020), I assumed that clustering of CD14 in the plasma membrane could be involved in this process. Previous studies of our laboratory revealed that CD14 undergoes clustering in the plasma membrane during LPS binding in J774 macrophage-like cells. The CD14 clustering, in turn, induces the generation of $PI(4,5)P_2$ that is involved in signaling pathways triggered by TLR4. Such signaling abilities of CD14 are linked with its raft localization and can be ascribed to local lipid changes concomitant with the raft clustering, subsequently affecting the inner leaflet of the plasma membrane (Płóciennikowska et al., 2015b). Therefore, to examine whether palmitoylation of flotillins is also associated with CD14 clustering, I studied it in a model system using J774 cells; CD14 clustering was induced by anti-CD14 antibody binding, as described earlier (Płóciennikowska et al., 2015b). For this purpose, cells were labeled with 17ODYA and then incubated at 4^0C with rat anti-CD14 IgG. Since the antibody is bivalent, it induced initial CD14 aggregation, however, the CD14-IgG complexes could not be internalized due to the low temperature; rat IgG was used in control cells. After incubation with the primary antibody, cells were subjected to a short incubation (10 min) with anti-rat IgG at 37^0C, which induced further CD14 clustering. Then cells were lysed, and lysates were subjected to click chemistry with biotin-azide followed by the enrichment of labeled proteins

on streptavidin beads, as shown in Fig. 4.14A (top panel B). The immunoblotting analysis uncovered a significant increase in palmitoylation of both flotillin-1 and flotillin-2 in cells incubated with anti-CD14 and anti-rat IgG that was about 2.3-fold higher than in control cells incubated with control rat IgG alone (Fig. 4.14B). Incubation of cells with control rat IgG and anti-rat IgG induced a markedly lower increase in palmitoylation of flotillin-1 and flotillin-2. Interestingly, flotillin palmitoylation also was elevated after incubation with the primary anti-CD14 antibody alone, this effect was stronger for flotillin-1 than flotillin-2 (about a 2-fold increase in comparison to rat IgG), although the difference did not reach the statistical significance (Fig. 4.14B).

To confirm these results, I cross-linked CD14 under different conditions: cells were incubated with the primary anti-CD14 IgG and the secondary anti-rat IgG at 4^0C (30 min each incubation) and then warmed briefly at 37^0C (10 min) (Fig. 4.14A, lower panel C). At these conditions, the rise in palmitoylation of flotillin-1 and -2 was statistically significant even after incubation with the primary anti-CD14 IgG only (about 1.5- and 2-fold over control cells not treated with any antibody, respectively; Fig. 4.14C). Palmitoylation of flotillin-1 increased further by about 1.5 fold after cross-linking of CD14 with the secondary antibody. An elevated palmitoylation of flotillin-1 and -2 was also detected in cells incubated with control rat and anti-rat IgG (Fig. 4.14C). On the other hand, palmitoylation of Jak1 and the PAG adaptor protein did not change or change moderately during CD14 cross-linking (Fig. 4.14B, C).

These data indicate that clustering of CD14 induced by cross-linking with antibodies (which also occurs during LPS binding) can be a signal for palmitoylation of flotillins despite CD14 and flotillins do not interact directly. This process can be stimulated by subtle changes in the distribution of CD14 in the outer leaflet of the plasma membrane, since it was observed after binding of the primary anti-CD14 IgG alone, and was detected also in cells incubated with control rat IgG and anti-rat IgG, possibly due to the binding of the IgG to FcγIIA receptor which associates with rafts (Kwiatkowska et al., 2003). The data indicate that CD14 can interact with both flotillins. However, after 1 h of cell stimulation with LPS, an increased amount of palmitoylated flotillin-1, not flotillin-2, was detected by mass spectrometry (Sobocińska et al., 2018b). For this reason, I aimed to identify zDHHC(s) that can catalyze flotillin-1 *S*-palmitoylation, and then investigate the contribution of these enzymes to LPS-induced production of pro-inflammatory cytokines.

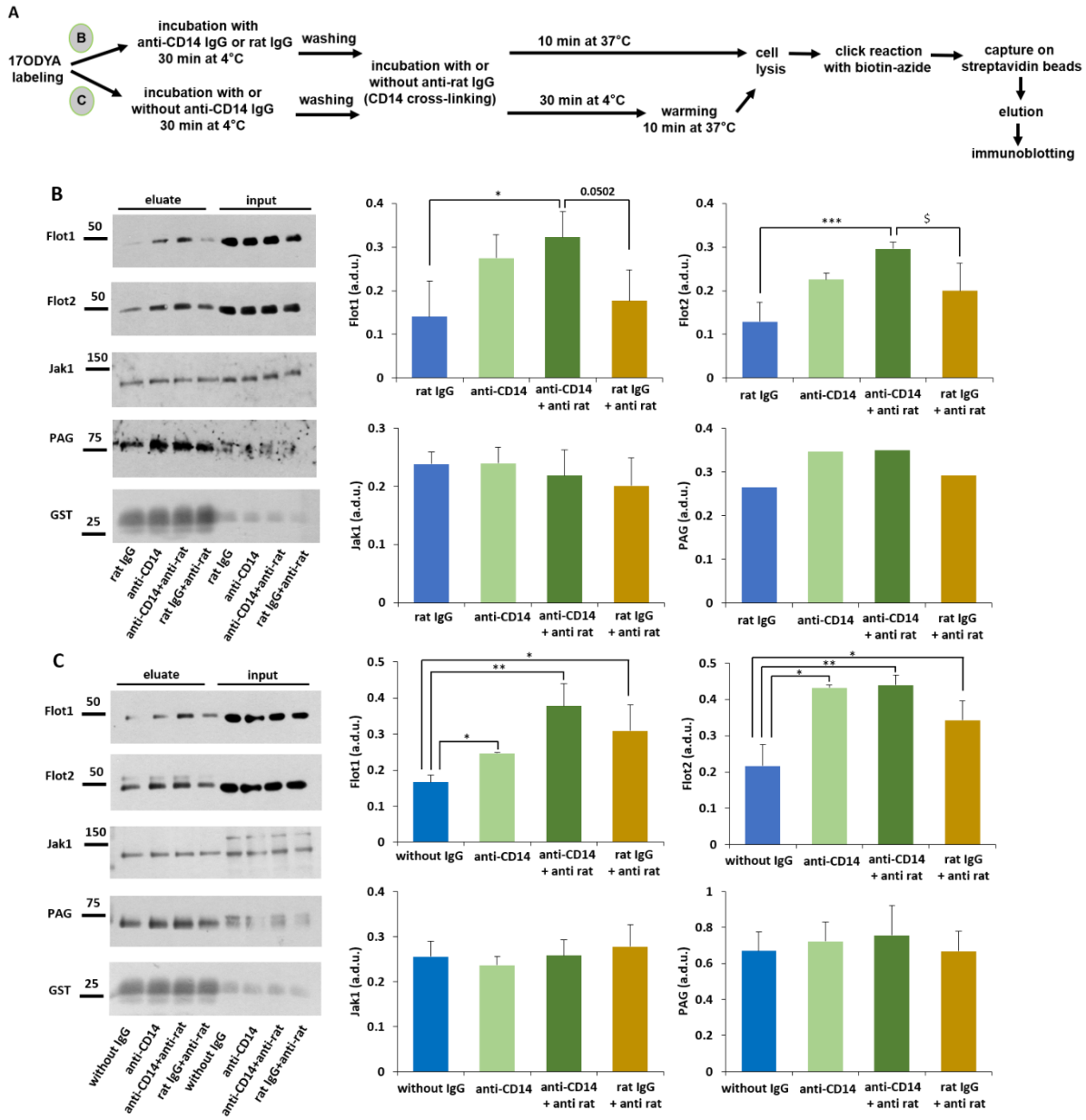

Figure 4.14 Palmitoylation of flotillins during CD14 clustering in J774 cells. (A) Scheme of the experimental procedure. Cells were labeled with 17ODYA (50 μM, 4 h, 37°C) and then exposed to antibodies, which forced clustering of CD14 in the plasma membrane. Cells were lysed, 17ODYA-labeled proteins were tagged with biotin-azide in click reaction and captured on streptavidin beads, eluted and separated by SDS-PAGE. **(B)** Cross-linking conditions included incubation of cells for 30 min at 4°C with anti-CD14 rat IgG followed by 10 min at 37°C with anti-rat IgG. In one series, anti-rat IgG was omitted during the second incubation. Controls included cells incubated with rat IgG alone or with rat IgG flowed by anti-rat IgG. **(C)** Cross-linking conditions included incubation of cells for 30 min at 4°C with anti-CD14 rat IgG followed by 30 min at 4°C with anti-rat IgG and next warming of the cells for 10 min at 37°C. In one series, anti-rat IgG were omitted during the second incubation. Controls included cells not treated with any antibody or incubated with rat IgG flowed by anti-rat IgG. **(B, C)** Immunoblotting analysis of palmitoylation of the indicated proteins in cells during CD14 cross-linking. For comparison, 2% of total cell lysate was also run as an input. Relative protein levels were quantified by densitometry and normalized against biotinylated GST that was added to cell lysates prior to their incubation with streptavidin beads. Molecular weight markers are shown on the left. Without IgG – cells not treated with any antibody. Data shown are mean ± s.d. from three or four experiments or from one for PAG in **(B)**. *, $ and ***, Significantly different at $p \leq .05$ and $p \leq .01$. (*) Show the difference of the indicated value *vs.* without IgG or rat IgG; ($) show the difference of the indicated value *vs.* rat IgG + anti-rat IgG.

4.14 Initial identification of zDHHC catalyzing *S*-palmitoylation of flotillin-1

To identify zDHHC(s), which catalyze *S*-palmitoylation of flotillin-1, all 23 members of the mouse zDHHC family (tagged at the C-terminus with HA) were co-expressed with mouse flotillin-1 in HEK293 cells, according to the method of Fukata et al. (2006). Since the collection of plasmids encoding palmitoyl acyltransferases of the zDHHC family was kindly provided by Dr. Fukata who originally named them "DHHC" proteins, in the following few sections I provide both names of these enzymes for clarity. This set of studies aimed to reveal zDHHC(s) whose co-expression enhanced flotillin-1 *S*-palmitoylation above the level observed in cells transfected with flotillin-1 alone. In the first step of this analysis, flotillin-1 was co-expressed with sets of three zDHHCs, as shown in Fig. 15A-C. Then, to detect flotillin-1 palmitoylation, I used a method developed at the beginning of my studies, which relied on metabolic cell labeling with 17ODYA and the click reaction with biotin-azide followed by the detection of palmitoylated proteins eluted from streptavidin beads (see Fig. 1). Immunoblotting analysis revealed that palmitoylation of flotillin-1 (the amount of flotillin-1 eluted from streptavidin beads) was markedly enhanced upon its co-expression with the following sets of DHHC/zDHHC: 1-3, 7-9 (the strongest effect) and 18-20. Less pronounced palmitoylation, but still above the control level, was detected in the presence of the following DHHCs: 13-15, 6+16+17 and 21-23 (Fig.4.15 A, C). DHHC13 corresponds to zDHHC24, DHHC22 to zDHHC13 and DHHC23 to zDHHC25. The activity of DHHC/zDHHC6 is controlled by DHHC/zDHHC16 and they both interact in the endoplasmic reticulum (Abrami et al., 2017), therefore I decided to combine these enzymes in one set. Interestingly, the increase in the amount of palmitoylated flotillin-1 was accompanied by an increase in the total amount of this protein seen in the input cell lysates. The latter effect was most pronounced in sets containing DHHC/zDHHC1-3 and 7-9, those that also had the strongest effect on palmitoylation of flotillin-1 (Fig.4.15A, C). The obtained data indicate that flotillin-1 can be *S*-palmitoylated by various zDHHCs and this modification can affect the flotillin-1 abundance in cells. The results also pointed to DHHC/zDHHC7-9 as the most promising candidates capable of successfully modifying flotillin-1 (Fig.4.15C).

It should be noted that individual zDHHCs were overproduced in different amounts. For example, DHHC/zDHHC5, which is known to catalyze *S*-palmitoylation of flotillin-2 (Li et al., 2012) and presumably flotillin-1 (Wan et al., 2013), was expressed at a relatively low level, in contrast to DHHC/zDHHC4. Also DHHC7, 13 (zDHHC24), 14, and 19 were fairly abundant.

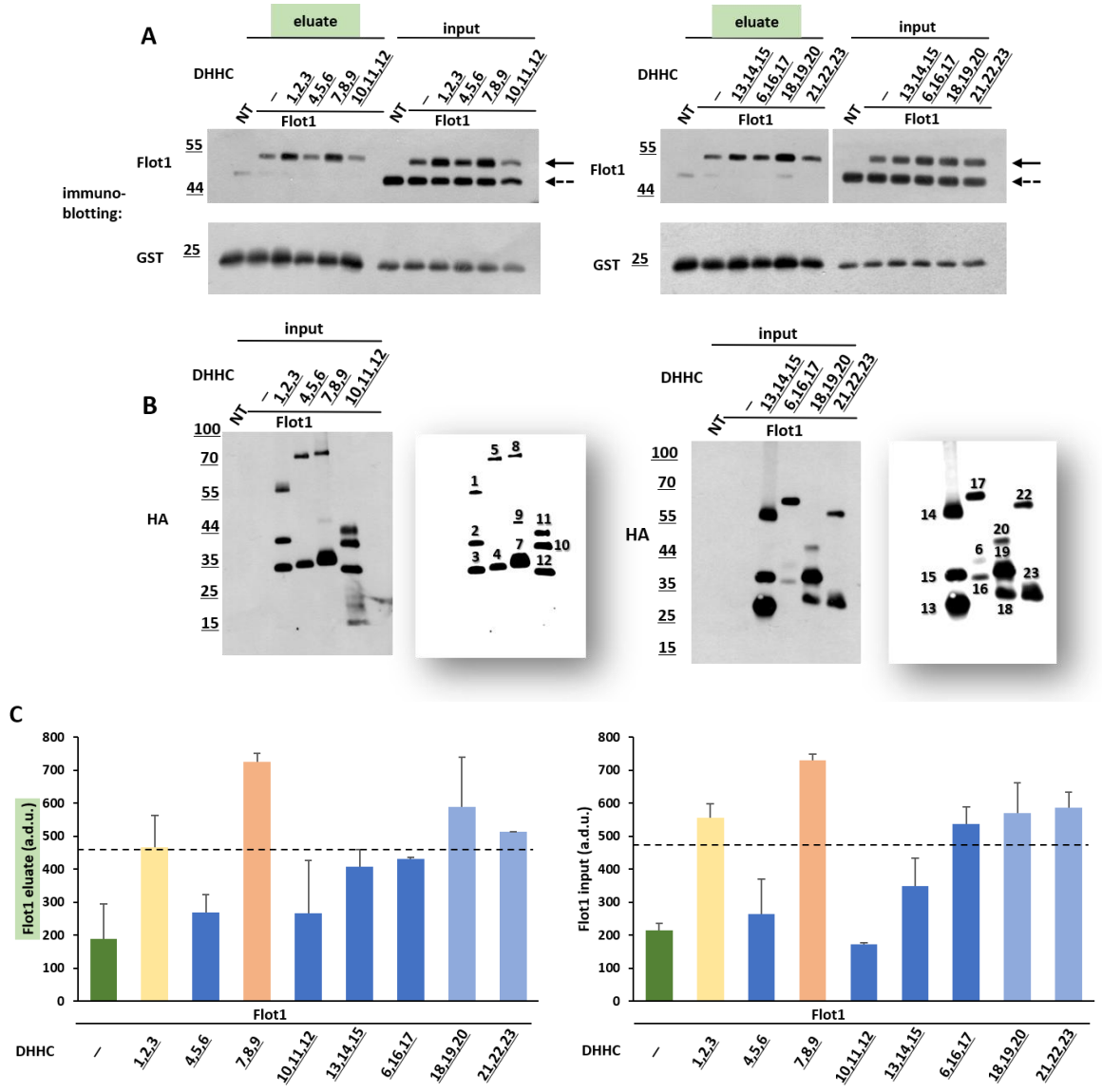

DHHC10=zDHHC11, DHHC11=zDHHC23, DHHC13=zDHHC24, DHHC22=zDHHC13, DHHC23=zDHHC25

Figure 4.15 Analysis of the influence of DHHC1-DHHC23 on palmitoylation of flotillin-1 - click chemistry. Flotillin-1 was overexpressed with or without DHHC enzymes in HEK293 cells using pCMV6-Entry-Myc-DDK and pEF-BOS plasmid, respectively. The plasmids were used at a 1:1:1:1 ratio (200 ng of Flot1 and 200 ng of each DHHC). pEF-BOS plasmid bore genes of individual DHHC-HA. After 24 h, cells were labeled with 17ODYA (50 µM, 1 h, 37^0C), lysed, 17ODYA-labeled proteins were tagged with biotin-azide in the click reaction and captured on streptavidin beads, eluted and separated by SDS-PAGE. The scheme of this experimental procedure is shown in Fig. 1. **(A)** Immunoblotting analysis of flotillin-1 palmitoylation (detection of flotillin-1 in eluates from streptavidin beads). For comparison, 2% of total cell lysate was also run as an input. Flotillin-1 was detected with an anti-flotillin-1 antibody. Positions of overexpressed and endogenous flotillin-1 in inputs and eluates are indicated by the solid and dashed arrows, respectively. Detection of biotinylated GST that was added to cell lysates prior to their incubation with streptavidin beads revealed the efficiency of elution of biotinylated proteins from streptavidin beads. **(B)** Input samples were probed with anti-HA to detect DHHCs. Additionally, the right panels show copies of blots with individual numbers of every single DHHC. Molecular weight markers are shown on the left. **(C)** The relative level of flotillin-1 was quantified in eluates and inputs by densitometry and normalized against GST. Dash-dotted lines show the mean of a.d.u. from all variants co-transfected with flotillin-1 and DHHCs. Data shown are mean ± s.d. from two experiments. NT - non-transfected cells; 1-23 – numbers of overexpressed DHHCs; a.d.u, arbitrary density units.

Furthermore, DHHC/zDHHC6, 9 and 16 were barely detectable while DHHC/zDHHC21 was often not detected at all (Fig.4.15B). This phenomenon could result from uneven transfection of cells with plasmids carrying DHHC/zDHHC genes of different sizes, as found earlier for CD14 and TLR4 (Płóciennikowska et al., 2016). DHHC/zDHHC9 requires GCP16 protein for stability (Swarthout et al., 2005). It was also possible that zDHHC interfered with each other's stability, as found for DHHC/zDHHC6 and 16 (Abrami et al., 2017). Therefore, in the next step, flotillin-1 was co-expressed with individual DHHC/zDHHC.

4.15 zDHHC3, 5, 7 and 8 catalyze *S*-palmitoylation of flotillin-1

To identify zDHHC catalyzing *S*-palmitoylation of flotillin-1, I focused on DHHC1-10 (and 16 for the reason mentioned above). Among those, DHHC10 corresponds to zDHHC11. This set of enzymes included DHHC/zDHHC7-9 most strongly affecting flotillin-1 palmitoylation in the initial analysis (see Fig. 4.15). Additionally, DHHC/zDHHC2, 5, and 8 are located in the plasma membrane (Chen et al., 2018) and can modify submembranous proteins, including flotillins. This selection left DHHC11-23 beyond the scope of this work.

Using the click-based approach I found a marked increase in the amount of palmitoylated flotillin-1 (the amount of flotillin-1 eluted from the streptavidin beads) in the presence of DHHC/zDHHC3, 5, 7 and 8 (Fig.4.16A, C). In contrast, no effect of DHHC/zDHHC1, 4, 9 was detected while DHHC/zDHHC2, 6, 16 and DHHC10 (zDHHC11) exerted a weak-to-moderate influence (Fig.4.16A, C). The increase in the total amount of flotillin-1 was again observed in cells co-transfected with DHHCs/zDHHCs. The amounts of the total and palmitoylated flotillin-1 often correlated, e.g., in the presence of DHHC/zDHHC3, 5, 7 and 8 (Fig.4.16A, C).

The expression level of the analyzed DHHCs/zDHHCs could give a hint as to the effectiveness of flotillin-1 palmitoylation (Fig. 4.16B). Thus, the strong palmitoylation of flotillin-1 in the presence of DHHC/zDHHC7 correlated with a high overproduction of this palmitoyl acyltransferase. However, highly expressed DHHC10 (zDHHC11) only moderately enhanced flotillin-1 palmitoylation casting doubt on the physiological importance of this process. Furthermore, DHHC/zDHHC2 and DHHC/zDHHC5 were expressed at a similar level, but DHHC/zDHHC2 palmitoylated flotillin-1 less efficiently. The same regularity was observed for DHHC/zDHHC4 and DHHC/zDHHC8 (Fig.4.16B).

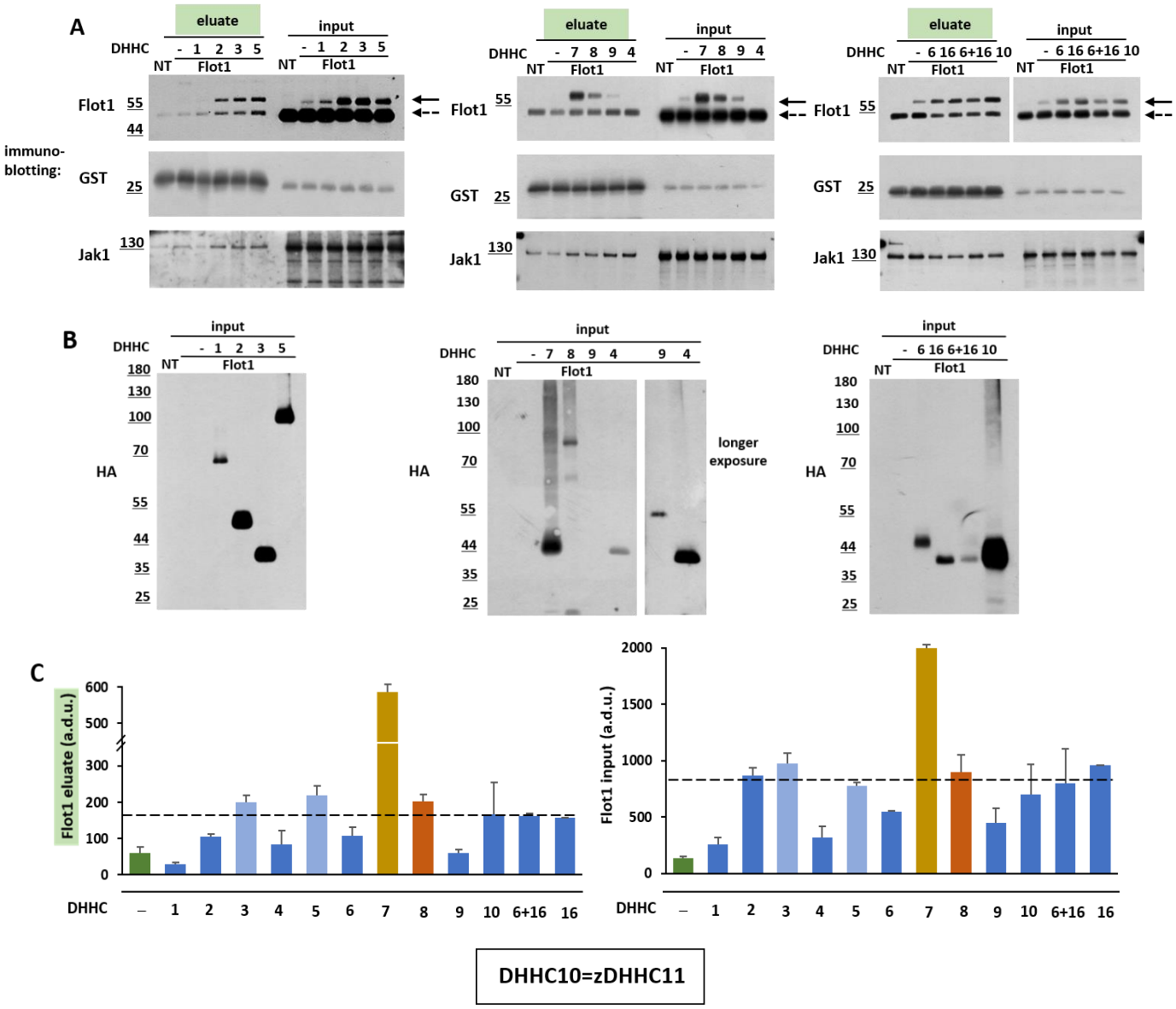

Figure 4.16 Analysis of the influence of selected DHHCs on palmitoylation of flotillin-1 - click chemistry. Flotillin-1 was overexpressed with or without DHHC enzymes in HEK293 cells using pCMV6-Entry-Myc-DDK and pEF-BOS plasmid, respectively. The plasmids were used at a 1:1 ratio (200 ng of Flot1 and 200 ng of DHHC). pEF-BOS plasmid bore genes of individual DHHC-HA. After 24h, cells were labeled with 17ODYA (50 µM, 1 h, 37^{0}C), lysed, 17ODYA-labeled proteins were tagged with biotin-azide in the click reaction and captured on streptavidin beads, eluted and separated by SDS-PAGE. The scheme of this experimental procedure is shown in Fig. 1. **(A)** Immunoblotting analysis of flotillin-1 palmitoylation (detection of flotillin-1 in eluates from streptavidin beads). For comparison, 2% of total cell lysate was also run as an input. Flotillin-1 was detected with an anti-flotillin-1 antibody. Positions of overexpressed and endogenous flotillin-1 in inputs and eluates are indicated by the solid and dashed arrows, respectively. Detection of biotinylated GST that was added to cell lysates prior to their incubation with streptavidin beads revealed the efficiency of elution of biotinylated proteins from streptavidin beads. Endogenous Jak1 is also shown in eluates and inputs. **(B)** Input samples were probed with anti-HA to detect DHHCs. Molecular weight markers are shown on the left. **(C)** The relative level of flotillin-1 in eluates and inputs was quantified by densitometry and normalized against GST. Dash-dotted lines show the mean of a.d.u. from all variants co-transfected with flotillin-1 and DHHC. Data shown are mean ± s.d. from two experiments. NT - non-transfected cells; 1-16 – numbers of overexpressed DHHC; a.d.u, arbitrary density units.

The relatively efficient palmitoylation of flotillin-1 by DHHC/zDHHC8 combined with a moderate expression of this palmitoyl acyltransferase drew our attention to this enzyme.

DHHC/zDHHC8 is found in the plasma membrane, Golgi apparatus and intracellular vesicles (Chen et al., 2018; Ernst et al., 2018). Inhibition of *S*-palmitoylation induces a shift of endogenous flotillin-1 from the plasma membrane to intracellular vesicles (Biernatowska et al., 2013) where it may be modified by zDHHC8. The other two DHHC/zDHHCs effective in palmitoylation of flotillin-1, zDHHC3 and zDHHC7, catalyze *S*-acylation of multiple proteins in the Golgi apparatus (Lemonidis et al., 2015). For these reasons, I eventually focused on zDHHC8 as an enzyme that could *S*-palmitoylate flotillin-1 more selectively and also on zDHHC5 likely to *S*-palmitoylate both flotillins. Since the DHHC and zDHHC names of zDHHC5 and zDHHC8 do not differ, in the following sections I use only their zDHHC names.

4.16 zDHHC8 catalyzes *S*-palmitoylation of flotillin-1 and flotillin-2 but not DGKε

To analyze flotillin-1 *S*-palmitoylation by zDHHC8 in more detail, I performed an ABE-based analysis on HEK293 cells transfected with zDHHC8 together with either flotillin-1 or flotillin-2 or DGKε. Immunoblotting analysis confirmed that co-expression of zDHHC8 with flotillin-1 led to a significant increase in *S*-palmitoylation of the protein (the amount of flotillin-1 in the eluate from streptavidin beads) and also in the total amount of flotillin-1 in the input lysate. The enrichment reached, respectively, about 4.1- and 2.3-fold above the control level, i.e., that in cells transfected with flotillin-1 alone (Fig. 4.17A-C). Subsequently, I reduced the amount of zDHHC8-encoding plasmid by half and transfect cells along with the same amount of flotillin-1-encoding plasmid as above. Under these conditions, the increase in the amount of *S*-palmitoylated flotillin-1 and the total pool of flotillin-1 was also statistically significant (about1.8-fold over the control) (Fig. 4.17A, right panel, B, C).

S-palmitoylation of flotillin-2 was up-regulated by zDHHC8 to a smaller extent (about 1.4-fold) than that of flotillin-1. The total amount of flotillin-2 was also increased in the presence of zDHHC8 *vs.* control, although the difference was not statistically significant. In contrast to both flotillins, zDHHC8 did not affect the *S*-palmitoylation of DGKε nor its total level in the input fraction (Fig. 4.17A-C). Endogenous Jak1 was used as a positive control for the recovery of palmitoylated proteins in all labeled samples. (Fig. 4.17A).

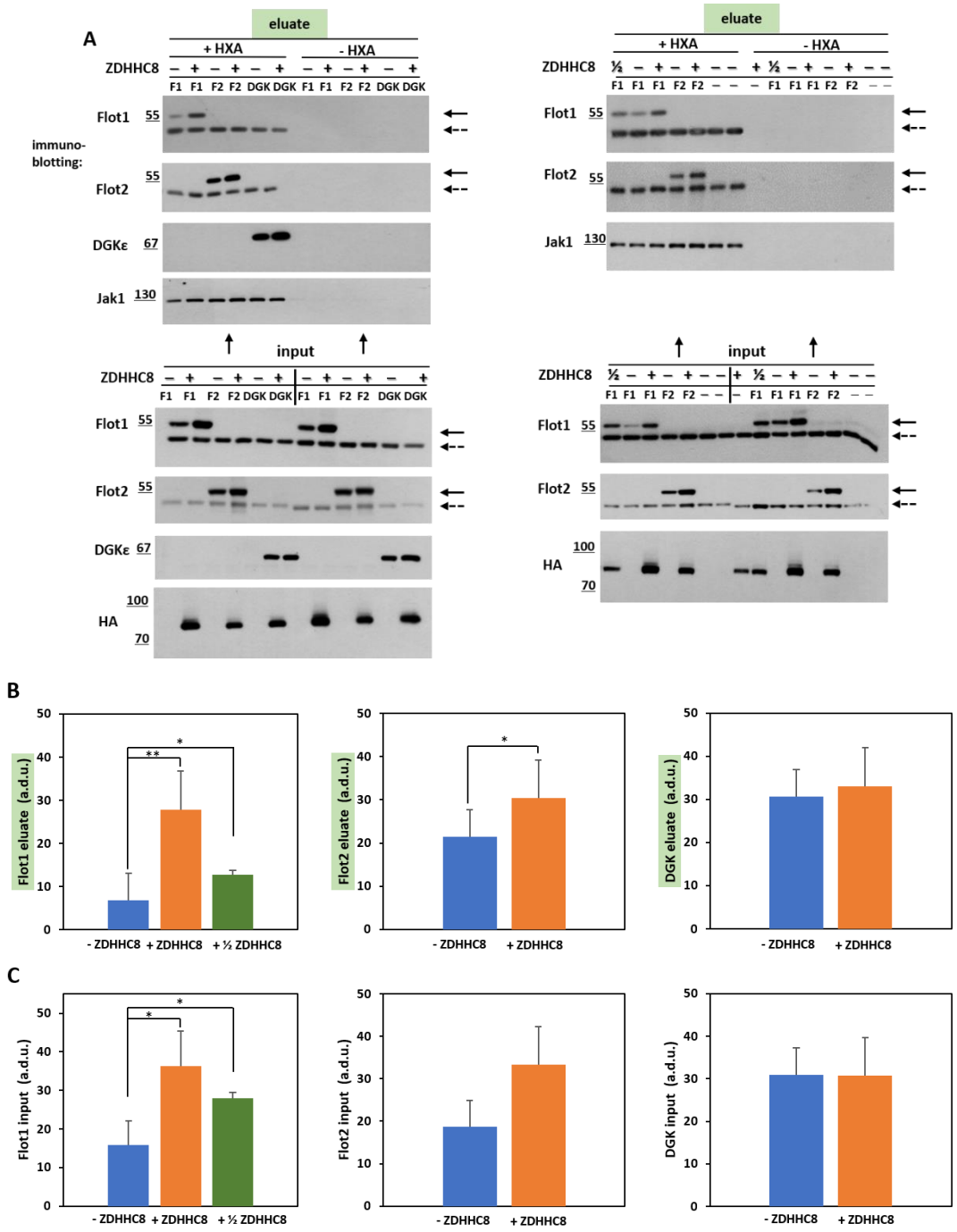

Figure 4.17 Analysis of the influence of DHHC/zDHHC8 on *S*-palmitoylation of flotillin-1 and other proteins. Flotillin-1, flotillin-2 and DGKε were overexpressed with or without zDHHC8 in HEK293 cells. The plasmids were used at a 1:1 ratio (200 ng of Flot1, Flot2 or DGKε and 200 ng of zDHHC8) or at a 1:0.5 ratio (200 ng of Flot1 and 100 ng of zDHHC8). After 24 h, cells were lysed, free thiol groups of proteins were blocked by alkylation, and palmitoyl moieties were released with hydroxylamine (HXA). The newly exposed thiol groups reacted with biotin-HPDP (input samples collected). Then, biotinylated proteins were captured on streptavidin beads, eluted and separated by SDS-PAGE. The scheme of this experimental procedure is shown in Fig. 4. **(A)** Immunoblotting analysis of *S*-palmitoylation of flotillin-1, flotillin-2 and DGKε (detection of these proteins in eluates from streptavidin beads). Endogenous *S*-palmitoylated Jak1 is also seen. Lower panels show indicated proteins in inputs. Proteins were detected with specific antibodies, including an anti-HA tag antibody revealing zDHHC8. Positions of overexpressed and endogenous flotillin-1 and flotillin-2 in inputs and eluates are indicated by the solid and dashed arrows, respectively. Molecular weight markers are shown on the left. **(B, C)** Relative protein levels were quantified by densitometry in eluates from streptavidin beads (**B**) and in inputs (**C**). Data shown are mean ± s.d. from three experiments. * and **, Significantly different at $p \leq .05$ and $p \leq .01$. F1 and F2 – flotillin1 and flotillin-2; a.d.u, arbitrary density units.

Interestingly, co-transfection of zDHHC8 with flotillin-1 (but not flotillin-2) in a plasmid ratio of 1:1 (ng:ng) led to an enrichment of zDHHC8 in comparison to cells expressing the enzyme alone or transfected at a 0.5:1 ratio to flotillin-1 (Fig. 4.17A, B), which indicated that at certain conditions the two proteins can affect each other. To sum up, the data indicate that zDHHC8 can *S*-palmitoylate flotillin-1 over flotillin-2 and does not modify DGKε.

4.17 Other zDHHCs catalyzing *S*-palmitoylation of flotillin-1 and flotillin-2

Finally, to get a broader picture of enzymes catalyzing *S*-palmitoylation of flotillin-1, I performed the ABE-based analysis of HEK293 cells co-expressing flotillin-1 and DHHC/zDHHC5, 7 or DHHC23 (zDHHC25), and also DHHC/zDHHC4 or DHHC10 (zDHHC11) as controls. These zDHHCs were selected on the basis of the data presented in Figures 15 and 16. Based on those data also the amount of zDHHC-carrying plasmids was reduced in some cases to balance the expression of these enzymes (Fig. 4.18).

Immunoblotting analysis showed that, among the selected palmitoyl acyltransferases, zDHHC5 was particularly effective in *S*-palmitoylating flotillin-1, which was accompanied by an elevation of the total amount of the protein. These two parameters increased about 5.7- and 3.4-fold, respectively, in comparison to flotillin-1 overexpressed alone (Fig.4.18A). zDHHC7 and DHHC23 (zDHHC25) also induced substantial *S*-palmitoylation of flotillin-1 and its accumulation in cells – about 4.0- and 5.7-fold increase induced by DHHC/zDHHC7, and 2.3- and 2.6-fold by DHHC13 (zDHHC24), respectively (Fig.4.18A, B). In contrast, neither *S*-palmitoylation of flotillin-1 nor its abundance in cells were up-regulated in the presence of DHHC/zDHHC4 or DHHC10 (zDHHC11), in agreement with the results of the click-based analysis shown above (Fig.4.18A, B; see Fig.4.16). In fact, some reduction of flotillin-1 abundance and *S*-palmitoylation was observed using the ABE (Fig.4.18A, B). Thus, in addition to zDHHC8 also zDHHC5, 7 and DHHC 23 (zDHHC25) can *S*-palmitoylate flotillin-1.

Finally, co-expression of flotillin-2 with zDHHC5 led to *S*-palmitoylation and enrichment of flotillin-2, the former expected from earlier data (Li et al., 2012). *S*-palmitoylation of flotillin-2 was up-regulated about 2.9-fold and its total pool about 3-fold *vs.* flotillin-2 expressed alone (Fig. 4.18C). Notably, flotillin-2 was co-expressed with half the amount of zDHHC5 used in flotillin-1 *S*-palmitoylation analysis.

Based on the data obtained from analyses of *S*-palmitoylation of flotillin-1 and flotillin-2, I chose zDHHC5 and zDHHC8 to test their contribution to the pro-inflammatory signaling induced by LPS.

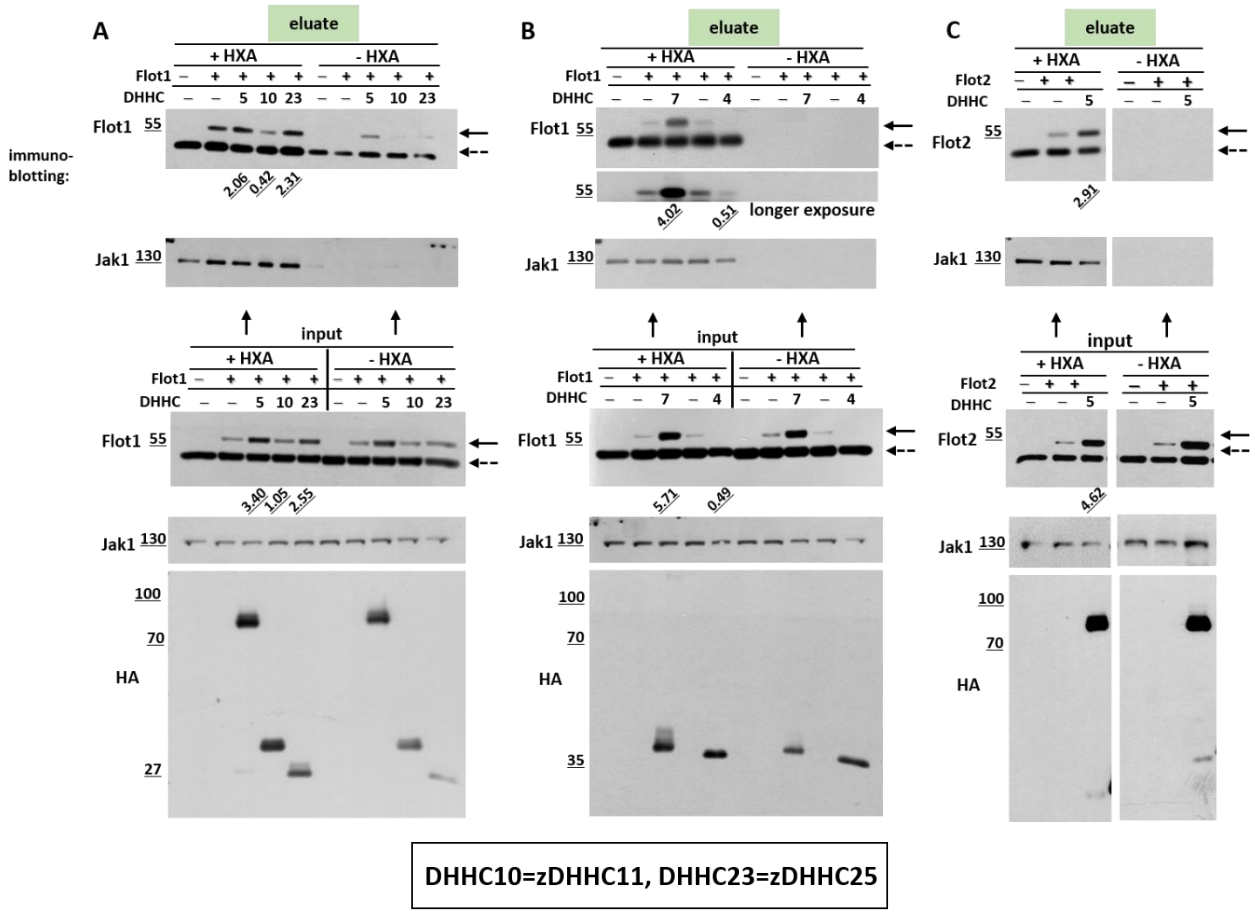

Figure 4.18 Analysis of the influence of DHHC4/5/7/10/23 on *S*-palmitoylation of flotillin-1 and flotillin-2. Flotillin-1 **(A, B)** and flotillin-2 **(C)** were overexpressed with or without indicated DHHC in HEK293 cells using pCMV6-Entry-Myc-DDK and pEF-BOS plasmid, respectively. The plasmids were used at a 1:1 ratio, i.e., 200 ng of Flot1 and 200 ng of DHHC/zDHHC5 **(A),** DHHC/zDHHC4 or DHHC/zDHHC7 **(B)** or at a 1:0.5 proportion, i.e., 200 ng of Flot1 and 100 ng of DHHC10 (zDHHC11) or DHHC23 (zDHHC25) **(A)** or Flot2 and zDHHC5 **(C)**. The proportions of plasmids varied in an attempt to equalize levels of overproduced DHHC. After 24h, cells were lysed, free thiol groups of proteins were blocked by alkylation, and palmitoyl moieties were released with hydroxylamine. The newly exposed thiol groups reacted with biotin-HPDP (input samples collected). Then, biotinylated proteins were captured on streptavidin beads, eluted and separated by SDS-PAGE. The scheme of this experimental procedure is shown in Fig.4.4 **(A, B)** Immunoblotting analysis of *S*-palmitoylation of flotillin-1 and **(C)** flotillin-2 (detection of these proteins in eluates from streptavidin beads). Endogenous *S*-palmitoylated Jak1 is also seen. Lower panels show analyzed proteins in inputs. Proteins were detected with specific antibodies, including an anti-HA tag antibody revealing DHHCs. Positions of overexpressed and endogenous flotillin-1 and flotillin-2 in inputs and eluates are indicated by the solid and dashed arrows, respectively. Molecular weight markers are shown on the left. The numbers below blots indicate the fold of enrichment of flotillin-1 or flotillin-2 co-expressed with respective DHHC *vs.* flotillin-1 or flotillin-2 expressed alone. NT- non-transfected cells, P4/5/7/10/23 – DHHC 4/5/7/10/23, respectively.

4.18. Silencing of *Zdhhc5* inhibits LPS-induced cytokine production

To determine the involvement of zDHHC5 and zDHHC8 in LPS-induced pro-inflammatory response, I silenced their expression in Raw264 cells with siRNA and analyzed

mRNA levels of CD14, TLR4 and flotillins, and two major pro-inflammatory cytokines, in cells stimulated with 10 ng/ml LPS. RT-qPCR analysis revealed that silencing of *Zdhhc5* and *Zdhhc8* was effective (Fig. 4.19A, B). zDHHC5 mRNA was reduced by as much as 85% prior to and after LPS stimulation in comparison to control cells treated with negative control siRNA (Fig. 4.19A). The analysis also uncovered a very low level of zDHHC8 mRNA in Raw264 cells - it was about 200-fold lower than the level of zDHHC5 mRNA. siRNA reduced it by 46%. In control cells, it was decreased to a comparable extent after LPS-stimulation in comparison to control cells treated with negative control siRNA (Fig. 4.19B). Depletion of zDHHC5 did not affect zDHHC8 mRNA and vice versa (Fig. 4.19A, B).

Silencing of either *Zdhhc5* or *Zdhhc8* led to only a non-significant reduction of the mRNA level of both flotillins before and after LPS-stimulation (Fig. 4.19C, D). Notably, flotillin-2 mRNA tended to decrease upon LPS stimulation (Fig. 4.19D) resembling the trend found earlier for the protein (Fig.4.11A,B). No changes in flotillin-1 expression were induced by LPS (Fig. 4.19C).

The level of CD14 mRNA in control cells rose after stimulation of cells with LPS, as found earlier for the CD14 protein (see Fig. 4.11), and this increase was nullified after zDHHC5 silencing (Fig. 19E). Moreover, the silencing of zDHHC5 significantly augmented the LPS-induced reduction of the TLR4 mRNA level (Fig. 4.19F). Thus, the depletion of zDHHC5 negatively affected the expression of *Cd14* and *Tlr4* in LPS-stimulated cells.

Further RT-qPCR analysis of Raw264 cells showed that the depletion of zDHHC5 also led to a significant reduction of TNFα and CCL5/RANTES mRNA levels, by 48% and 26%, respectively, in comparison to control cells. No effect of zDHHC8 silencing was detected (Fig. 4.19G, H). TNFα is *S*-palmitoylated, however, the detected changes in its mRNA indicate an upstream regulation of those changes.

Taken together, obtained results showed that despite the marked influence of zDHHC8 on the flotillin-1 palmitoylation in model studies in HEK293 cells, this palmitoyl acyltransferase does not seem to be important for LPS-induced signaling in Raw264 cells, possibly due to its very low expression in these cells. In contrast, the zDHHC5 participation is required for the LPS-induced production of TNFα and CCL5/RANTES, also affecting the expression of *Cd14* and *Tlr4*.

To define the impact of the zDHHC5 and zDHHC8 depletion on pro-inflammatory responses of Raw264 cells more precisely, I quantified the amount of cytokines secreted by cells stimulated with 10 ng/ml LPS using mouse cytokine array membranes.

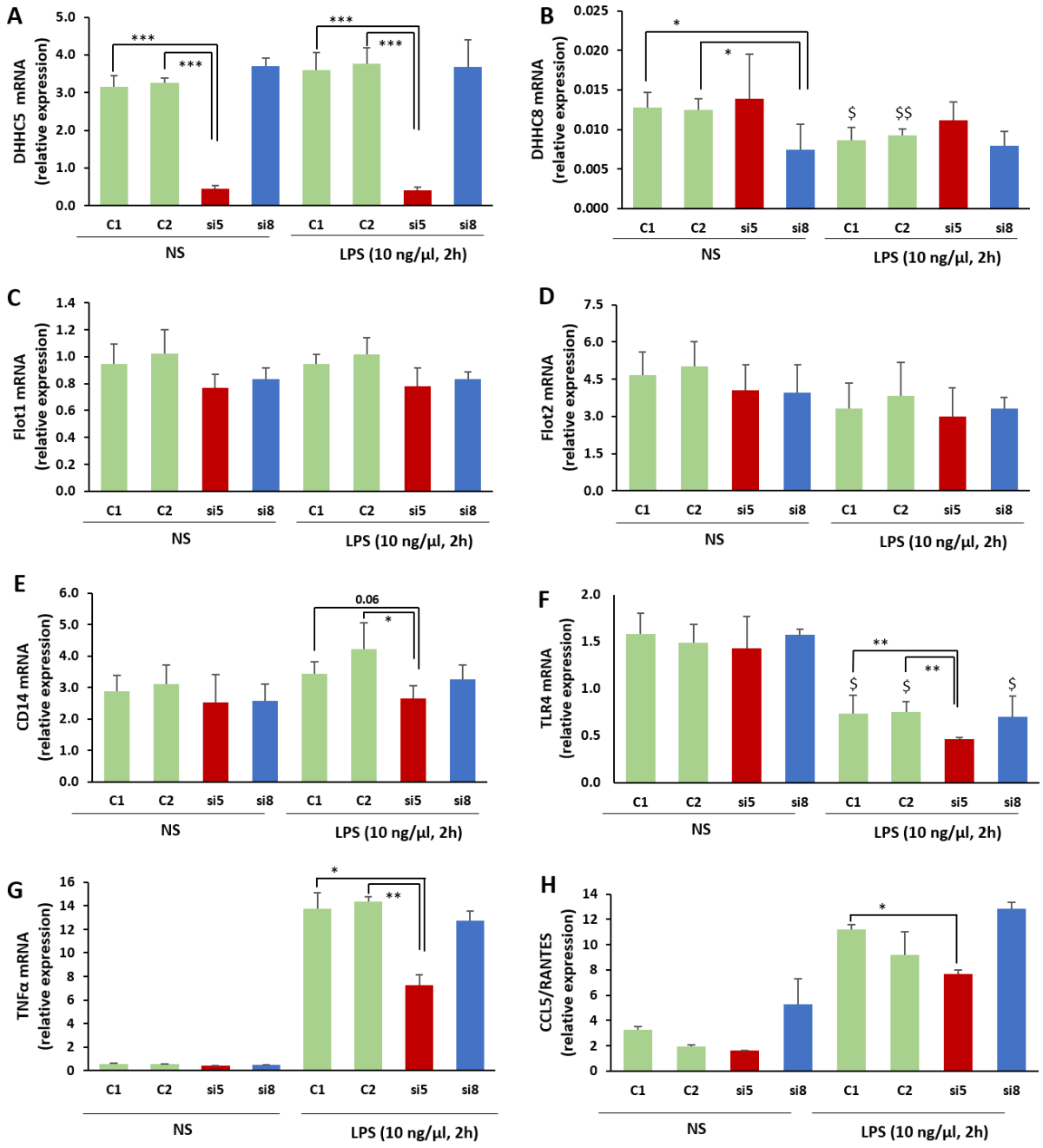

Figure 4.19 Analysis of the influence of *Zdhhc5* and *Zdhhc8* silencing on the expression of selected genes in Raw264 cells. Cells were transfected with siRNA targeting zDHHC5 or zDHHC8 or with negative control siRNA or Lipofectamine RNAiMAX alone for 24 h and next left unstimulated or stimulated with 10 ng/ml LPS for 2 h. Analysis was performed using RT-qPCR. *Zdhhc5* **(A)**, *Zdhhc8* **(B)**, *Flot1* **(C)**, *Flot2* **(D)**, *Tlr4* **(F)** and *Ccl5* **(H)** transcripts were quantified relative to *Tbp*, while that of *Cd14* **(E)** and *Tnfa* **(G)** relative to *Hprt* due to comparable abundance of those transcripts. Data shown are mean ± s.d. from three experiments (**A-F**) and one run in triplicate **(G, H)**. *, $ and **, $$ and ***, Significantly different at $p \leq .05$ and $p \leq .01$ and $p \leq .001$. (*) Show the difference of the indicated value *vs.* C1 or C2; ($) show the difference of the indicated value *vs.* the corresponding one in non-stimulated cells. C1, C2 – control cells treated with Lipofectamine RNAiMAX only (C1) or negative control siRNA (C2); si5, si8 – cells treated with siRNA specific against *Zdhhc5* (si5) or *Zdhhc8* (si8).

Silencing of zDHHC5 inhibited the production of CCL5/RANTES (despite its low production after 2-h stimulation with 10 ng/ml LPS), the interleukin-1 receptor antagonist (IL-1Ra) and IP10; the reduction reached about 95%, 66% and 51%, respectively, of average control level. All these mediators are produced in the TRIF-dependent pathway of TLR4 (Björkbacka et al., 2004; Tarassishin et al., 2011). Also, a moderate reduction of TNFα and MIP-2 production (by 27% and 34%, respectively) was observed. MIP-1α and MIP-1β were not affected (Fig.20A, B). Thus, considering the strong impact on cytokine production induced in the TRIF-dependent manner, we can conclude that the silencing of *Zdhhc5* resembled the effect of the depletion of flotillins (see Fig 4.13).

Performed analysis showed some inhibitory effect of zDHHC8 depletion on LPS-induced TNFα and IL-1Ra production (Fig.4.20A, B).

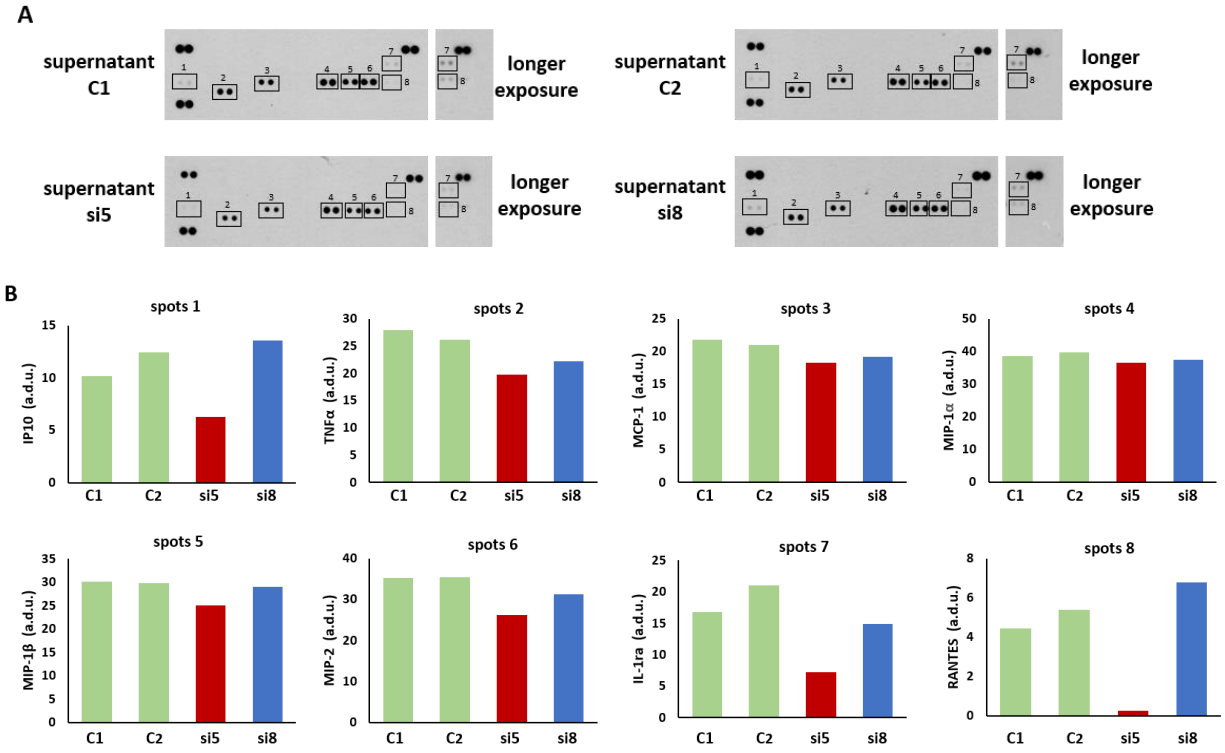

Figure 4.20 Analysis of the influence of *Zdhhc5* and *Zdhhc8* silencing on the cytokine production in LPS-stimulated Raw264 cells. Cells were transfected with siRNA targeting zDHHC5 or zDHHC8 or with negative control siRNA or Lipofectamine RNAiMAX alone for 24 h and stimulated with 10 ng/ml LPS for 2 h. **(*A*)** Immunoblotting analysis of cytokines in cell culture supernatants using cytokine array membranes. **(B)** Profiles of secreted cytokines quantified by densitometry. Data show one representative experiment of two. C1, C2 – control cells treated with Lipofectamine RNAiMAX only (C1) or negative control siRNA (C2); si5, si8 – cells transfected with siRNA specific against *Zdhhc5* (si5) or *Zdhhc8* (si8); a.d.u, arbitrary density units.

5. Discussion

The main aim of this study was to determine the role of flotillins and their *S*-palmitoylation in LPS-triggered pro-inflammatory response. Obtained results indicate that participation of flotillins is required for the maximal pro-inflammatory signaling in LPS-stimulated cells.

To achieve my goal, I obtained clones of Raw264 macrophage-like cells stably depleted of flotillin-2. I decided to target flotillin-2 with shRNA because the initial RT-qPCR analysis showed that its level was over 4-fold higher than that of flotillin-1. Four of the five shRNAs used were effective in depleting flotillin-2 at the mRNA and protein levels and allowed to obtain cell clones used in further studies. Interestingly, three effective shRNA targeted the 3'-untranslated region (3'-UTR) of flotillin-2 mRNA. This could facilitate future rescue studies, as the flotillin-2 encoding sequence re-introduced into the selected clones would not be affected by RNAi targeting the 3'-UTR.

I found that the lack of flotillin-2 led to the profound down-regulation of flotillin-1 at the protein level and also moderate at the mRNA level in some clones. The phenomenon of loss of both flotillins after directed depletion of one of these proteins has been described previously and is linked to the hetero-dimerization of flotillins, which apparently reinforce each other's stability (Babuke and Tikkanen, 2007; Kwiatkowska, Matveichuk et al., 2020). Flotillin-2 dominates flotillin-1 in Raw264 cells and in the two other macrophage-like cells, which explains why its depletion could lead to the disappearance of flotillin-1 especially at the protein level. Indeed, a negative influence of flotillin-2 knock-down on flotillin-1 is more frequently observed, while only profound depletion of flotillin-1 has the opposite effect (Hoehne et al., 2005, Berger et al., 2013, Jang et al., 2015). Due to the disappearance of both flotillins, it is difficult to pinpoint the function(s) of each of these proteins individually. Such individual functions are possible given differences in structure and post-translational modifications of flotillin-1 and -2. These include, e.g., single *S*-palmitoylation of flotillin-1 and *N*-myristoylation combined with triple *S*-palmitoylation of flotillin-2 (Morrow et al., 2002; Li et al., 2012). Indeed, some specific functions are attributed to flotillin-1 (Kwiatkowska, Matveichuk et al., 2020), as discussed below.

In flotillin-depleted Raw264 cells, LPS-induced TLR4-mediated responses were diminished. The TRIF-dependent signaling pathway leading to activation (phosphorylation) of the IRF3 transcription factor was inhibited and the following production of CCL5/RANTES was reduced. Also, the MyD88-dependent signaling leading to IκB phosphorylation and activation of the NFκB transcription factor, and TNFα

production was reduced. The latter, however, was affected more severely in cells stimulated with low LPS concentration (10 ng/ml).

One can notice that the involvement of flotillins in LPS-induced signaling was manifested in conditions that required CD14 involvement for TLR4 activation. CD14 binds LPS monomers and transfers them to the MD2/TLR4 complexes triggering pro-inflammatory signaling, including the MyD88-dependent pathway originating from the plasma membrane and the TRIF-dependent one, which is triggered from endosomes after endocytosis of CD14/TLR4/MD2 complexes (Jiang et al., 2005; Kagan et al., 2008; Ciesielska et al., 2021). At higher LPS concentrations (≥ 100 ng/ml), the requirement of CD14 for activation of the MyD88-dependent signaling can be alleviated, as LPS can be delivered to MD2-TLR4 by, e.g., BSA or soluble CD14 (Płóciennikowska et al., 2015a). On the other hand, the TRIF-dependent signaling is dependent on TLR4 endocytosis that is governed by CD14 (Zanoni et al., 2011). Earlier studies of our group indicated that LPS-induced clustering of CD14 triggers $PI(4,5)P_2$ generation which contributes to the TLR4 signaling (Płóciennikowska et al., 2015b; 2016).

A line of data obtained in the course of this study indicates that flotillins modulate the level of CD14 in cells and thereby affect the LPS-induced signaling. I found that depletion of flotillin-2 and -1: (i) decreased the level of CD14 mRNA in some clones (RT-qPCR); (ii) reduced the total cellular level of CD14 (immunoblotting); (ii) lowered the level of CD14 on the cell surface (flow cytometry). Notably, no such changes were observed for TLR4, pointing to the specificity of flotillin-CD14 interactions. In the next chapter, I discuss possible mechanisms by which flotillins can affect the CD14 level.

5.1 How can flotillins modulate the cellular level of CD14

Several mechanisms can be considered to explain the influence of flotillins on the CD14 level, including changes in (1) the *Cd14* gene expression and (2) the CD14 protein dynamics.

Ad 1). It has been found that flotillins can affect the expression of several genes through their influence on the membrane pool of sphingosine and the cellular level of its derivative, sphingosine-1-phosphate (S1P) which in turn inhibits histone deacetylases (Riento et al., 2018). Flotillins are membrane-bound proteins that localize to both the plasma membrane and endosomal/lysosomal compartments. Due to structural features including hydrophobic stretches and acylation(s) described in the Introduction, flotillin-1 and -2 associate with the cytosolic leaflet of plasma membrane nanodomains (rafts) and

can bind sphingosine, a lipid involved in diverse cellular processes. Analysis of the membrane content of mouse embryonic fibroblasts (MEFs) obtained from knock-out mice lacking flotillin-1 or flotillin-1 and -2 revealed a decrease in the raft sphingosine level, accompanied by a decrease in cellular S1P level. Flotillin-1 knockout followed by S1P depletion led to a reduction in histone acetylation and thereby diminished the expression of several genes, including the genes encoding bone-marrow stromal antigen 2 (Bst2) and interferon-stimulated protein 15 (Riento et al., 2018). Our preliminary studies did not reveal changes in the Bst2 mRNA level in flotillin-depleted clones of Raw264 cells (not shown). This undermines the link between flotillins and S1P and the expression of the CD14-encoding gene in these cells. On the other hand, previous studies of our group indicated that silencing of the gene encoding sphingomyelin synthase 1 (an enzyme converting ceramide into sphingomyelin) in J774 macrophage-like cells, also reduced the CD14 mRNA level (Prymas et al., 2020), therefore, the influence of sphingolipids on *Cd14* expression in flotillin-depleted cells cannot be ruled out. This is likely because the *Cd14* promoter activity is regulated (positively and negatively) by ceramide via Sp1 and Sp3 transcription factors (Wooten and Ogretman, 2005). The link between flotillins, sphingolipids, and CD14 is an interesting topic for further studies. Recently, a direct relation between *S*-palmitoylation of flotillin-1 in the endoplasmic reticulum and the activity of a Snail transcription factor has also been discovered. Non-palmitoylated flotillin-1 is sumoylated, migrates from the endoplasmic reticulum to the nucleus, and stabilizes Snail. Genes whose transcription is thereby induced encode proteins essential for endothelial-to-mesenchymal transition and metastasis of prostate cancer cells (Jang et al., 2019). However, since LPS-stimulation induces rather than inhibits flotillin-1 *S*-palmitoylation a similar mechanism of regulation of *Cd14* expression seems unlikely.

Ad2-1). The flotillin influence on the CD14 level can be related to the high dynamics of this protein in macrophages. CD14 undergoes endocytosis even in resting cells, after LPS binding it behaves like a "TAXI protein" (transporter associated with the execution of inflammation) and mediates endocytosis of TLR4 (Tan and Kagan, 2017).

Flotillins form assemblies at the inner leaflet of the plasma membrane in the membrane regions that have some properties of plasma membrane rafts. Thus, flotillins are isolated in a so-called detergent-resistant membrane (DRM) fraction of a low density during ultracentrifugation of detergent cell lysates, as do rafts, and recent data suggest that flotillins locate in more "heavy" subfraction of DRMs abundant in proteins (Jang et al., 2015). Moreover, immunofluorescent and electron microscopy studies indicate that

flotillins co-localize with typical raft proteins – the GPI-anchored ones, especially after their cross-linking. Flotillins were found to be involved in the internalization of these raft proteins and also of cholera toxin which binds to GM1 ganglioside in rafts (Glebov et al., 2006; Aït-Slimane et al., 2009; Frick et al., 2007). On the other hand, silencing of flotillin-1 expression with siRNA reduced the endocytosis of CD59 (a GPI-anchored protein) by about 50% only, casting doubts on the importance of the flotillin-1 involvement in this process (Glebov et al., 2006).

A recent study investigating the internalization of cytotoxic drug - cisplatin - by human retinal pigment epithelial cells has renewed our understanding of the role of flotillins in endocytosis. The study revealed that the uptake of a fluid phase can be induced by treating cells with ultrasounds, microbubbles, and desipramine (USMB). This fluid-phase uptake resulted in enhanced cellular uptake of cisplatin and required the participation of flotillin-1 and -2, zDHHC5, and Fyn tyrosine kinase of the Src family (Fekri et al., 2019). The data suggest that *S*-palmitoylation of flotillins by zDHHC5 is crucial for flotillin-mediated endocytosis (Fekri et al., 2019).

Based on results of the study on USMB and data on so-called massive endocytosis which also engages zDHHC2 and zDHHC5 and rafts (Hilgemann et al., 2020), and given the "raftophilic" nature of flotillins, the following mechanisms controlling flotillin-mediated endocytosis (with CD14 as a cargo) can be considered (Fig. 5.1): upon a stimulus, like USMB, Fyn kinase catalyzes the phosphorylation of flotillins and also activates zDHHC5. Next, zDHHC5 catalyzes *S*-palmitoylation of flotillins and other (sub)membranous proteins. *S*-palmitoylation of the MAGUK family adaptor proteins is an intriguing possibility since MMP1 (a raft protein) from the MAGUK family binds flotillins (Biernatowska et al., 2017), yet zDHHC(s) catalyzing MPP1 *S*-palmitoylation remains unknown. The formation of flotillin-based submembranous complexes is likely to take place at the plasma membrane rafts since *S*-palmitoylation of flotillin-2 can enhance its association with rafts (Neumann-Giesen et al., 2004). *S*-palmitoylation of flotillin-1 can determine its association with the plasma membrane (Morrow et al., 2002; Jang et al., 2015). On the other hand, local accumulation of saturated palmitic acid residues in rafts can facilitate the coalescence of these ordered membrane domains (Hilgeman et al., 2020, Podkalicka et al., 2015). The combination of all these factors facilitates flotillin–zDHHC5–MAGUK proteins–Fyn kinase interactions, protein phosphorylation and *S*-palmitoylation, and raft coalescence. They are followed by the invagination of the membrane that is governed by flotillin hetero-oligomers. Concomitantly, the entrapped fluid phase and

plasma membrane proteins are internalized. The preferred cargo of the flotillin-positive vesicles would be GPI-anchored proteins due to their raft localization. A similar chain of events can be triggered by cross-linking of GPI-anchored proteins with antibodies or by LPS-induced clustering of CD14 due to the co-localization of these proteins with Fyn kinase in rafts (Fig. 5.1).

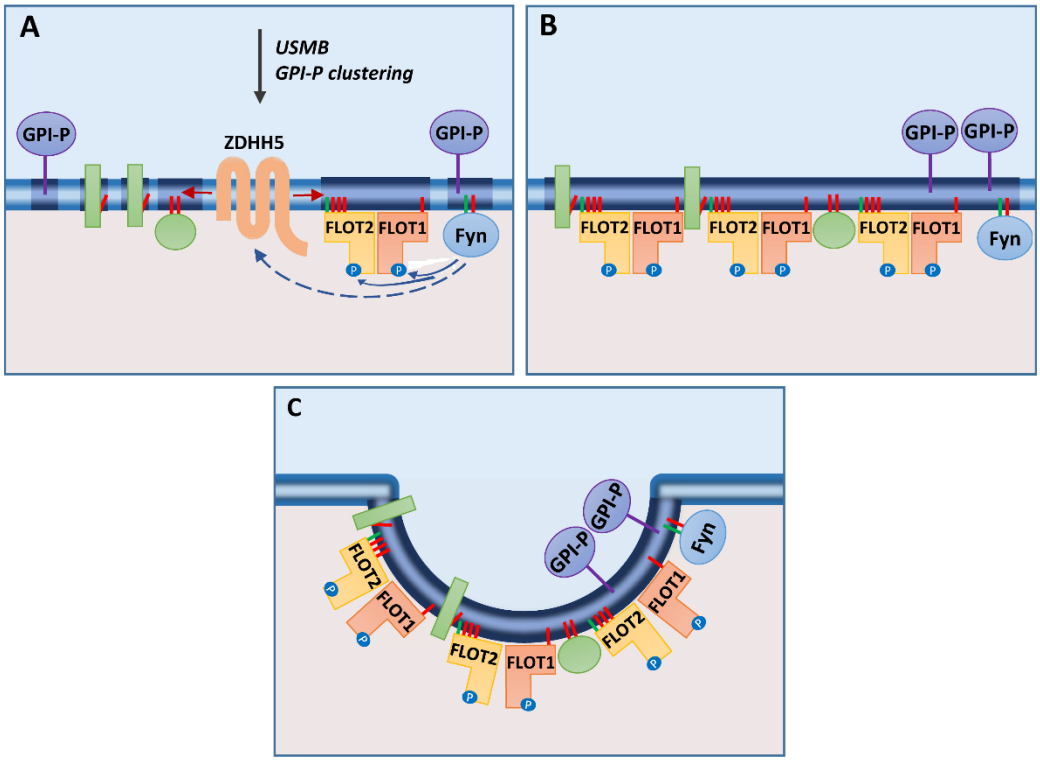

Figure 5.1 Flotillin-dependent endocytosis. (**A**) Endocytosis is triggered by ultrasound, microbubbles, and desipramine (USMB) or clustering of GPI-anchored proteins (GPI-P). Fyn kinase activates zDHHC5 (directly or indirectly) and phosphorylates flotillins. (**B**) *S*-palmitoylation of flotillins and other proteins which are anchored in rafts (navy-blue shaded fragment of the plasma membrane) causes coalescence of rafts. (**C**) Flotillins can facilitate invagination of the membrane which leads to pinching off of a vesicle. *N*-myristoylation and *S*-palmitoylation are indicated by green and red bars, respectively. Green rectangles and spheres represent *S*-palmitoylated transmembrane and peripheral membrane proteins, respectively. From Kwiatkowska, Matveichuk et al. (2020).

Results of my studies show that cross-linking of CD14 with antibodies that precedes its internalization induces *S*-palmitoylation of both flotillin-1 and flotillin-2, which is consistent with the mechanism described above. However, in this scenario, depletion of flotillins inhibits CD14 endocytosis which should lead to CD14 accumulation on the cell surface, whereas the opposite was observed in flotillin-deficient cells.

This discrepancy can be reconciled in light of the results of our group's recent studies. Ciesielska et al. (2022) found that about 25% of the cell surface CD14 can be endocytosed and then returned to the plasma membrane in a short period of time in non-stimulated cells,

without the participation of newly synthesized CD14. CD14 recycling is dependent on the participation of sorting nexins SNX1, SNX2, and SNX6. Inhibition of CD14 recycling caused by SNX1 silencing facilitated CD14 degradation, ultimately leading to a reduction of the total amount of CD14 and also to down-regulation of its cell surface pool (Ciesielska et al., 2022). These effects resemble those caused by flotillin depletion.

Furthermore, flotillins are engaged in the recycling of some plasma membrane receptors, including T cell receptor (TCR) which associates with rafts for signal transduction (Horejsi and Hrdinka, 2014). In this case, flotillins determine a rapid sorting of TCR toward Rab5- and next Rab11-positive recycling endosomes. Notably, flotillins are not involved in either TCR endocytosis from the plasma membrane or in the return of the receptor from the Rab11-bearing endosomes to the plasma membrane. Instead, flotillins participate in "pre-early endosomal sorting" of TCR, which coincides with its internalization from the plasma membrane (Redpath et al., 2019). In other words, flotillins direct TCR toward recycling endosomes and this may be promoted by flotillin-dependent clustering of TCR-bearing rafts. Moreover, flotillins also assist the trafficking of metalloproteinase MT1-MMP. The enzyme is internalized from the plasma membrane to Rab7-positive endosomes in cancer cells. That process is followed by MT1-MMP exocytosis from invadopodia and results in a local enrichment of this enzyme facilitating the migration of cancer cells through the extracellular matrix (Planchon et al., 2018).

It is currently unknown what triggers CD14 recycling, whether flotillins are indeed involved in this process and what the role of flotillin-1 and/or flotillin-2 *S*-palmitoylation is therein. Flotillin-depleted Raw264 cell clones appear to be a very good tool for future studies addressing these questions. The contribution of flotillins to CD14 recycling can explain the reduction of the CD14 level that I found in resting cells. This CD14 depletion could result in the reduction of CD14-dependent macrophage responses to LPS found in this study, which was also seen in SNX1-depleted cells (Ciesielska et al., 2022).

It should be remembered, however, that stimulation of cells with LPS induced an increase in the amount of *S*-palmitoylated flotillin-1 without affecting flotillin-2, as we found by mass spectrometry analysis (Sobocińska et al., 2018b). These results are in agreement with a growing body of data pointing to unique functions of flotillin-1, as discussed below.

Ad2-2) It has recently been shown that flotillin-1 can function independently of flotillin-2 and that some of its activities are regulated by *S*-palmitoylation of its Cys34 (Kwiatkowska, Matveichuk et al., 2020). Based on data obtained in my studies (decreased level of CD14 protein in flotillin-deficient Raw264 cells and increased amounts of *S*-palmitoylated flotillin-1 in LPS-stimulated cells), it can be speculated that *S*-palmitoylation of flotillin-1 could regulate the intracellular trafficking of *de novo* synthesized CD14 from the endoplasmic reticulum to the plasma membrane, as shown for IGF-1R.

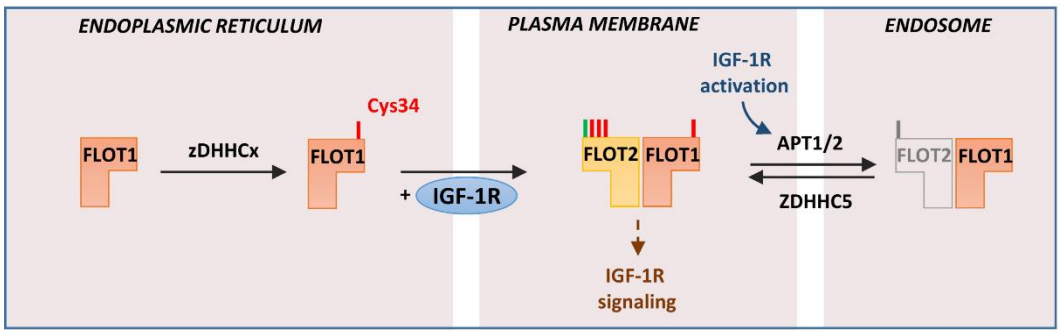

Figure 5.2 Regulation of IGF-1R trafficking and activity by *S*-palmitoylated flotillin-1. *S*-palmitoylation of newly synthesized flotillin-1 by zDHHCx (zDHHC6/zDHHC16?) at the membrane of the endoplasmic reticulum induces its translocation to the plasma membrane accompanied by IGF-1R trafficking. At the plasma membrane, flotillin-1 forms hetero-oligomers with flotillin-2 and undergoes cycles of depalmitoylation and *S*-palmitoylation which are necessary for sustained signaling of IGF-1R. These reactions can be catalyzed by APT1/2 or ABHD17 thioesterases and zDHHC5, respectively. Since *S*-palmitoylation o flotillin-1 is required for its association with the plasma membrane, flotillin-1 depalmitoylation can lead to its translocation to endosomes, either alone or with flotillin-2. From Kwiatkowska, Matveichuk et al. (2020), modified.

In the study of Jang and co-workers, a knockdown of flotillin-1 with shRNA in HeLa/HEK293 cells and "rescue" experiments with flotillin-1 muted in the palmitoylation site (Cys34Ala) precluded the localization of IGF-1R in the plasma membrane (Jang et al., 2015). Inhibition of IGF-1R-induced signaling and cell proliferation followed. Since the depletion of flotillin-1 or expression of Cys34Ala-mutated flotillin-1 led to a concomitant depletion of flotillin-2, the authors inhibited the activity of proteasomes, allowing flotillin-2 to re-appear without palmitoylated flotillin-1, and to associate with the plasma membrane in flotillin-1 depleted cells. However, the IGF-1R was not recruited to the plasma membrane in these conditions. Therefore, it has been proposed that flotillin-1 is *S*-palmitoylated by an unidentified zDHHC localized to the endoplasmic reticulum (zDHHCx in Fig. 5.2). My analysis indicates that zDHHC6 and zDHHC16 can be these enzymes. *S*-palmitoylation of flotillin-1 in the endoplasmic reticulum is crucial for the proper trafficking of flotillin-1 and the IGF-1R to the plasma membrane (Fig. 5.2).

Interestingly, the activation of the IGF-1R occurs in rafts enriched in hetero-oligomers of flotillin-1 and -2, and *S*-palmitoylation of flotillin-1 seems to be required for the assembly of these oligomers. Furthermore, Jang's team established that sustained IGF-1R signaling requires de- and re-palmitoylation of flotillin-1 (Jang et al., 2015). In the latter case, the involvement of zDHHC5 can be considered, as my analysis shows. It is tempting to speculate that a similar sequence of events is triggered by LPS. In LPS-stimulated cells the synthesis of CD14 is induced; the concomitant up-regulation of flotillin-1 level and its *S*-palmitoylation (all revealed in my analyses) can determine the transport of the newly synthesized CD14 toward the plasma membrane and facilitate LPS-induced signaling.

5.2. Role of zDHHC5 and zDHHC8 in *S*-palmitoylation of flotillins

I aimed to identify zDHHC(s) that can catalyze *S*-palmitoylation of flotillins, and then investigate the contribution of these enzymes to the LPS-induced production of pro-inflammatory cytokines. To achieve this goal, I co-expressed 23 palmitoyl acyltransferases of the zDHHC family with flotillin-1 or -2 in HEK293 cells, according to the method developed by Fukata (Fukata et al., 2006). This approach was performed to reveal zDHHC(s) whose co-expression enhanced flotillin-1 or -2 palmitoylation above the level observed in cells transfected with flotillin-1 or -2 alone. To detect flotillin palmitoylation, I used a method based on metabolic labeling cells with 17ODYA with a subsequent click reaction with biotin-azide, followed by the detection of palmitoylated proteins eluted from streptavidin beads. I verified the results of those analyzes using the ABE technique. Obtained data showed that flotillin-1 can be *S*-palmitoylated by several zDHHCs and this modification can affect the flotillin-1 abundance in cells. Studies performed on SARS-CoV-2 S protein using the ABE technique in model studies analogous to those carried out by myself have shown that this viral protein is *S*-palmitoylated by as many as 11 zDHHC (Li et. al. 2022), so flotillin-1 is no exception.

Next, I focused on zDHHC1-9, zDHHC11 (corresponding to DHHC10), and zDHHC16 as the most promising in terms of flotillin-1 palmitoylation. I found a marked increase in the amount of palmitoylated flotillin-1 in the presence of zDHHC3, 5, 7, and 8. zDHHC3 and zDHHC7 (localized in the Golgi apparatus) (Mukai et al., 2004; Ohno et al., 2006; Brigidi et al., 2015; Zaballa and van der Goot, 2018) are effective in palmitoylation of flotillin-1, and they also catalyze *S*-palmitoylation of multiple other proteins, above 40 and 25, respectively (Lemonidis et al., 2015; https://swisspalm.org). I assumed that *S*-palmitoylation of endogenous flotillins can depend on their cellular localization,

determining availability for zDHHCs. For this reason, in further studies, I focused on zDHHC8 and zDHHC5 which are located in the plasma membrane and in the membrane of intracellular vesicles (endosomes) (Mukai et al., 2004; Brigidi et al., 2015), as this location of zDHHC reflects the location of flotillins. Interestingly, in the case of zDHHC2, the third palmitoyl acyltransferase located in the plasma membrane, I found less efficacy in *S*-palmitoylation of flotillin-1, indicating the importance of the two other enzymes. Both zDHHC5 and zDHHC8 *S*-palmitoylate flotillin-1 and -2, and zDHHC8 prefers flotillin-1. While *S*-palmitoylation of flotillin-2 by zDHHC5 has been reported (Li et al., 2012) and the ability of zDHHC5 to *S*-palmitoylate flotillin-1 has been indicated (Wan et al., 2013), the finding of flotillin-1 and -2 *S*-palmitoylation by zDHHC8 is novel. I observed that *S*-palmitoylation of flotillins was accompanied by their accumulation in cells. The same effect was described for flotillin-1 by Wan et al. (2013). On the other hand, Li et al. (2012) reported that in zDHHC5-depleted cells in which *S*-palmitoylation of flotillin-2 was reduced, its oligomers were not detected. It can therefore be postulated that *S*-palmitoylation of flotillins facilitates their homo-oligomerization, which protects them from degradation and leads to their accumulation in cells.

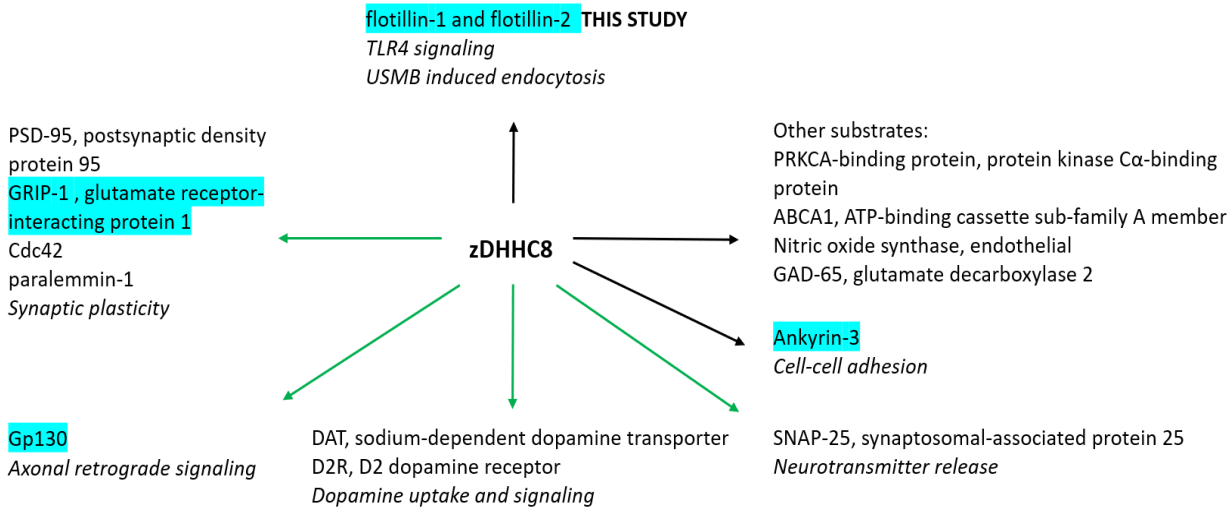

Figure 5.3 Identified substrates of human, mouse and rat zDHHC8, according to SwissPalm (16.05.22). The blue background indicates proteins which are also *S*-palmitoylated by zDHHC5; green arrows indicate substrates of zDHHC8 involved in various aspects of neuronal activity.

zDHHC5 and zDHHC8 are closely related palmitoyl acyltransferases which have an extended C-terminal part not found in other enzymes of the zDHHC family (Fukata et al., 2004; Thomas et al., 2012). A unique feature of the C-terminus of zDHHC5 and zDHHC8 is the common amino acid sequence enabling binding of the PDZ domain. Accordingly,

both zDHHC5 and zDHHC8 *S*-palmitoylate GRIP1 and bind/*S*-palmitoylate PSD-95 protein (of the MAGUK family) which contains several PDZ domains (Mukai et al., 2008; Thomas et al., 2012; Brigidi et al., 2015). On the other hand, MPP1, another member of the MAGUK family binds flotillins (Biernatowska et al., 2017), suggesting the formation of flotillin-MAGUK proteins-zDHHC5/8 complexes, as described above for the mechanism of endocytosis. *S*-palmitoylation of GRIP1 by zDHHC5/8 drives its association with endosomes, which in turn results in stimulation of AMPA-receptor recycling. *S*-palmitoylation of GRIP1 by zDHHC5 requires the involvement of the PDZ-binding domain of zDHHC5 (Thomas et al., 2012). Studies on MDCK epithelial cells showed that zDHHC5/8 and zDHHC14 are localized in the plasma membrane. However, only zDHHC5/8 are required for *S*-palmitoylation and association of ankyrin-G with the lateral part of the epithelial plasma membrane. A necessary condition for the proper organization of the lateral membrane is also the interaction between ankyrin-G and βII-spectrin which recognizes both phosphoinositides and palmitoylated ankyrin-G (He et al., 2014). Recently, Gp130 was reported to be the third common substrate for the zDHHC5/8 palmitoyl acyltransferases (Collura et al., 2020). These findings reinforce our observations by indicating that the zDHHC5/8 tandem can catalyze *S*-palmitoylation of flotillin-1 and flotillin-2.

According to the Human Protein Atlas database (https://proteinatlas.org), the expression of the zDHHC8-encoding gene is not tissue-specific. zDHHC8 was found in the plasma membrane of HEK293T cells, neurons, polarized epithelial cells, and in the Golgi apparatus, and intracellular vesicles, including endosomes (Thomas et al., 2012; He et al., 2014; Ernst et al., 2018). zDHHC8 is phosphorylated by some PKC serine kinases and is *S*-palmitoylated by unknown palmitoyl acyltransferase. Our data indicate that its expression in Raw264 cells is very low. The importance of zDHHC8 for neuronal functioning has been best documented so far. As mentioned above, both zDHHC8 and zDHHC5 were found to robustly palmitoylate Gp130 in dorsal root ganglion axons being involved in axonal retrograde signaling (Collura et al., 2020). zDHHC8 also *S*-palmitoylates two other neuronal proteins: GRIP1b (together with zDHHC5) and PSD-95, which is a scaffolding protein that regulates the organization of the postsynaptic density of dendrites and, together with GRIP1, modulates the local turnover of AMPA-type glutamate receptors (Mukai et al., 2008; Thomas et al., 2012). zDHHC8 also palmitoylates Cdc42 (a brain-specific form) which promotes stabilization of spines, a dendritic protrusion - the postsynaptic element at most synapses in the brain. A list of human and mouse zDHHC8

substrates is shown in Fig. 5.3. Not surprisingly, zDHHC8 deficiency is linked with the development of mental illnesses, including schizophrenia (Faul et al., 2005; Mukai et al., 2008). zDHHC8 could also promote the formation and multiplication of seizures in humans and could be a key target in epilepsy treatment as an AMPA receptor modulator (Yang et al., 2018).

Results of my study indicate that in model conditions zDHHC8 can *S*-palmitoylate flotillin-1 and to a lower extent also flotillin-2, but does not modify DGKε. Moreover, co-transfection of zDHHC8 with flotillin-1 (but not flotillin-2) led to an enrichment of zDHHC8 in comparison to cells overexpressing the enzyme alone, indicating that at certain conditions the two proteins can affect each other. Despite the clear influence of zDHHC8 on flotillin-1 *S*-palmitoylation in model studies, this palmitoyl acyltransferase does not appear to be important for LPS-induced signaling in Raw264 cells, possibly due to its low expression in these cells. It seems that zDHHC5 rather than zDHHC8 activity is involved in TLR4 signaling in macrophages. I found that silencing of zDHHC5, but not the minor zDHHC8, inhibited LPS-induced expression of *Tnfa* and *Ccl5* encoding two cytokines generated in MyD88- and TRIF-dependent manner, respectively. It also markedly inhibited the production of TNFα and CCL5/RANTES, and also other cytokines (IL-1Ra, IP10) produced in the TRIF-dependent manner. As mentioned earlier, zDHHC5 is located in the plasma membrane where it *S*-palmitoylates several substrates including flotillin-2, but can also be present in endosomal compartments. zDHHC5 is phosphorylated by Fyn tyrosine kinase of the Src family and *S*-palmitoylated by zDHHC20 (Plain et al., 2020). zDHHC5 is more extensively studied than zDHHC8 and has a wider pool of identified substrates (Fig. 5.4). In fibroblasts, knockdown of zDHHC5 led to inhibition of so-called massive endocytosis (MEND). zDHHC5-flotillin-1/2-Fyn kinase triad is involved in USBM-induced endocytosis (Fekri et al., 2019). In neurons, it contributes to the synaptic plasticity of dendrites by regulating the recycling and stability of AMPA receptors in the postsynaptic membrane. This process requires interaction of zDHHC5 with Fyn kinase and PSD-95 scaffolding protein at the postsynaptic membrane in resting conditions, and also involves zDHHC8, and the GRIP1 protein, as described above. Increased neuronal activity reduces the activity of Fyn kinase and leads to disassembly of the zDHHC5/PSD95 with subsequent endocytosis of zDHHC5, its translocation to recycling endosomes, and local *S*-palmitoylation of δ-catenin. After the fusion of the recycling endosomes with the postsynaptic membrane, δ-catenin increases the stabilization of AMPA receptors in the membrane.

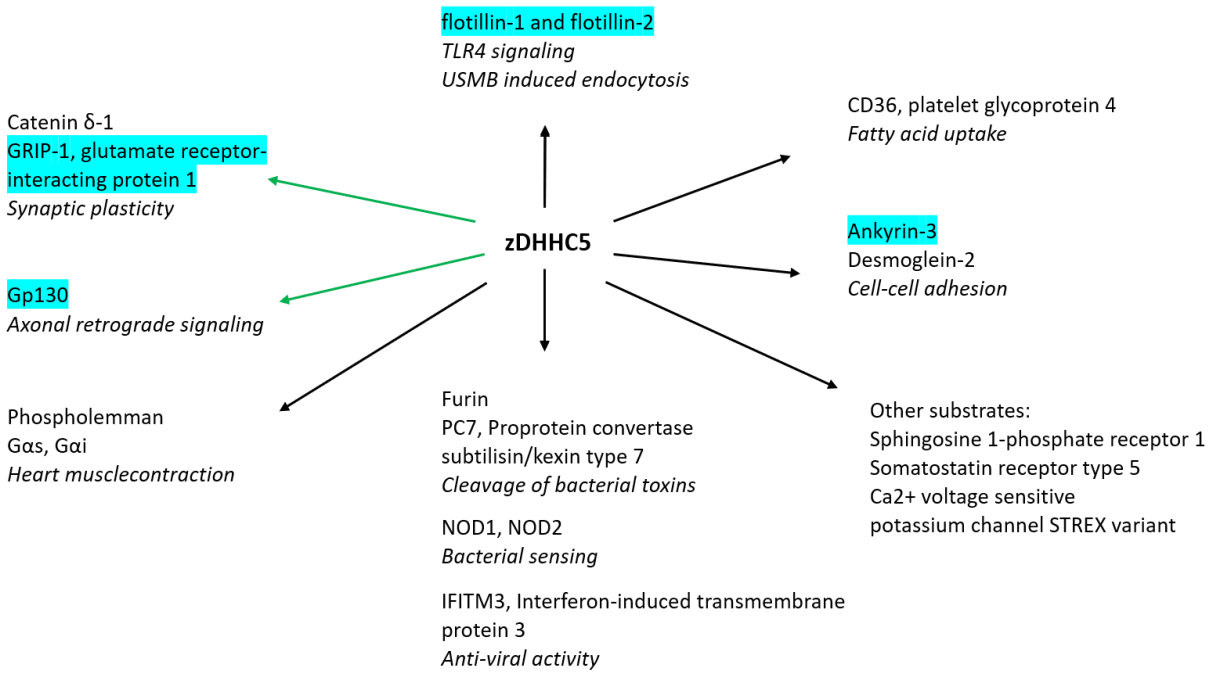

Figure 5.4 Identified substrates of human, mouse and rat zDHHC5, according to SwissPalm (16.05.22) and Woodley and Collins (2021). The blue background indicates proteins which are also *S*-palmitoylated by zDHHC8; green arrows indicate substrates of zDHHC5 involved in various aspects of neuronal activity.

Concomitantly, the PSD-95-based submembranous protein complex is rebuilt (Woodley and Collins, 2021). Deletion of the *ZdhhcC5* gene in a region of chromosome 11 is connected with bipolar disorder (Fallin et al., 2004). A novel study reported that zDHHC5 regulates Ras activity in pancreatic cancer (Ritho and Dixon, 2022). zDHHC5 is also engaged in antiviral and antibacterial innate immunity reactions. It *S*-palmitoylates nucleotide oligomerization domain (NOD)-like receptor 1 (NOD1) and NOD2, crucial for recognition of bacteria which invade a cell, and interferon-induced transmembrane protein 3 (IFITM3) with antiviral activity (Woodley and Collins, 2021). It should be noted, however, that none of the zDHHC5 substrates, except for flotillins, were found to be involved in TLR4-induced signaling. Therefore, the inhibitory effect of *Zdhhc5* silencing toward LPS-induced cytokine production is likely related to the impaired *S*-palmitoylation of flotillin-1 and flotillin-2.

Given the properties of zDHHC5 on one hand and flotillin functions described in the previous chapter on the other, it can be speculated that zDHHC5 can *S*-palmitoylate flotillin-1 and -2 under the plasma membrane. My studies indicate that *S*-palmitoylation of flotillin-1 and -2 can be triggered by clustering of CD14, which is the first known event to occur upon LPS binding by CD14 (Płóciennkowska et al., 2015b). Flotillins can facilitate

CD14 clustering, as described for several other plasma membrane proteins (Kwiatkowska, Matveichuk et al., 2020), and can be involved in the subsequent endocytosis of CD14 (in resting cells) or CD14/TLR4 (in LPS-stimulated cells) and CD14 recycling, as described above for TCR. Palmitoylation/depalmitoylation cycles of flotillin-1 and its interaction with flotillin-2 guarantee sustained signaling of the IGF-1R (Jang et al., 2015), and an analogous scenario for TLR4 signaling can be envisioned. In addition, it seems likely that TLR4-triggered signaling induces *S*-palmitoylation of flotillin-1 in the endoplasmic reticulum by zDHHC6/16 required for newly synthesized CD14 transport from the endoplasmic reticulum to the plasma membrane. The possible interactions between CD14 and flotillins, and zDHHCs involved are shown in Fig. 5.5.

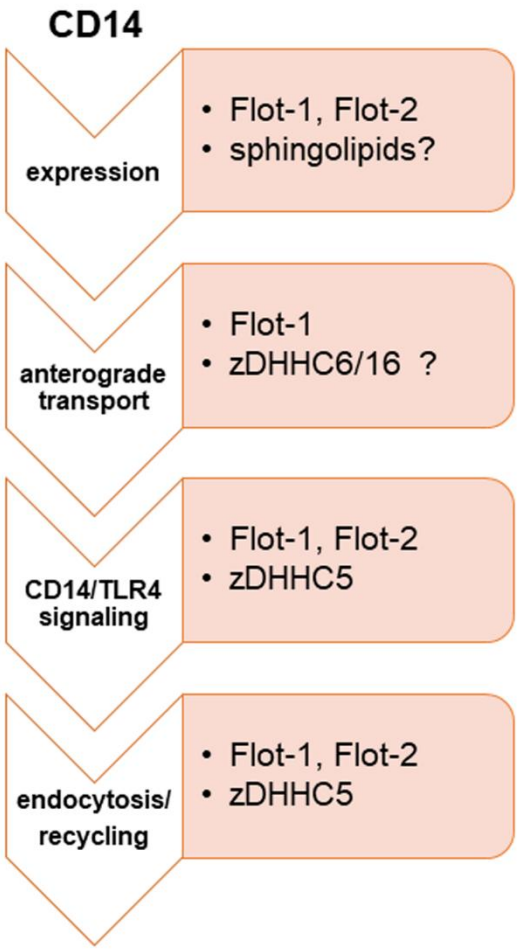

Figure 5.5. Schematic diagram of the interactions between CD14 and flotillins, and zDHHCs involved in these processes (see text for details).

The activation of CD14/TLR4 helps to combat bacterial infections but when exaggerated can lead to potentially fatal sepsis. Moreover, a low-grade inflammation induced by LPS leads to so-called metabolic endotoxemia linked with several human diseases, like type 2 diabetes. These facts fuel interest in molecular mechanisms of activation of macrophages by LPS and the presented study reveals that flotillins are

involved in these processes. Proteins bearing the SPFH domain, including flotillins, have recently been optimistically hailed as promising therapeutic targets in "a myriad of diseases" (Wang et al., 2020). This hope is based on the anti-cancer and anti-inflammatory *in vitro* activity of small natural cyclic compounds, flavaglines, targeting prohibitin-1/2 of the SPFH family. These molecules are believed to affect the conformation of prohibitins interfering thereby with their scaffolding functions. Analogous small molecules targeting flotillins have not yet been discovered, but this is likely given the successful synthesis of several prohibitin-blocking compounds (Wang et al., 2020).

5.3 Methodological aspects of detection of palmitoylated proteins in LPS-stimulated cells

I used two non-radioactive methods in my studies to detect palmitoylated proteins. The first one is based on metabolic labeling of living cells with a palmitic acid analogue, 17ODYA, followed by a so-called "click" reaction, and the second one, so-called ABE in which palmitic acid moieties of proteins are substituted with biotin. I developed a modification of the click chemistry-based technique. For this purpose, 17ODYA bound to proteins was subjected to the click reaction with biotin and subsequently labeled proteins were enriched on streptavidin-coupled beads. Due to forceful biotin-streptavidin binding (Chivers et al., 2011), the elution of bound proteins is troublesome. I found a combination of solutions, including H_2O and β-mercaptoethanol which allowed the proteins to be recovered from the beads. I also obtained an internal standard which allowed me to assess the protein elution efficiency. It was biotinylated GST added to cell lysates before their incubation with streptavidin beads. Successful elution of streptavidin-bound proteins allows a subsequent simultaneous immunoblotting analysis of several proteins, both endogenous and overproduced, provided that specific antibodies are available. Thereby, the detected changes in the amount of palmitoylated proteins are in control of each other. As could be expected, I found that stimulation of Raw264 cells with 100 ng/ml LPS for 1 h induced synthesis and concomitant palmitoylation of tmTNFα - the transmembrane precursor of this major pro-inflammatory cytokine. LPS also induced an increase in the amount of palmitoylated eiF5A2, an eukaryotic translation factor, and flotillin-1, raft protein which became the subject of this study. These results were consistent with mass spectrometry analysis of LPS-induced changes in protein palmitoylation in Raw264 cells for which 17ODYA-labeling of proteins was used (Sobocińska et al., 2018b). Interestingly, eIF5A2 and eIF5A1 are the only known eukaryotic proteins containing a unique amino

acid hypusine. It is synthesized at the ε-amino group of lysine during post-translational modification called hypusination. Two enzymes - deoxyhypusine synthase (DHS) and deoxyhypusine hydroxylase (DOHH) - are responsible for this modification, which is essential for the functioning of eIF5As proteins. eIF5A2 is mainly localized in the nucleus but tends to localize in the cytoplasm after hypusination. eiF5A2 is a potential biomarker in many types of human cancer (Wu et al., 2020). My analysis indicates that eiF5A2 is palmitoylated and this eIF5A2 modification was highly upregulated in LPS-stimulated cells, suggesting its contribution to eiF5A2 functioning in LPS-induced protein synthesis. eiF5A2 palmitoylation site(s) is not identified, however, the protein was found in palmitoylomes of several human and murine cells (https://swisspalm.org).

Additionally, the variation of the click-based technique used by me is also useful in detecting GPI-anchored proteins, like CD14. Tagging of either N- or C-terminus of these proteins can hinder their proper synthesis and attachment of the GPI anchor. I found that 17ODYA incorporates into the GPI anchor of CD14 which explains the results of the high through-put proteomic analysis of 17ODYA-labeled proteins (Sobocińska et al., 2018b).

Both the click-based and the ABE techniques have pros and cons, as indicated in the Introduction. Therefore, the best option is to use both methods for the detection of protein palmitoylation. This approach allowed me to reveal the previously unknown *S*-palmitoylation of OPAL1 adaptor protein.

5.4 OPAL1, its functions and *S*-palmitoylation

OPAL1 (WBP1L) is a transmembrane adaptor protein expressed in T and B lymphocytes, neutrophils, monocytes, and macrophages where it is located in the plasma membrane and endosomal compartments. Studies of Brdicka's group showed that OPAL1 binds and activates the NEDD4-family E3 ubiquitin ligases, which then catalyze the ubiquitination of the CXRC4 receptor. As a result, the receptor undergoes proteasomal degradation and its signaling cascade, including ERK1/2 and Akt phosphorylation, is down-regulated. Since the CXCR4 receptor is involved in the maintenance of hematopoiesis, OPAL1 is also involved in this process (Borna et al., 2020). On the other hand, recent studies showed that OPAL1 belongs to a group of genes whose expression is considered a part of the "signature genes" of ETV6-RUNX1-linked lymphoblastic leukemia. This type of childhood acute lymphoblastic leukemia is associated with the presence of ETV6-RUNX1 fusion protein formed by translocation of the *ETV6* gene fragment and its fusion with *RUNX1* encoding a transcription factor. ETV6 is a

transcriptional repressor and *WBP1L* is one of its target genes. In the fusion protein encoded by ETV6-RUNX1, ETV6 is inactive and therefore no longer represses *WBP1L* expression (Chen et al., 2021). As a result, OPAL1-dependent activation of NEDD4-family E3 ubiquitin ligases is enhanced and the CXRC4 receptor, their substrate, is down-regulated, which altogether explains why a high level of OPAL1 mRNA is a good prognostic marker for the treatment of leukemia. Additionally, the study of Cardenas' group showed that methylation of the *WBP1L* gene is altered in the placenta of smokers which resulted in 135-g lower birth weight in newborn babies (Cardenas et al., 2019).

My studies performed in the collaboration with Dr. Brdicka's group show that OPAL1 undergoes *S*-palmitoylation. We established that the modification takes place in the CCCVC motif located at the border of the transmembrane and the cytoplasmic fragments of OPAL1. This location of *S*-palmitoylated cysteine residues is found in several other proteins, including hemagglutinin A of influenza virus (Sobocińska et al., 2018a), adaptor proteins PAG and LAT. Palmitoylation of the latter two proteins determines their raft localization. In turn, enzymes that bind to the above-mentioned adaptor proteins are involved in signaling pathways of raft-associated immunoreceptors, including TCR, FcεRI, and FcγIIA (Stepanek et al., 2014).

At present, we can only speculate on the consequences of OPAL1 *S*-palmitoylation. Among substrates of NEDD4 and ITCH (two members of the NEDD4 family of E3 ubiquitin ligases) is RNF11, a protein that associates with membranes of early and recycling endosomes. RNF11 is *N*-myristoylated and *S*-palmitoylated to then be ubiquitinated and degraded. RNF11 overexpression contributes to tumorigenesis (Santonico et al., 2010). If *S*-palmitoylated OPAL1 is also present in rafts of early and recycling endosomes, co-localization of OPAL1-NEDD4 with *S*-palmitoylated RNF11 therein would facilitate the ubiquitination of RNF11 leading to a reduction of RNF11 level. This chain of events would be consistent with the anti-cancer properties of OPAL1.

6. Summary and conclusions

The data presented in this dissertation provide insights into the role of flotillins and their *S*-palmitoylation in the pro-inflammatory signaling triggered by LPS. Specifically, the results indicate that:

1. During stimulation of Raw264 macrophage-like cells with LPS, the cellular level of flotillin-1 and the amount of its *S*-palmitoylated form increase. The positive association between these two phenomena was confirmed by model studies in which flotillin-1 was overproduced together with individual zDHHCs catalyzing its *S*-palmitoylation. LPS does not induce such flotillin-2 changes.

2. Participation of flotillins is required for the maximal pro-inflammatory response induced by LPS.

3. Flotillins are involved in cell activation by low LPS concentration, to a greater extent in the TRIF-dependent endosomal TLR4 signaling pathway than in the MyD88-dependent pathway. Those are processes that require CD14 involvement.

4. Flotillins regulate the cellular level of CD14, affecting the amount of its mRNA, the total amount of CD14 in cells, and its pool located on the surface of the plasma membrane. No such changes were observed for TLR4.

5. On the other hand, clustering of CD14 in the plasma membrane induces *S*-palmitoylation of flotillin-1 and flotillin-2.

6. *S*-palmitoylation of flotillin-1 and flotillin-2 is catalyzed by zDHHC5 and zDHHC8, and potentially some other zDHHCs.

7. The participation of zDHHC5 is required for the response to LPS triggered in both signaling pathways of the TLR4 with emphasis on the TRIF-dependent pathway and may be associated with its participation in *S*-palmitoylation of flotillins.

Taken together, the data indicate that flotillins modulate the cellular level of CD14 and interact (indirectly) with CD14, thereby affecting the intensity of the LPS-induced pro-inflammatory response. Flotillins are likely to be involved in CD14 endocytosis and recycling, as well as in the transport of newly synthesized CD14 to the plasma membrane, all events can be regulated by *S*-palmitoylation of flotillins catalyzed among others by zDHHC5.

8. The above results were obtained, i.a., owing to the development of a modification of a technique for detecting palmitoylated protein. It involves enrichment of 17ODYA (palmitic acid analogue)-labeled proteins and their recovery from streptavidin-coupled beads. The advantage of this technique is that it allows simultaneous identification of several endogenous palmitoylated proteins as well as proteins ectopically expressed in cells.

9. The described technique allowed the detection of *S*-palmitoylation of an adaptor protein OPAL1, which was confirmed with an application of a classical ABE technique. *S*-palmitoylation can determine raft localization of OPAL1.

7. Publications by Orest V. Matveichuk

1. Sobocińska J., Roszczenko-Jasińska P., Zaręba-Kozioł M., Hromada-Judycka A., **Matveichuk O.V**., Traczyk G., Łukasiuk K., Kwiatkowska K. Lipopolysaccharide upregulates palmitoylated enzymes of the phosphatidylinositol cycle: An insight from proteomic studies. *Molecular and Cellular Proteomics* (2018) 17(2):233-254. doi: 10.1074/mcp.RA117.000050.

2. Borna S., Drobek A., Kralova J., Glatzova D., Splichalova I., Fabisik M., Pokorna J., Skopcova T., Angelisova P., Kanderova V., Starkova J., Stanek P., **Matveichuk O.V.,** Pavliuchenko N., Kwiatkowska K., Protty M.B., Tomlinson M.G., Alberich-Jorda M., Korinek V., Brdicka T. Transmembrane adaptor protein WBP1L regulates CXCR4 signalling and murine haematopoiesis. *Journal of Cellular and Molecular Medicine* (2020) 24(2):1980-1992. doi: 10.1111/jcmm.14895.

3. Kwiatkowska K.*, **Matveichuk O.V.*,** Fronk J., Ciesielska A. Flotillins: At the intersection of protein *S*-palmitoylation and lipid-mediated signaling. *International Journal of Molecular Sciences* (2020) 21(7):2283. doi: 10.3390/ijms21072283.

* These authors contributed equally to this work.

8. Literature

1. Abrami L, Dallavilla T, Sandoz PA, et al. Identification and dynamics of the human ZDHHC16-ZDHHC6 palmitoylation cascade. *Elife*. 2017;6:e27826. Published 2017 Aug 15. doi:10.7554/eLife.27826

2. Aït-Slimane T, Galmes R, Trugnan G, Maurice M. Basolateral internalization of GPI-anchored proteins occurs via a clathrin-independent flotillin-dependent pathway in polarized hepatic cells. *Mol Biol Cell*. 2009;20(17):3792-3800. doi:10.1091/mbc.e09-04-0275

3. Aksoy E, Taboubi S, Torres D, et al. The p110δ isoform of the kinase PI(3)K controls the subcellular compartmentalization of TLR4 signaling and protects from endotoxic shock [published correction appears in Nat Immunol. 2013 Aug;14(8):877. Berenjeno-Martin, Inma [corrected to Berenjeno, Inma M]]. *Nat Immunol*. 2012;13(11):1045-1054. doi:10.1038/ni.2426

4. Amaddii M, Meister M, Banning A, et al. Flotillin-1/reggie-2 protein plays dual role in activation of receptor-tyrosine kinase/mitogen-activated protein kinase signaling. *J Biol Chem*. 2012;287(10):7265-7278. doi:10.1074/jbc.M111.287599

5. Anderson KV, Bokla L, Nüsslein-Volhard C. Establishment of dorsal-ventral polarity in the Drosophila embryo: the induction of polarity by the Toll gene product. *Cell*. 1985;42(3):791-798. doi:10.1016/0092-8674(85)90275-2

6. Anwar MA, Basith S, Choi S. Negative regulatory approaches to the attenuation of Toll-like receptor signaling. *Exp Mol Med*. 2013;45(2):e11. Published 2013 Feb 22. doi:10.1038/emm.2013.28

7. Aramsangtienchai P, Spiegelman NA, He B, et al. HDAC8 Catalyzes the Hydrolysis of Long Chain Fatty Acyl Lysine. *ACS Chem Biol*. 2016;11(10):2685-2692. doi:10.1021/acschembio.6b00396

8. Babuke T, Tikkanen R. Dissecting the molecular function of reggie/flotillin proteins. *Eur J Cell Biol*. 2007;86(9):525-532. doi:10.1016/j.ejcb.2007.03.003

9. Berger J, Howard AD, Brink L, et al. COOH-terminal requirements for the correct processing of a phosphatidylinositol-glycan anchored membrane protein. *J Biol Chem*. 1988;263(20):10016-10021.

10. Berger T, Ueda T, Arpaia E, et al. Flotillin-2 deficiency leads to reduced lung metastases in a mouse breast cancer model. *Oncogene*. 2013;32(41):4989-4994. doi:10.1038/onc.2012.499

11. Bickel PE, Scherer PE, Schnitzer JE, Oh P, Lisanti MP, Lodish HF. Flotillin and epidermal surface antigen define a new family of caveolae-associated integral membrane proteins. *J Biol Chem*. 1997;272(21):13793-13802. doi:10.1074/jbc.272.21.13793

12. Biernatowska A, Podkalicka J, Majkowski M, et al. The role of MPP1/p55 and its palmitoylation in resting state raft organization in HEL cells. *Biochim Biophys Acta*. 2013;1833(8):1876-1884. doi:10.1016/j.bbamcr.2013.03.009

13. Björkbacka H, Fitzgerald KA, Huet F, et al. The induction of macrophage gene expression by LPS predominantly utilizes Myd88-independent signaling cascades. *Physiol Genomics*. 2004;19(3):319-330. doi:10.1152/physiolgenomics.00128.2004

14. Blaskovic S, Blanc M, van der Goot FG. What does S-palmitoylation do to membrane proteins?. *FEBS J*. 2013;280(12):2766-2774. doi:10.1111/febs.12263

15. Bodrikov V, Pauschert A, Kochlamazashvili G, Stuermer CAO. Corrigendum to "Reggie-1 and reggie-2 (flotillins) participate in Rab11a-dependent cargo trafficking, spine synapse formation and LTP-related AMPA receptor (GluA1) surface exposure in mouse hippocampal neurons" (Exp. Neurol. 289, Pages 31-45). *Exp Neurol*. 2017;293:200. doi:10.1016/j.expneurol.2017.02.016

16. Borna S, Drobek A, Kralova J, et al. Transmembrane adaptor protein WBP1L regulates CXCR4 signalling and murine haematopoiesis. *J Cell Mol Med*. 2020;24(2):1980-1992. doi:10.1111/jcmm.14895

17. Borzęcka K, Płóciennikowska A, Björkelund H, Sobota A, Kwiatkowska K. CD14 mediates binding of high doses of LPS but is dispensable for TNF-α production. *Mediators Inflamm*. 2013;2013:824919. doi:10.1155/2013/824919

18. Borzęcka-Solarz K, Dembińska J, Hromada-Judycka A, et al. Association of Lyn kinase with membrane rafts determines its negative influence on LPS-induced signaling. *Mol Biol Cell*. 2017;28(8):1147-1159. doi:10.1091/mbc.E16-09-0632

19. Bradford MM. A rapid and sensitive method for the quantitation of microgram quantities of protein utilizing the principle of protein-dye binding. *Anal Biochem*. 1976;72:248-254. doi:10.1006/abio.1976.9999

20. Brigidi GS, Santyr B, Shimell J, Jovellar B, Bamji SX. Activity-regulated trafficking of the palmitoyl-acyl transferase DHHC5. *Nat Commun*. 2015;6:8200. Published 2015 Sep 3. doi:10.1038/ncomms9200

21. Bufler P, Stiegler G, Schuchmann M, et al. Soluble lipopolysaccharide receptor (CD14) is released via two different mechanisms from human monocytes and CD14 transfectants. *Eur J Immunol*. 1995;25(2):604-610. doi:10.1002/eji.1830250244

22. Burnaevskiy N, Peng T, Reddick LE, Hang HC, Alto NM. Myristoylome profiling reveals a concerted mechanism of ARF GTPase deacylation by the bacterial protease IpaJ. *Mol Cell*. 2015;58(1):110-122. doi:10.1016/j.molcel.2015.01.040

23. Cani PD, Amar J, Iglesias MA, et al. Metabolic endotoxemia initiates obesity and insulin resistance. *Diabetes*. 2007;56(7):1761-1772. doi:10.2337/db06-1491

24. Cardenas A, Lutz SM, Everson TM, Perron P, Bouchard L, Hivert MF. Mediation by Placental DNA Methylation of the Association of Prenatal Maternal Smoking and Birth

Weight [published correction appears in Am J Epidemiol. 2020 Oct 1;189(10):1212]. *Am J Epidemiol*. 2019;188(11):1878-1886. doi:10.1093/aje/kwz184

25. Carty M, Goodbody R, Schröder M, Stack J, Moynagh PN, Bowie AG. The human adaptor SARM negatively regulates adaptor protein TRIF-dependent Toll-like receptor signaling. *Nat Immunol*. 2006;7(10):1074-1081. doi:10.1038/ni1382

26. Chaplin DD. Overview of the immune response. *J Allergy Clin Immunol*. 2010;125(2 Suppl 2):S3-S23. doi:10.1016/j.jaci.2009.12.980

27. Charollais J, Van Der Goot FG. Palmitoylation of membrane proteins (Review). *Mol Membr Biol*. 2009;26(1):55-66. doi:10.1080/09687680802620369

28. Charron G, Zhang MM, Yount JS, et al. Robust fluorescent detection of protein fatty-acylation with chemical reporters. *J Am Chem Soc*. 2009;131(13):4967-4975. doi:10.1021/ja810122f

29. Chen B, Sun Y, Niu J, Jarugumilli GK, Wu X. Protein Lipidation in Cell Signaling and Diseases: Function, Regulation, and Therapeutic Opportunities. *Cell Chem Biol*. 2018;25(7):817-831. doi:10.1016/j.chembiol.2018.05.003

30. Chen CY, Shih YC, Hung YF, Hsueh YP. Beyond defense: regulation of neuronal morphogenesis and brain functions via Toll-like receptors. *J Biomed Sci*. 2019;26(1):90. Published 2019 Nov 4. doi:10.1186/s12929-019-0584-z

31. Chen D, Camponeschi A, Nordlund J, et al. RAG1 co-expression signature identifies ETV6-RUNX1-like B-cell precursor acute lymphoblastic leukemia in children. *Cancer Med*. 2021;10(12):3997-4003. doi:10.1002/cam4.3928

32. Chesarino NM, Hach JC, Chen JL, et al. Chemoproteomics reveals Toll-like receptor fatty acylation. *BMC Biol*. 2014;12:91. Published 2014 Nov 5. doi:10.1186/s12915-014-0091-3

33. Chiang CY, Veckman V, Limmer K, David M. Phospholipase Cγ-2 and intracellular calcium are required for lipopolysaccharide-induced Toll-like receptor 4 (TLR4) endocytosis and interferon regulatory factor 3 (IRF3) activation. *J Biol Chem*. 2012;287(6):3704-3709. doi:10.1074/jbc.C111.328559

34. Chivers CE, Koner AL, Lowe ED, Howarth M. How the biotin-streptavidin interaction was made even stronger: investigation via crystallography and a chimaeric tetramer. *Biochem J*. 2011;435(1):55-63. doi:10.1042/BJ20101593

35. Chowdhury SM, Zhu X, Aloor JJ, et al. Proteomic Analysis of ABCA1-Null Macrophages Reveals a Role for Stomatin-Like Protein-2 in Raft Composition and Toll-Like Receptor Signaling. *Mol Cell Proteomics*. 2015;14(7):1859-1870. doi:10.1074/mcp.M114.045179

36. Ciesielska A, Krawczyk M, Sas-Nowosielska H, Hromada-Judycka A, Kwiatkowska K. CD14 recycling modulates LPS-induced inflammatory responses of murine macrophages. *Traffic*. 2022;23(6):310-330. doi:10.1111/tra.12842

37. Ciesielska A, Matyjek M, Kwiatkowska K. TLR4 and CD14 trafficking and its influence on LPS-induced pro-inflammatory signaling. *Cell Mol Life Sci*. 2021;78(4):1233-1261. doi:10.1007/s00018-020-03656-y

38. Collura KM, Niu J, Sanders SS, Montersino A, Holland SM, Thomas GM. The palmitoyl acyltransferases ZDHHC5 and ZDHHC8 are uniquely present in DRG axons and control retrograde signaling via the Gp130/JAK/STAT3 pathway. *J Biol Chem*. 2020;295(46):15427-15437. doi:10.1074/jbc.RA120.013815

39. Cremona ML, Matthies HJ, Pau K, et al. Flotillin-1 is essential for PKC-triggered endocytosis and membrane microdomain localization of DAT [published correction appears in Nat Neurosci. 2011 Dec;14(2):1617]. *Nat Neurosci*. 2011;14(4):469-477. doi:10.1038/nn.2781

40. Dattaroy D, Seth RK, Das S, et al. Sparstolonin B attenuates early liver inflammation in experimental NASH by modulating TLR4 trafficking in lipid rafts via NADPH oxidase activation. *Am J Physiol Gastrointest Liver Physiol*. 2016;310(7):G510-G525. doi:10.1152/ajpgi.00259.2015

41. Davda D, El Azzouny MA, Tom CT, et al. Profiling targets of the irreversible palmitoylation inhibitor 2-bromopalmitate. *ACS Chem Biol*. 2013;8(9):1912-1917. doi:10.1021/cb400380s

42. Deguine J, Barton GM. MyD88: a central player in innate immune signaling. *F1000Prime Rep*. 2014;6:97. Published 2014 Nov 4. doi:10.12703/P6-97

43. Deng Y, Ge P, Tian T, et al. Prognostic value of flotillins (flotillin-1 and flotillin-2) in human cancers: A meta-analysis. *Clin Chim Acta*. 2018;481:90-98. doi:10.1016/j.cca.2018.02.036

44. Drisdel RC, Alexander JK, Sayeed A, Green WN. Assays of protein palmitoylation. *Methods*. 2006;40(2):127-134. doi:10.1016/j.ymeth.2006.04.015

45. Edgar AJ, Polak JM. Flotillin-1: gene structure: cDNA cloning from human lung and the identification of alternative polyadenylation signals. *Int J Biochem Cell Biol*. 2001;33(1):53-64. doi:10.1016/s1357-2725(00)00069-8

46. El-Husseini Ael-D, Schnell E, Dakoji S, et al. Synaptic strength regulated by palmitate cycling on PSD-95. *Cell*. 2002;108(6):849-863. doi:10.1016/s0092-8674(02)00683-9

47. Ernst AM, Syed SA, Zaki O, et al. S-Palmitoylation Sorts Membrane Cargo for Anterograde Transport in the Golgi. *Dev Cell*. 2018;47(4):479-493.e7. doi:10.1016/j.devcel.2018.10.024

48. Esparza GA, Teghanemt A, Zhang D, Gioannini TL, Weiss JP. Endotoxin albumin complexes transfer endotoxin monomers to MD-2 resulting in activation of TLR4. *Innate Immun*. 2012;18(3):478-491. doi:10.1177/1753425911422723

49. Fallin MD, Lasseter VK, Wolyniec PS, et al. Genomewide linkage scan for bipolar-disorder susceptibility loci among Ashkenazi Jewish families. *Am J Hum Genet*. 2004;75(2):204-219. doi:10.1086/422474

50. Faul T, Gawlik M, Bauer M, et al. ZDHHC8 as a candidate gene for schizophrenia: analysis of a putative functional intronic marker in case-control and family-based association studies. *BMC Psychiatry*. 2005;5:35. Published 2005 Oct 14. doi:10.1186/1471-244X-5-35

51. Fekri F, Abousawan J, Bautista S, et al. Targeted enhancement of flotillin-dependent endocytosis augments cellular uptake and impact of cytotoxic drugs. *Sci Rep*. 2019;9(1):17768. Published 2019 Nov 28. doi:10.1038/s41598-019-54062-9

52. Fitzgerald KA, Kagan JC. Toll-like Receptors and the Control of Immunity. *Cell*. 2020;180(6):1044-1066. doi:10.1016/j.cell.2020.02.041

53. Fitzgerald KA, Rowe DC, Barnes BJ, et al. LPS-TLR4 signaling to IRF-3/7 and NF-kappaB involves the toll adapters TRAM and TRIF [published correction appears in J Exp Med. 2003 Nov 3;198(9):following 1450]. *J Exp Med*. 2003;198(7):1043-1055. doi:10.1084/jem.20031023

54. FOLCH J, LEES M, SLOANE STANLEY GH. A simple method for the isolation and purification of total lipides from animal tissues. *J Biol Chem*. 1957;226(1):497-509.

55. Fork C, Hitzel J, Nichols BJ, Tikkanen R, Brandes RP. Flotillin-1 facilitates toll-like receptor 3 signaling in human endothelial cells. *Basic Res Cardiol*. 2014;109(6):439. doi:10.1007/s00395-014-0439-4

56. Forrester MT, Hess DT, Thompson JW, et al. Site-specific analysis of protein S-acylation by resin-assisted capture. *J Lipid Res*. 2011;52(2):393-398. doi:10.1194/jlr.D011106

57. Fraser NJ, Howie J, Wypijewski KJ, Fuller W. Therapeutic targeting of protein S-acylation for the treatment of disease. *Biochem Soc Trans*. 2020;48(1):281-290. doi:10.1042/BST20190707

58. Frick M, Bright NA, Riento K, Bray A, Merrified C, Nichols BJ. Coassembly of flotillins induces formation of membrane microdomains, membrane curvature, and vesicle budding. *Curr Biol*. 2007;17(13):1151-1156. doi:10.1016/j.cub.2007.05.078

59. Fukata Y, Bredt DS, Fukata M. Protein Palmitoylation by DHHC Protein Family. In: Kittler JT, Moss SJ, eds. *The Dynamic Synapse: Molecular Methods in Ionotropic Receptor Biology*. Boca Raton (FL): CRC Press/Taylor & Francis; 2006.

60. Fukata M, Fukata Y, Adesnik H, Nicoll RA, Bredt DS. Identification of PSD-95 palmitoylating enzymes. *Neuron*. 2004;44(6):987-996. doi:10.1016/j.neuron.2004.12.005

61. Ganeshan K, Chawla A. Metabolic regulation of immune responses. *Annu Rev Immunol*. 2014;32:609-634. doi:10.1146/annurev-immunol-032713-120236

62. Gay NJ, Gangloff M. Structure and function of Toll receptors and their ligands. *Annu Rev Biochem*. 2007;76:141-165. doi:10.1146/annurev.biochem.76.060305.151318

63. Gay NJ, Symmons MF, Gangloff M, Bryant CE. Assembly and localization of Toll-like receptor signalling complexes. *Nat Rev Immunol*. 2014;14(8):546-558. doi:10.1038/nri3713

64. Genest M, Comunale F, Planchon D, et al. Upregulated flotillins and sphingosine kinase 2 derail AXL vesicular traffic to promote epithelial-mesenchymal transition. *J Cell Sci*. 2022;135(7):jcs259178. doi:10.1242/jcs.259178

65. Glebov OO, Bright NA, Nichols BJ. Flotillin-1 defines a clathrin-independent endocytic pathway in mammalian cells. *Nat Cell Biol*. 2006;8(1):46-54. doi:10.1038/ncb1342

66. Guan X, Fierke CA. Understanding Protein Palmitoylation: Biological Significance and Enzymology. *Sci China Chem*. 2011;54(12):1888-1897. doi:10.1007/s11426-011-4428-2

67. Guo H, Callaway JB, Ting JP. Inflammasomes: mechanism of action, role in disease, and therapeutics. *Nat Med*. 2015;21(7):677-687. doi:10.1038/nm.3893

68. Hach JC, McMichael T, Chesarino NM, Yount JS. Palmitoylation on conserved and nonconserved cysteines of murine IFITM1 regulates its stability and anti-influenza A virus activity. *J Virol*. 2013;87(17):9923-9927. doi:10.1128/JVI.00621-13

69. He M, Abdi KM, Bennett V. Ankyrin-G palmitoylation and βII-spectrin binding to phosphoinositide lipids drive lateral membrane assembly. *J Cell Biol*. 2014;206(2):273-288. doi:10.1083/jcb.201401016

70. Henrick BM, Yao XD, Zahoor MA, Abimiku A, Osawe S, Rosenthal KL. TLR10 Senses HIV-1 Proteins and Significantly Enhances HIV-1 Infection. *Front Immunol*. 2019;10:482. Published 2019 Mar 15. doi:10.3389/fimmu.2019.00482

71. Hilgemann DW, Lin MJ, Fine M, Deisl C. On the existence of endocytosis driven by membrane phase separations. *Biochim Biophys Acta Biomembr*. 2020;1862(1):183007. doi:10.1016/j.bbamem.2019.06.006

72. Hoehne M, de Couet HG, Stuermer CA, Fischbach KF. Loss- and gain-of-function analysis of the lipid raft proteins Reggie/Flotillin in Drosophila: they are posttranslationally regulated, and misexpression interferes with wing and eye development. *Mol Cell Neurosci*. 2005;30(3):326-338. doi:10.1016/j.mcn.2005.07.007

73. Horejsi V, Hrdinka M. Membrane microdomains in immunoreceptor signaling. *FEBS Lett*. 2014;588(15):2392-2397. doi:10.1016/j.febslet.2014.05.047

74. Husebye H, Halaas Ø, Stenmark H, et al. Endocytic pathways regulate Toll-like receptor 4 signaling and link innate and adaptive immunity. *EMBO J*. 2006;25(4):683-692. doi:10.1038/sj.emboj.7600991

75. Ivaldi C, Martin BR, Kieffer-Jaquinod S, et al. Proteomic analysis of S-acylated proteins in human B cells reveals palmitoylation of the immune regulators CD20 and CD23. *PLoS One*. 2012;7(5):e37187. doi:10.1371/journal.pone.0037187

76. Jang D, Kwon H, Choi M, Lee J, Pak Y. Sumoylation of Flotillin-1 promotes EMT in metastatic prostate cancer by suppressing Snail degradation. *Oncogene*. 2019;38(17):3248-3260. doi:10.1038/s41388-018-0641-1

77. Jang D, Kwon H, Jeong K, Lee J, Pak Y. Essential role of flotillin-1 palmitoylation in the intracellular localization and signaling function of IGF-1 receptor. *J Cell Sci*. 2015;128(11):2179-2190. doi:10.1242/jcs.169409

78. Jennings BC, Linder ME. DHHC protein S-acyltransferases use similar ping-pong kinetic mechanisms but display different acyl-CoA specificities. *J Biol Chem*. 2012;287(10):7236-7245. doi:10.1074/jbc.M111.337246

79. Jenne A, Famulok M. Disruption of the streptavidin interaction with biotinylated nucleic acid probes by 2-mercaptoethanol. *Biotechniques*. 1999;26(2):249-254. doi:10.2144/99262bm15

80. Jiang H, Khan S, Wang Y, et al. SIRT6 regulates TNF-α secretion through hydrolysis of long-chain fatty acyl lysine. *Nature*. 2013;496(7443):110-113. doi:10.1038/nature12038

81. Jiang H, Zhang X, Chen X, Aramsangtienchai P, Tong Z, Lin H. Protein Lipidation: Occurrence, Mechanisms, Biological Functions, and Enabling Technologies. *Chem Rev*. 2018;118(3):919-988. doi:10.1021/acs.chemrev.6b00750

82. Jiang Z, Georgel P, Du X, et al. CD14 is required for MyD88-independent LPS signaling. *Nat Immunol*. 2005;6(6):565-570. doi:10.1038/ni1207

83. Józefowski S, Czerkies M, Łukasik A, et al. Ceramide and ceramide 1-phosphate are negative regulators of TNF-α production induced by lipopolysaccharide. *J Immunol*. 2010;185(11):6960-6973. doi:10.4049/jimmunol.0902926

84. Kagan JC, Medzhitov R. Phosphoinositide-mediated adaptor recruitment controls Toll-like receptor signaling. *Cell*. 2006;125(5):943-955. doi:10.1016/j.cell.2006.03.047

85. Kagan JC, Su T, Horng T, Chow A, Akira S, Medzhitov R. TRAM couples endocytosis of Toll-like receptor 4 to the induction of interferon-beta. *Nat Immunol*. 2008;9(4):361-368. doi:10.1038/ni1569

86. Kaiser HJ, Lingwood D, Levental I, et al. Order of lipid phases in model and plasma membranes. *Proc Natl Acad Sci U S A*. 2009;106(39):16645-16650. doi:10.1073/pnas.0908987106

87. Kawai T, Akira S. The role of pattern-recognition receptors in innate immunity: update on Toll-like receptors. *Nat Immunol*. 2010;11(5):373-384. doi:10.1038/ni.1863

88. Kawai T, Akira S. TLR signaling. *Cell Death Differ*. 2006;13(5):816-825. doi:10.1038/sj.cdd.4401850

89. Kawai T, Akira S. Toll-like receptors and their crosstalk with other innate receptors in infection and immunity. *Immunity*. 2011;34(5):637-650. doi:10.1016/j.immuni.2011.05.006

90. Kim JI, Lee CJ, Jin MS, et al. Crystal structure of CD14 and its implications for lipopolysaccharide signaling. *J Biol Chem*. 2005;280(12):11347-11351. doi:10.1074/jbc.M414607200

91. Kim YC, Lee SE, Kim SK, et al. Toll-like receptor mediated inflammation requires FASN-dependent MYD88 palmitoylation. *Nat Chem Biol*. 2019;15(9):907-916. doi:10.1038/s41589-019-0344-0

92. Kong E, Peng S, Chandra G, et al. Dynamic palmitoylation links cytosol-membrane shuttling of acyl-protein thioesterase-1 and acyl-protein thioesterase-2 with that of proto-oncogene H-ras product and growth-associated protein-43. *J Biol Chem*. 2013;288(13):9112-9125. doi:10.1074/jbc.M112.421073

93. Kulma M, Kacprzyk-Stokowiec A, Kwiatkowska K, Traczyk G, Sobota A, Dadlez M. R468A mutation in perfringolysin O destabilizes toxin structure and induces membrane fusion. *Biochim Biophys Acta Biomembr*. 2017;1859(6):1075-1088. doi:10.1016/j.bbamem.2017.03.001

94. Kusumi A, Fujiwara TK, Morone N, et al. Membrane mechanisms for signal transduction: the coupling of the meso-scale raft domains to membrane-skeleton-induced compartments and dynamic protein complexes. *Semin Cell Dev Biol*. 2012;23(2):126-144. doi:10.1016/j.semcdb.2012.01.018

95. Kwiatkowska K, Frey J, Sobota A. Phosphorylation of FcgammaRIIA is required for the receptor-induced actin rearrangement and capping: the role of membrane rafts. *J Cell Sci*. 2003;116(Pt 3):537-550. doi:10.1242/jcs.00254

96. Kwiatkowska K, Matveichuk OV, Fronk J, Ciesielska A. Flotillins: At the Intersection of Protein *S*-Palmitoylation and Lipid-Mediated Signaling. *Int J Mol Sci*. 2020;21(7):2283. Published 2020 Mar 26. doi:10.3390/ijms21072283

97. Laemmli UK. Cleavage of structural proteins during the assembly of the head of bacteriophage T4. *Nature*. 1970;227(5259):680-685. doi:10.1038/227680a0

98. Lemaitre B, Nicolas E, Michaut L, Reichhart JM, Hoffmann JA. The dorsoventral regulatory gene cassette spätzle/Toll/cactus controls the potent antifungal response in Drosophila adults. *Cell*. 1996;86(6):973-983. doi:10.1016/s0092-8674(00)80172-5

99. Lemonidis K, Sanchez-Perez MC, Chamberlain LH. Identification of a Novel Sequence Motif Recognized by the Ankyrin Repeat Domain of zDHHC17/13 S-Acyltransferases. *J Biol Chem*. 2015;290(36):21939-21950. doi:10.1074/jbc.M115.657668

100. Levental I, Grzybek M, Simons K. Raft domains of variable properties and compositions in plasma membrane vesicles. *Proc Natl Acad Sci U S A*. 2011;108(28):11411-11416. doi:10.1073/pnas.1105996108

101. Levental I, Lingwood D, Grzybek M, Coskun U, Simons K. Palmitoylation regulates raft affinity for the majority of integral raft proteins. *Proc Natl Acad Sci U S A*. 2010;107(51):22050-22054. doi:10.1073/pnas.1016184107

102. Levy S, Shoham T. Protein-protein interactions in the tetraspanin web. *Physiology (Bethesda)*. 2005;20:218-224. doi:10.1152/physiol.00015.2005

103. Liang X, Nazarian A, Erdjument-Bromage H, Bornmann W, Tempst P, Resh MD. Heterogeneous fatty acylation of Src family kinases with polyunsaturated fatty acids regulates raft localization and signal transduction. *J Biol Chem*. 2001;276(33):30987-30994. doi:10.1074/jbc.M104018200

104. Li Y, Martin BR, Cravatt BF, Hofmann SL. DHHC5 protein palmitoylates flotillin-2 and is rapidly degraded on induction of neuronal differentiation in cultured cells. *J Biol Chem*. 2012;287(1):523-530. doi:10.1074/jbc.M111.306183

105. Li D, Liu Y, Lu Y, Gao S, Zhang L. Palmitoylation of SARS-CoV-2 S protein is critical for S-mediated syncytia formation and virus entry. *J Med Virol*. 2022;94(1):342-348. doi:10.1002/jmv.27339

106. Lin DT, Conibear E. ABHD17 proteins are novel protein depalmitoylases that regulate N-Ras palmitate turnover and subcellular localization. *Elife*. 2015;4:e11306. Published 2015 Dec 23. doi:10.7554/eLife.11306

107. Lin SC, Lo YC, Wu H. Helical assembly in the MyD88-IRAK4-IRAK2 complex in TLR/IL-1R signalling. *Nature*. 2010;465(7300):885-890. doi:10.1038/nature09121

108. Lingwood D, Simons K. Lipid rafts as a membrane-organizing principle. *Science*. 2010;327(5961):46-50. doi:10.1126/science.1174621

109. Lobo S, Greentree WK, Linder ME, Deschenes RJ. Identification of a Ras palmitoyltransferase in Saccharomyces cerevisiae. *J Biol Chem*. 2002;277(43):41268-41273. doi:10.1074/jbc.M206573200

110. Lorent JH, Diaz-Rohrer B, Lin X, et al. Structural determinants and functional consequences of protein affinity for membrane rafts [published correction appears in Nat Commun. 2018 May 1;9(1):1805]. *Nat Commun*. 2017;8(1):1219. Published 2017 Oct 31. doi:10.1038/s41467-017-01328-3

111. Malgapo MIP, Linder ME. Substrate recruitment by zDHHC protein acyltransferases. *Open Biol*. 2021;11(4):210026. doi:10.1098/rsob.210026

112. Manček-Keber M, Jerala R. Postulates for validating TLR4 agonists. *Eur J Immunol*. 2015;45(2):356-370. doi:10.1002/eji.201444462

113. Martin BR, Cravatt BF. Large-scale profiling of protein palmitoylation in mammalian cells. *Nat Methods*. 2009;6(2):135-138. doi:10.1038/nmeth.1293

114. Martin BR. Chemical approaches for profiling dynamic palmitoylation. *Biochem Soc Trans*. 2013;41(1):43-49. doi:10.1042/BST20120271

115. Merrick BA, Dhungana S, Williams JG, et al. Proteomic profiling of S-acylated macrophage proteins identifies a role for palmitoylation in mitochondrial targeting of phospholipid scramblase 3. *Mol Cell Proteomics*. 2011;10(10):M110.006007. doi:10.1074/mcp.M110.006007

116. Mitchell DA, Vasudevan A, Linder ME, Deschenes RJ. Protein palmitoylation by a family of DHHC protein S-acyltransferases. *J Lipid Res*. 2006;47(6):1118-1127. doi:10.1194/jlr.R600007-JLR200

117. Mitchell JA, Paul-Clark MJ, Clarke GW, McMaster SK, Cartwright N. Critical role of toll-like receptors and nucleotide oligomerisation domain in the regulation of health and disease. *J Endocrinol*. 2007;193(3):323-330. doi:10.1677/JOE-07-0067

118. Morrow IC, Rea S, Martin S, et al. Flotillin-1/reggie-2 traffics to surface raft domains via a novel golgi-independent pathway. Identification of a novel membrane targeting domain and a role for palmitoylation. *J Biol Chem*. 2002;277(50):48834-48841. doi:10.1074/jbc.M209082200

119. Motshwene PG, Moncrieffe MC, Grossmann JG, et al. An oligomeric signaling platform formed by the Toll-like receptor signal transducers MyD88 and IRAK-4. *J Biol Chem*. 2009;284(37):25404-25411. doi:10.1074/jbc.M109.022392

120. Mukai J, Dhilla A, Drew LJ, et al. Palmitoylation-dependent neurodevelopmental deficits in a mouse model of 22q11 microdeletion. *Nat Neurosci*. 2008;11(11):1302-1310. doi:10.1038/nn.2204

121. Mukai J, Liu H, Burt RA, et al. Evidence that the gene encoding ZDHHC8 contributes to the risk of schizophrenia. *Nat Genet*. 2004;36(7):725-731. doi:10.1038/ng1375

122. Munderloh C, Solis GP, Bodrikov V, et al. Reggies/flotillins regulate retinal axon regeneration in the zebrafish optic nerve and differentiation of hippocampal and N2a neurons. *J Neurosci*. 2009;29(20):6607-6615. doi:10.1523/JNEUROSCI.0870-09.2009

123. Neumann-Giesen C, Falkenbach B, Beicht P, et al. Membrane and raft association of reggie-1/flotillin-2: role of myristoylation, palmitoylation and oligomerization and induction of filopodia by overexpression. *Biochem J*. 2004;378(Pt 2):509-518. doi:10.1042/BJ20031100

124. Neumann-Giesen C, Fernow I, Amaddii M, Tikkanen R. Role of EGF-induced tyrosine phosphorylation of reggie-1/flotillin-2 in cell spreading and signaling to the actin cytoskeleton. *J Cell Sci*. 2007;120(Pt 3):395-406. doi:10.1242/jcs.03336

125. Ohno Y, Kashio A, Ogata R, Ishitomi A, Yamazaki Y, Kihara A. Analysis of substrate specificity of human DHHC protein acyltransferases using a yeast expression system. *Mol Biol Cell*. 2012;23(23):4543-4551. doi:10.1091/mbc.E12-05-0336

126. Ohno Y, Kihara A, Sano T, Igarashi Y. Intracellular localization and tissue-specific distribution of human and yeast DHHC cysteine-rich domain-containing proteins. *Biochim Biophys Acta*. 2006;1761(4):474-483. doi:10.1016/j.bbalip.2006.03.010

127. Pandey S, Singh S, Anang V, Bhatt AN, Natarajan K, Dwarakanath BS. Pattern Recognition Receptors in Cancer Progression and Metastasis. *Cancer Growth Metastasis*. 2015;8:25-34. Published 2015 Jul 23. doi:10.4137/CGM.S24314

128. Park BS, Song DH, Kim HM, Choi BS, Lee H, Lee JO. The structural basis of lipopolysaccharide recognition by the TLR4-MD-2 complex. *Nature*. 2009;458(7242):1191-1195. doi:10.1038/nature07830

129. Patel MN, Carroll RG, Galván-Peña S, et al. Inflammasome Priming in Sterile Inflammatory Disease. *Trends Mol Med*. 2017;23(2):165-180. doi:10.1016/j.molmed.2016.12.007

130. Patra MC, Choi S. Insight into Phosphatidylinositol-Dependent Membrane Localization of the Innate Immune Adaptor Protein Toll/Interleukin 1 Receptor Domain-Containing Adaptor Protein. *Front Immunol*. 2018;9:75. Published 2018 Jan 29. doi:10.3389/fimmu.2018.00075

131. Pedro MP, Vilcaes AA, Tomatis VM, Oliveira RG, Gomez GA, Daniotti JL. 2-Bromopalmitate reduces protein deacylation by inhibition of acyl-protein thioesterase enzymatic activities. *PLoS One*. 2013;8(10):e75232. Published 2013 Oct 2. doi:10.1371/journal.pone.0075232

132. Perera PY, Vogel SN, Detore GR, Haziot A, Goyert SM. CD14-dependent and CD14-independent signaling pathways in murine macrophages from normal and CD14 knockout mice stimulated with lipopolysaccharide or taxol. *J Immunol*. 1997;158(9):4422-4429

133. Philippe JM, Jenkins PM. Spatial organization of palmitoyl acyl transferases governs substrate localization and function. *Mol Membr Biol*. 2019;35(1):60-75. doi:10.1080/09687688.2019.1710274

134. Phuyal S, Hessvik NP, Skotland T, Sandvig K, Llorente A. Regulation of exosome release by glycosphingolipids and flotillins. *FEBS J*. 2014;281(9):2214-2227. doi:10.1111/febs.12775

135. Plain F, Howie J, Kennedy J, et al. Control of protein palmitoylation by regulating substrate recruitment to a zDHHC-protein acyltransferase. *Commun Biol*. 2020;3(1):411. Published 2020 Jul 31. doi:10.1038/s42003-020-01145-3

136. Planchon D, Rios Morris E, Genest M, et al. MT1-MMP targeting to endolysosomes is mediated by upregulation of flotillins. *J Cell Sci*. 2018;131(17):jcs218925. Published 2018 Sep 5. doi:10.1242/jcs.218925

137. Płóciennikowska A, Hromada-Judycka A, Borzęcka K, Kwiatkowska K. Co-operation of TLR4 and raft proteins in LPS-induced pro-inflammatory signaling. *Cell Mol Life Sci*. 2015;72(3):557-581. doi:10.1007/s00018-014-1762-5 (a)

138. Płóciennikowska A, Hromada-Judycka A, Dembińska J, Roszczenko P, Ciesielska A, Kwiatkowska K. Contribution of CD14 and TLR4 to changes of the PI(4,5)P2 level in LPS-stimulated cells. *J Leukoc Biol*. 2016;100(6):1363-1373. doi:10.1189/jlb.2VMA1215-577R

139. Płóciennikowska A, Zdioruk MI, Traczyk G, Świątkowska A, Kwiatkowska K. LPS-induced clustering of CD14 triggers generation of PI(4,5)P2. *J Cell Sci*. 2015;128(22):4096-4111. doi:10.1242/jcs.173104 (b)

140. Podkalicka J, Biernatowska A, Majkowski M, Grzybek M, Sikorski AF. MPP1 as a Factor Regulating Phase Separation in Giant Plasma Membrane-Derived Vesicles. *Biophys J*. 2015;108(9):2201-2211. doi:10.1016/j.bpj.2015.03.017

141. Poggi M, Kara I, Brunel JM, et al. Palmitoylation of TNF alpha is involved in the regulation of TNF receptor 1 signalling. *Biochim Biophys Acta*. 2013;1833(3):602-612. doi:10.1016/j.bbamcr.2012.11.009

142. Poltorak A, He X, Smirnova I, et al. Defective LPS signaling in C3H/HeJ and C57BL/10ScCr mice: mutations in Tlr4 gene. *Science*. 1998;282(5396):2085-2088. doi:10.1126/science.282.5396.2085

143. Prymas K, Świątkowska A, Traczyk G, et al. Sphingomyelin synthase activity affects TRIF-dependent signaling of Toll-like receptor 4 in cells stimulated with lipopolysaccharide. *Biochim Biophys Acta Mol Cell Biol Lipids*. 2020;1865(2):158549. doi:10.1016/j.bbalip.2019.158549

144. Pust S, Klokk TI, Musa N, et al. Flotillins as regulators of ErbB2 levels in breast cancer. *Oncogene*. 2013;32(29):3443-3451. doi:10.1038/onc.2012.357

145. Raetz CR, Whitfield C. Lipopolysaccharide endotoxins. *Annu Rev Biochem*. 2002;71:635-700. doi:10.1146/annurev.biochem.71.110601.135414

146. Raghupathy R, Anilkumar AA, Polley A, et al. Transbilayer lipid interactions mediate nanoclustering of lipid-anchored proteins. *Cell*. 2015;161(3):581-594. doi:10.1016/j.cell.2015.03.048

147. Redpath GMI, Ecker M, Kapoor-Kaushik N, et al. Flotillins promote T cell receptor sorting through a fast Rab5-Rab11 endocytic recycling axis. *Nat Commun*. 2019;10(1):4392. Published 2019 Sep 26. doi:10.1038/s41467-019-12352-w

148. Ren W, Jhala US, Du K. Proteomic analysis of protein palmitoylation in adipocytes. *Adipocyte*. 2013;2(1):17-28. doi:10.4161/adip.22117

149. Resh MD. Covalent lipid modifications of proteins. *Curr Biol*. 2013;23(10):R431-R435. doi:10.1016/j.cub.2013.04.024

150. Resh MD. Fatty acylation of proteins: new insights into membrane targeting of myristoylated and palmitoylated proteins. *Biochim Biophys Acta*. 1999;1451(1):1-16. doi:10.1016/s0167-4889(99)00075-0

151. Resh MD. Fatty acylation of proteins: The long and the short of it. *Prog Lipid Res*. 2016;63:120-131. doi:10.1016/j.plipres.2016.05.002

152. Resman N, Vasl J, Oblak A, et al. Essential roles of hydrophobic residues in both MD-2 and toll-like receptor 4 in activation by endotoxin. *J Biol Chem*. 2009;284(22):15052-15060. doi:10.1074/jbc.M901429200

153. Riento K, Frick M, Schafer I, Nichols BJ. Endocytosis of flotillin-1 and flotillin-2 is regulated by Fyn kinase. *J Cell Sci*. 2009;122(Pt 7):912-918. doi:10.1242/jcs.039024

154. Riento K, Zhang Q, Clark J, et al. Flotillin proteins recruit sphingosine to membranes and maintain cellular sphingosine-1-phosphate levels. *PLoS One*. 2018;13(5):e0197401. Published 2018 May 22. doi:10.1371/journal.pone.0197401

155. Rivera-Milla E, Stuermer CA, Málaga-Trillo E. Ancient origin of reggie (flotillin), reggie-like, and other lipid-raft proteins: convergent evolution of the SPFH domain. *Cell Mol Life Sci*. 2006;63(3):343-357. doi:10.1007/s00018-005-5434-3

156. Rietschel ET, Kirikae T, Schade FU, et al. Bacterial endotoxin: molecular relationships of structure to activity and function. *FASEB J*. 1994;8(2):217-225. doi:10.1096/fasebj.8.2.8119492

157. Ritho J, Dixon SJ. Excited to see you: New imaging approaches to detect ferrous iron in vivo. *Cell Chem Biol*. 2022;29(1):3-4. doi:10.1016/j.chembiol.2021.12.012

158. Rocks O, Peyker A, Kahms M, et al. An acylation cycle regulates localization and activity of palmitoylated Ras isoforms. *Science*. 2005;307(5716):1746-1752. doi:10.1126/science.1105654

159. Rosadini CV, Kagan JC. Early innate immune responses to bacterial LPS. *Curr Opin Immunol*. 2017;44:14-19. doi:10.1016/j.coi.2016.10.005

160. Roth AF, Feng Y, Chen L, Davis NG. The yeast DHHC cysteine-rich domain protein Akr1p is a palmitoyl transferase. *J Cell Biol*. 2002;159(1):23-28. doi:10.1083/jcb.200206120

161. Roth AF, Wan J, Bailey AO, et al. Global analysis of protein palmitoylation in yeast. *Cell*. 2006;125(5):1003-1013. doi:10.1016/j.cell.2006.03.042

162. Rowe DC, McGettrick AF, Latz E, et al. The myristoylation of TRIF-related adaptor molecule is essential for Toll-like receptor 4 signal transduction. *Proc Natl Acad Sci U S A*. 2006;103(16):6299-6304. doi:10.1073/pnas.0510041103

163. Ruiz-García, A., López-López, S., García-Ramírez, J. J., Baladrón, V., Ruiz-Hidalgo, M. J., López-Sanz, L., Ballesteros, Á., Laborda, J., Monsalve, E. M., & Díaz-Guerra, M. J. (2016). The Tetraspanin TSPAN33 Controls TLR-Triggered Macrophage Activation through Modulation of NOTCH Signaling. *Journal of immunology (Baltimore, Md. : 1950)*, *197*(8), 3371–3381. https://doi.org/10.4049/jimmunol.1600421

164. Ryu JK, Kim SJ, Rah SH, et al. Reconstruction of LPS Transfer Cascade Reveals Structural Determinants within LBP, CD14, and TLR4-MD2 for Efficient LPS Recognition and Transfer. *Immunity*. 2017;46(1):38-50. doi:10.1016/j.immuni.2016.11.007

165. Sanders SS, Hou J, Sutton LM, et al. Huntingtin interacting proteins 14 and 14-like are required for chorioallantoic fusion during early placental development. *Dev Biol*. 2015;397(2):257-266. doi:10.1016/j.ydbio.2014.11.018

166. Santonico E, Belleudi F, Panni S, Torrisi MR, Cesareni G, Castagnoli L. Multiple modification and protein interaction signals drive the Ring finger protein 11 (RNF11) E3 ligase to the endosomal compartment. *Oncogene*. 2010;29(41):5604-5618. doi:10.1038/onc.2010.294

167. Schappe MS, Desai BN. Measurement of TLR4 and CD14 Receptor Endocytosis Using Flow Cytometry. *Bio Protoc*. 2018;8(14):e2926. doi:10.21769/BioProtoc.2926

168. Schulte T, Paschke KA, Laessing U, Lottspeich F, Stuermer CA. Reggie-1 and reggie-2, two cell surface proteins expressed by retinal ganglion cells during axon regeneration. *Development*. 1997;124(2):577-587. doi:10.1242/dev.124.2.577

169. Skotte NH, Sanders SS, Singaraja RR, et al. Palmitoylation of caspase-6 by HIP14 regulates its activation. *Cell Death Differ*. 2017;24(3):433-444. doi:10.1038/cdd.2016.139

170. Senyilmaz D, Virtue S, Xu X, et al. Regulation of mitochondrial morphology and function by stearoylation of TFR1. *Nature*. 2015;525(7567):124-128. doi:10.1038/nature14601

171. Shoham T, Rajapaksa R, Kuo CC, Haimovich J, Levy S. Building of the tetraspanin web: distinct structural domains of CD81 function in different cellular compartments. *Mol Cell Biol*. 2006;26(4):1373-1385. doi:10.1128/MCB.26.4.1373-1385.2006

172. Simmons DL, Tan S, Tenen DG, Nicholson-Weller A, Seed B. Monocyte antigen CD14 is a phospholipid anchored membrane protein. *Blood*. 1989;73(1):284-289

173. Simons K, Ikonen E. Functional rafts in cell membranes. *Nature*. 1997;387(6633):569-572. doi:10.1038/42408

174. Sobocińska J, Roszczenko-Jasińska P, Ciesielska A, Kwiatkowska K. Protein Palmitoylation and Its Role in Bacterial and Viral Infections. *Front Immunol*. 2018;8:2003. Published 2018 Jan 19. doi:10.3389/fimmu.2017.02003 (a)

175. Sobocińska J, Roszczenko-Jasińska P, Zaręba-Kozioł M, et al. Lipopolysaccharide Upregulates Palmitoylated Enzymes of the Phosphatidylinositol Cycle: An Insight from Proteomic Studies. *Mol Cell Proteomics*. 2018;17(2):233-254. doi:10.1074/mcp.RA117.000050 (b)

176. Solis GP, Hülsbusch N, Radon Y, Katanaev VL, Plattner H, Stuermer CA. Reggies/flotillins interact with Rab11a and SNX4 at the tubulovesicular recycling compartment and function in transferrin receptor and E-cadherin trafficking. *Mol Biol Cell*. 2013;24(17):2689-2702. doi:10.1091/mbc.E12-12-0854

177. Song Y, Shou LM, Ai LY, Bei Y, Chen MT. Mini-Review: The Non-Immune Functions of Toll-Like Receptors. *Crit Rev Eukaryot Gene Expr*. 2019;29(1):37-45. doi:10.1615/CritRevEukaryotGeneExpr.2018027399

178. Spinelli M, Fusco S, Grassi C. Nutrient-Dependent Changes of Protein Palmitoylation: Impact on Nuclear Enzymes and Regulation of Gene Expression. *Int J Mol Sci*. 2018;19(12):3820. Published 2018 Nov 30. doi:10.3390/ijms19123820

179. Steimle A, Autenrieth IB, Frick JS. Structure and function: Lipid A modifications in commensals and pathogens. *Int J Med Microbiol*. 2016;306(5):290-301. doi:10.1016/j.ijmm.2016.03.001

180. Stepanek O, Draber P, Horejsi V. Palmitoylated transmembrane adaptor proteins in leukocyte signaling. *Cell Signal*. 2014;26(5):895-902. doi:10.1016/j.cellsig.2014.01.007

181. Stone MB, Shelby SA, Núñez MF, Wisser K, Veatch SL. Protein sorting by lipid phase-like domains supports emergent signaling function in B lymphocyte plasma membranes. *Elife*. 2017;6:e19891. Published 2017 Feb 1. doi:10.7554/eLife.19891

182. Strauss K, Goebel C, Runz H, et al. Exosome secretion ameliorates lysosomal storage of cholesterol in Niemann-Pick type C disease. *J Biol Chem*. 2010;285(34):26279-26288. doi:10.1074/jbc.M110.134775

183. Stuermer CA, Lang DM, Kirsch F, Wiechers M, Deininger SO, Plattner H. Glycosylphosphatidyl inositol-anchored proteins and fyn kinase assemble in noncaveolar plasma membrane microdomains defined by reggie-1 and -2. *Mol Biol Cell*. 2001;12(10):3031-3045. doi:10.1091/mbc.12.10.3031

184. Suzuki, M., Tachibana, I., Takeda, Y., He, P., Minami, S., Iwasaki, T., Kida, H., Goya, S., Kijima, T., Yoshida, M., Kumagai, T., Osaki, T., & Kawase, I. (2009). Tetraspanin CD9 negatively regulates lipopolysaccharide-induced macrophage

activation and lung inflammation. *Journal of immunology (Baltimore, Md. : 1950), 182*(10), 6485–6493. https://doi.org/10.4049/jimmunol.0802797

185. Swarthout JT, Lobo S, Farh L, et al. DHHC9 and GCP16 constitute a human protein fatty acyltransferase with specificity for H- and N-Ras. *J Biol Chem*. 2005;280(35):31141-31148. doi:10.1074/jbc.M504113200

186. Takeda K, Kaisho T, Akira S. Toll-like receptors. *Annu Rev Immunol*. 2003;21:335-376. doi:10.1146/annurev.immunol.21.120601.141126

187. Takeuchi O, Akira S. Pattern recognition receptors and inflammation. *Cell*. 2010;140(6):805-820. doi:10.1016/j.cell.2010.01.022

188. Tan Y, Kagan JC. A cross-disciplinary perspective on the innate immune responses to bacterial lipopolysaccharide. *Mol Cell*. 2014;54(2):212-223. doi:10.1016/j.molcel.2014.03.012

189. Tan Y, Kagan JC. Innate Immune Signaling Organelles Display Natural and Programmable Signaling Flexibility. *Cell*. 2019;177(2):384-398.e11. doi:10.1016/j.cell.2019.01.039

190. Tan Y, Kagan JC. Microbe-inducible trafficking pathways that control Toll-like receptor signaling. *Traffic*. 2017;18(1):6-17. doi:10.1111/tra.12454

191. Tan Y, Zanoni I, Cullen TW, Goodman AL, Kagan JC. Mechanisms of Toll-like Receptor 4 Endocytosis Reveal a Common Immune-Evasion Strategy Used by Pathogenic and Commensal Bacteria. *Immunity*. 2015;43(5):909-922. doi:10.1016/j.immuni.2015.10.008

192. Thalwieser Z, Király N, Fonódi M, Csortos C, Boratkó A. Protein phosphatase 2A-mediated flotillin-1 dephosphorylation up-regulates endothelial cell migration and angiogenesis regulation. *J Biol Chem*. 2019;294(52):20196-20206. doi:10.1074/jbc.RA119.007980

193. Tarassishin L, Suh HS, Lee SC. Interferon regulatory factor 3 plays an anti-inflammatory role in microglia by activating the PI3K/Akt pathway. *J Neuroinflammation*. 2011;8:187. Published 2011 Dec 30. doi:10.1186/1742-2094-8-187

194. Thomas GM, Hayashi T, Chiu SL, Chen CM, Huganir RL. Palmitoylation by DHHC5/8 targets GRIP1 to dendritic endosomes to regulate AMPA-R trafficking. *Neuron*. 2012;73(3):482-496. doi:10.1016/j.neuron.2011.11.021

195. Towbin H, Staehelin T, Gordon J. Electrophoretic transfer of proteins from polyacrylamide gels to nitrocellulose sheets: procedure and some applications. *Proc Natl Acad Sci U S A*. 1979;76(9):4350-4354. doi:10.1073/pnas.76.9.4350

196. Triantafilou M, Triantafilou K. Lipopolysaccharide recognition: CD14, TLRs and the LPS-activation cluster. *Trends Immunol*. 2002;23(6):301-304. doi:10.1016/s1471-4906(02)02233-0

197. Ullah MO, Sweet MJ, Mansell A, Kellie S, Kobe B. TRIF-dependent TLR signaling, its functions in host defense and inflammation, and its potential as a therapeutic target. *J Leukoc Biol*. 2016;100(1):27-45. doi:10.1189/jlb.2RI1115-531R

198. Van Acker T, Eyckerman S, Vande Walle L, et al. The small GTPase Arf6 is essential for the Tram/Trif pathway in TLR4 signaling. *J Biol Chem*. 2014;289(3):1364-1376. doi:10.1074/jbc.M113.499194

199. Vartak N, Papke B, Grecco HE, et al. The autodepalmitoylating activity of APT maintains the spatial organization of palmitoylated membrane proteins. *Biophys J*. 2014;106(1):93-105. doi:10.1016/j.bpj.2013.11.024

200. Veit M. Palmitoylation of virus proteins. *Biol Cell*. 2012;104(9):493-515. doi:10.1111/boc.201200006

201. Verkruyse LA, Hofmann SL. Lysosomal targeting of palmitoyl-protein thioesterase. *J Biol Chem*. 1996;271(26):15831-15836. doi:10.1074/jbc.271.26.15831

202. Wan J, Savas JN, Roth AF, et al. Tracking brain palmitoylation change: predominance of glial change in a mouse model of Huntington's disease. *Chem Biol*. 2013;20(11):1421-1434. doi:10.1016/j.chembiol.2013.09.018

203. Wang C, Deng L, Hong M, Akkaraju GR, Inoue J, Chen ZJ. TAK1 is a ubiquitin-dependent kinase of MKK and IKK. *Nature*. 2001;412(6844):346-351. doi:10.1038/35085597

204. Wang D, Tabti R, Elderwish S, et al. SFPH proteins as therapeutic targets for a myriad of diseases. *Bioorg Med Chem Lett*. 2020;30(22):127600. doi:10.1016/j.bmcl.2020.127600

205. Werner HB, Kuhlmann K, Shen S, et al. Proteolipid protein is required for transport of sirtuin 2 into CNS myelin. *J Neurosci*. 2007;27(29):7717-7730. doi:10.1523/JNEUROSCI.1254-07.2007

206. Wessel D, Flügge UI. A method for the quantitative recovery of protein in dilute solution in the presence of detergents and lipids. *Anal Biochem*. 1984;138(1):141-143. doi:10.1016/0003-2697(84)90782-6

207. Wong SW, Kwon MJ, Choi AM, Kim HP, Nakahira K, Hwang DH. Fatty acids modulate Toll-like receptor 4 activation through regulation of receptor dimerization and recruitment into lipid rafts in a reactive oxygen species-dependent manner. *J Biol Chem*. 2009;284(40):27384-27392. doi:10.1074/jbc.M109.044065

208. Woodley KT, Collins MO. Regulation and function of the palmitoyl-acyltransferase ZDHHC5. *FEBS J*. 2021;288(23):6623-6634. doi:10.1111/febs.15709

209. Wooten LG, Ogretmen B. Sp1/Sp3-dependent regulation of human telomerase reverse transcriptase promoter activity by the bioactive sphingolipid ceramide. *J Biol Chem*. 2005;280(32):28867-28876. doi:10.1074/jbc.M413444200

210. Wu GQ, Xu YM, Lau ATY. Recent insights into eukaryotic translation initiation factors 5A1 and 5A2 and their roles in human health and disease. *Cancer Cell Int*. 2020;20:142. Published 2020 Apr 29. doi:10.1186/s12935-020-01226-7

211. Yamamoto M, Sato S, Mori K, et al. Cutting edge: a novel Toll/IL-1 receptor domain-containing adapter that preferentially activates the IFN-beta promoter in the Toll-like receptor signaling. *J Immunol*. 2002;169(12):6668-6672. doi:10.4049/jimmunol.169.12.6668

212. Yang Q, Zheng F, Hu Y, et al. ZDHHC8 critically regulates seizure susceptibility in epilepsy. *Cell Death Dis*. 2018;9(8):795. Published 2018 Jul 23. doi:10.1038/s41419-018-0842-0

213. Yang Y, Wang H, Kouadir M, Song H, Shi F. Recent advances in the mechanisms of NLRP3 inflammasome activation and its inhibitors. *Cell Death Dis*. 2019;10(2):128. Published 2019 Feb 12. doi:10.1038/s41419-019-1413-8

214. Yang X, Claas C, Kraeft SK, et al. Palmitoylation of tetraspanin proteins: modulation of CD151 lateral interactions, subcellular distribution, and integrin-dependent cell morphology. Mol Biol Cell. 2002;13(3):767-781. doi:10.1091/mbc.01-05-0275

215. Yount JS, Zhang MM, Hang HC. Visualization and Identification of Fatty Acylated Proteins Using Chemical Reporters. *Curr Protoc Chem Biol*. 2011;3(2):65-79. doi:10.1002/9780470559277.ch100225

216. Zaballa ME, van der Goot FG. The molecular era of protein S-acylation: spotlight on structure, mechanisms, and dynamics. *Crit Rev Biochem Mol Biol*. 2018;53(4):420-451. doi:10.1080/10409238.2018.1488804

217. Zanoni I, Ostuni R, Marek LR, et al. CD14 controls the LPS-induced endocytosis of Toll-like receptor 4. *Cell*. 2011;147(4):868-880. doi:10.1016/j.cell.2011.09.051

218. Zhang MM, Tsou LK, Charron G, Raghavan AS, Hang HC. Tandem fluorescence imaging of dynamic S-acylation and protein turnover. *Proc Natl Acad Sci U S A*. 2010;107(19):8627-8632. doi:10.1073/pnas.0912306107

219. Zhang, M., Zhou, L., Xu, Y., Yang, M., Xu, Y., Komaniecki, G. P., Kosciuk, T., Chen, X., Lu, X., Zou, X., Linder, M. E., & Lin, H. (2020). A STAT3 palmitoylation cycle promotes T_H17 differentiation and colitis. *Nature*, *586*(7829), 434–439. https://doi.org/10.1038/s41586-020-2799-2

220. Ziemlińska E, Sobocińska J, Świątkowska A, et al. Palm Oil-Rich Diet Affects Murine Liver Proteome and *S*-Palmitoylome. *Int J Mol Sci*. 2021;22(23):13094. Published 2021 Dec 3. doi:10.3390/ijms222313094

221. Zou K, Abdullah M, Michikawa M. Current Biomarkers for Alzheimer's Disease: From CSF to Blood. *J Pers Med*. 2020;10(3):85. Published 2020 Aug 12. doi:10.3390/jpm10030085